SCUOLA DI DOTTORATO

UNIVERSITÀ DEGLI STUDI DELL'INSUBRIA

DIPARTIMENTO DI

BIOTECNOLOGIE E SCIENZE DELLA VITA

PhD Course in

LIFE SCIENCES AND BIOTECHNOLOGY

XXXVIII cycle

Molecular mechanisms of vascular senescence and calcification

Doctoral Dissertation of:

Federica Macrì

Supervisor: **Prof. Davide Vigetti**

Tutor: **Dr. Angela Raucci**

Coordinator of the PhD Program: **Prof. Silvia Sacchi**

Academic year 2024/2025

TABLE OF CONTENTS

TABLE OF FIGURES

TABLE OF TABLES

ABSTRACT

Vascular aging increases the cardiovascular disease risk, including vascular calcification (VC). A key event in VC is the vascular smooth muscle cells (VSMCs) trans-differentiation into an osteogenic phenotype, which is facilitated by senescence. High Mobility Group Box-1 (HMGB1) plays a role in senescence and the senescence-associated secretory phenotype (SASP), but its involvement in vascular aging and calcification remains unclear. Preliminary results from our lab showed that aortas from old mice had significantly lower HMGB1 protein levels compared with young animals. Senescent human aortic smooth muscle cells (HASMCs) displayed reduced HMGB1 expression and no protein translocation. HASMCs silenced for HMGB1 (shB1/HASMCs) had larger nuclei and lower proliferation compared to control cells (shCTR/HASMCs). Herein, we found that shB1/HASMCs had elevated p21 levels and senescence-associated β-galactosidase activity, and showed an anti-inflammatory SASP profile, with reduced IL-6, IL-1β, IL-8, and MCP-1 compared with shCTR/HASMCs. HMGB1 silencing also modulated the release of extracellular matrix (ECM) proteins involved in tissue mineralization and increased the expression of osteoblastic inducers. These observations were confirmed comparing aortas from $Hmgb1^{+/+}$/$Hmgb1^{+/-}$ mice. Furthermore, shB1/HASMCs grown in hyperphosphatemic conditions exhibited enhanced calcification and lower inflammation than control cells and, transcriptomics revealed changes in biomineralization, cell fate commitment, immune response, and tissue migration pathways. Aortas from $Hmgb1^{+/-}$ mice treated with Vitamin D showed increased calcification and diminished IL-6 compared with $Hmgb1^{+/+}$ mice. Finally, HMGB1 content was found lower in aortas isolated from older healthy individuals and chronic kidney disease patients, and HMGB1 levels negatively correlated with calcium content in abdominal aortic aneurysms patients. Our findings demonstrate that nuclear HMGB1 downregulation during vascular aging promotes senescence, an anti-inflammatory SASP, ECM disruption and the expression of calcification modulators that promote VSMCs osteoblastic trans-differentation and eventually VC. Also, HMGB1 loss may serve as a VSMC senescence and calcification marker.

ABBREVIATIONS

AAASP	Age-Associated Arterial Secretory Phenotype
AGEs	Advanced glycation end-products
ALP	Alkaline Phosphatase
Ang II	Angiotensin II
BGN	Biglycan
BMP-2	Bone morphogenic protein 2
CAVD	Calcific aortic valve disease
CDK	Cyclin-dependent kinase
CKD	Chronic kidney disease
CVD	Cardiovascular disease
DAMP	Damage associated molecular pattern
DDR	DNA damage response
DDSBs	DNA double-strand breaks
EC	Endothelial cells
ECM	Extra Cellular Matrix
HASMCs	Human aortic smooth muscle cells
hcFbs	Human cardiac fibroblasts
hDPCs	Human dental pulp cells
HMECs	Human Mammary Epithelial Cells
HMG	High mobility group
HMGB1	High Mobility Group Box-1
IL6	Interleukin 6
LGL1	Lethal Giant Larve
LKB1	Liver kinase B1
LPS	Lipopolisaccaride

MEFs	Mouse embryonic fibroblasts
MGP	Matrix -Gla Protein
MiDAS	Senescence associated with mitochondrial dysfunction
MIP	Macrophage inflammatory protein
MMPs	Matrix metalloproteases
MSX2	Msh homeobox 2
NAPs	Nuclear aggregates of polyamines
NESs	Nuclear export signals
NFkB	Nuclear factor kappa-light-chain-enhancer of activated B cells
NLs	Nuclear localization signal
nSMAse2	Neutral sphingomyelinase-2
OPG	Osteoprotegerin
OPN	Osteopontin
PASS	Pro-inflammatory Arterial Stiffness Syndrome
PDGF	Platelet - derived growth factor
PPi	Inorganic pyrophosphate
RAG	Recombination activating gene
RAGE	Receptor for advanced glycation end-products
RANKL	Receptor Activator of Nuclear Factor kappa-B ligand
RUNX2	Runt Related Transcription Factor 2
SAHF	Senescence - associated heterochromatic foci
SASP	Senescence-Associated Secretory Phenotype
SA-β-gal	Senescence-associated-β-galactosidase
shCTRL	Short Hairpin Control
shHMGB1	Short Hairpin HMGB1
SOX-9	SRY-box transcription factor 9
T2DM	Type 2 diabetes mellitus

TADs	Topologically associating domains
TGF-β	Transforming growth factor-β
TNAP	Tissue non specific alkaline phosphatase
TLR	Toll-like receptor
TNF	Tumor necrosis factor
TNX	Tenascin X
VC	Vascular Calcification
VCi	Vascular calcification of tonaca intima
VCm	Vascular calcification of tonaca media
VSMCs	Vascular smooth muscle cells
α-SMA	α-smooth muscle actin

1. INTRODUCTION

1.1 Structure and physiology of Vascular Smooth Muscle Cells

The different structure of blood vessels indicates their role in supplying oxygen and nutrients to the entire body while minimizing energy loss within the vascular wall. The arteries and veins have three layers. The endothelial layer, known as tunica intima, consists of a single layer of flattened cells encased by a thin layer of subendothelial connective tissue along with several circularly arranged elastic bands referred to as the internal elastic lamina. The tunica media or middle layer contains elastic fibers arranged in circles, along with connective tissue and polysaccharide materials. Particularly in arteries, the tunica media contains abundant vascular smooth muscle cells (VSMCs) organized in a spiral formation around the vessel lumen that regulate the diameter of the vessel. The outermost layer is the tunica adventitia, primarily composed of connective tissue, but it also houses nerves that serve the vessel along with nutrient capillaries known as vasa vasorum.

VSMCs are the predominant cell type in blood vessels and are essential for their physiological operation, especially for vasoconstriction, vasodilation, and the production of vascular extracellular matrix (Lacolley et al., 2017). Throughout their development, VSMCs experience ultrastructural alterations and display distinct phenotypic states associated with the expression of a growing number of cytoskeletal and extracellular components (Chamley-Campbell et al., 1979). At first, they exhibit a proliferative and migratory phenotype, synthesize ECM proteins (collagen and elastin) and show α-smooth muscle actin (α-SMA) and thrombospondin; during the middle stage of differentiation, they produce transgelin, SM-actinin and metavinculin. Fully developed and distinctly differentiated VSMCs exhibit a resting and contractile phenotype, expressing smoothelin, desmin, and various contractile proteins that play a role in regulating hemodynamic resistance. All these phenotypes exist in the media of every artery throughout the arterial network, predominantly consisting of contractile cells. In mature vessels, progenitors of VSMCs remain in the adventitia layer while the transcription of VSMC marker genes is suppressed to maintain the progenitor phenotype. Morphologically, we can distinguish between two primary categories of VMSCs: spindle-shaped cells, which have a contractile phenotype, and epithelioid cells, which demonstrate a synthetic phenotype (Majesky et al., 2007). Additionally, elongated and aging VSMCs have also been reported (Majesky et al., 2007). The diversity of VSMCs can affect the characteristics of the vascular tree and make one susceptible to vascular diseases. Crucially, VSMCs can shift back from the resting contractile phenotype to their previous migratory, secretory, and proliferative phenotype, along with ECM remodeling, resulting in arterial stiffness. The capability of VSMCs is termed "plasticity," which is influenced by various elements like blood flow, blood pressure, ligand-receptor interactions, reactive

oxygen species, growth factors, and regulatory transcriptional pathways (Lacolley et al., 2017).

1.2 Vascular Aging

The process of tissue aging takes place when cells gradually diminish their capacity to proliferate, which is crucial to substitute the harmed ones that naturally accumulate over time (Di Micco et al. 2021). Genetics, changed metabolism, poor diet and insufficient physical activity are among the factors which contribute to this issue. Aging plays a crucial role in development, regeneration, and reprogramming of the tissues, but it also acts as the main risk factor for the onset of age-related diseases like cardiovascular disease (CVD), diabetes, cancer, and neurodegenerative disorders (Lopez-Otín et al. 2023). Regarding vascular aging, large-diameter vessels such as the aorta, are primarily affected by age-related changes. The endothelial cells (ECs), the VSMCs, and the pericytes experience changes in their phenotype that affect both the intima and media layers. These changes result from persistent inflammation, mechanical stimuli and cellular death and an epigenetic occurrence (Lacolley, Regnault, and Avolio 2018). Increased elastin breakdown and collagen accumulation in the tunica media leads to thickening of the intima (Costantino, Paneni, and Cosentino 2016). Eventually, the elastic and collagen elements deteriorate significantly, resulting in the expansion, stretching, and rigidity of the aortic walls (Ohyama et al. 2018). The reduction in elasticity is also associated with the rise of inflammation and vascular permeability. All these elements result in a functional imbalance of the aorta, which is not restricted to the failure of the vessel, yet this subsequently causes cardiac issues. Additionally, the interplay among VSMCs, immune cells, and platelets plays a crucial role in the progression of arterial aging (Lacolley, Regnault, and Avolio 2018) (Figure 1). In atherosclerosis, which is a common age-associated vascular condition, the thickening of the blood vessels wall in the lumen begins with the activation of ECs. Activated ECs elicit the monocyte intrusion that triggers inflammation in the intima. Inflammatory cytokines and growth factors stimulate intimal VSMCs, leading to rapid proliferation and promoting intimal expansion. In reaction to platelet-derived growth factor (PDGF), the medial VSMCs move towards the media, enhancing intimal growth (Frismantiene et al. 2018). Wang and colleagues discuss the concept of a Pro-inflammatory Arterial Stiffness Syndrome (PASS) as a hallmark of aging in large arteries. With advancing age, large-elastic-artery walls (such as the aorta) undergo structural and functional transformations characterised by increased stiffness, extracellular matrix remodelling (elastin fragmentation, collagen deposition), vascular smooth muscle cell (VSMC) phenotypic shifts, oxidative stress, and low-grade chronic inflammation. These changes lead to both increased pulse-wave velocity and altered arterial haemodynamics, which in turn predispose to cardiovascular disease. Thus, the aged arterial phenotype is not

merely passive degeneration, but a biologically active process governed by inflammatory and remodelling pathways (Wang et al., 2018).

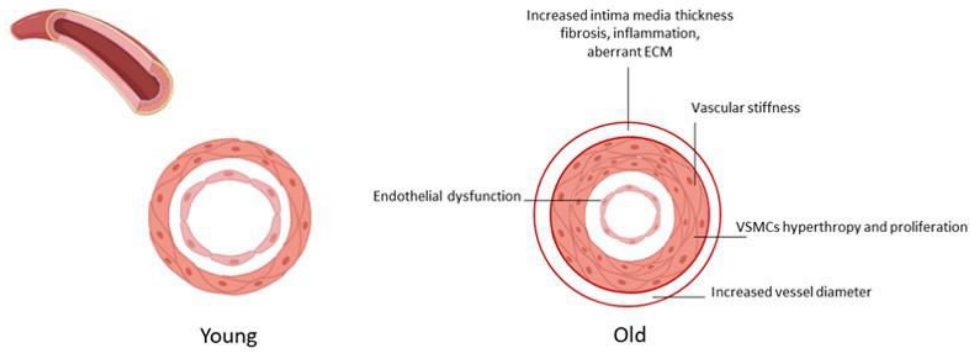

Figure 1. Vascular aging. Morphological changes are in most cases organ-specific and include vascular wall thickening, collagen deposition, perivascular fibrosis and vessel dilatation. ECM: extracellular matrix¸ VSMCs: Vascular smooth muscle cells. (Costantino et al., 2016).

1.3 Senescence and senescence associated secretory phenotype

Many cellular and molecular features have been recognized to characterize the mammalian aging such as telomere reduction, genomic instability, epigenetic alterations, decline in proteostasis, deregulation of nutrient detection, exhaustion of stem cells, mitochondrial impairment and cellular aging (López-Otín et al. 2023). Aging was found in 1961 by Hayflick, when he noticed that human fibroblasts in culture did not proliferate indefinitely but stopped their growth even with ideal conditions. This phenomenon was believed to be due to “aging” and was named “senescence”. He observed that cells exhibiting reduced mitotic activity, therefore those entering senescence, were marked by irregularly shaped and sized nuclei (Hayflick et al., 1961). Bodnar et al. showed that the process of cell division and the shortening of telomeres are the mechanisms that lead to senescence. This type of senescence is known as "replicative" senescence (Bodnar et al., 1998). Furthermore, an additional kind of senescence associated with the shortening of telomeres is referred to as “telomere-initiated” senescence. In this instance, the shortening of the telomere is caused by the lack of the T-loop configuration, which typically safeguards the DNA single-strand. In either scenario, cells become senescent and initiate DNA damage response (DDR). Senescence can be triggered also by oncogenes and stress factors. (D'adda et al., 2003; Morgan et al., 2018). Furthermore, when there is heightened oxidative stress resulting from the buildup of impaired mitochondria, the aging process is referred to “senescence associated with mitochondrial dysfunction” (MiDAS)

(Di Micco et al. 2021).
Typically, senescent cells are marked by a gradually flattening form, resistance to programmed cell death, the elevation of senescence-associated-β-galactosidase (SA-β-gal) activity, the existence of nuclear senescence-associated heterochromatic foci (SAHF) and the increase of the cyclin-dependent kinase (CDK) inhibitors p21 and p16 and the tumor suppressor p53. The increased expression of p16 e p21 establishes and maintains the senescence-associated growth arrest (Di Micco et al. 2021; Campisi et al., 2011). Finally, senescent cells remain metabolically active and develop the so called "senescence-associated secretory phenotype (SASP)", consisting in the secretion of pro-inflammatory molecules, such as interleukin-6 and IL-8, enzymes for ECM remodeling, growth factors, and soluble receptors that function in a paracrine way, affect nearby cells changing the microenvironment. Therefore, various markers are used to detect senescent cells, including indicators of apoptosis resistance (e.g. DCR2 and Bcl-xL), secreted factors (e.g. IL-6 and IL- 8), activator of DDR and indicators of cell cycle halt mechanisms (e.g. p16, p21, and p53) (Burton et al., 2014). Senescence yields both positive and negative effects based on the biological con-text (Powers et al., 2009). Particularly, in the early stages of life, senescence is es-sential to maintain adequate embryonic growth. Subsequently, senescence is as-sociated with tumor suppression expansion, and enhances wound healing and tissue repair remodeling following an injury (Powers et al., 2009). In contrast, senescent cells build up as age progresses, resulting in tissue impairment and misguided remodeling, ultimately contributing to age-associated the progression of diseases (Majesky 2007; Koga et al., 2011). Senescence of stem and/or progenitor cells influenced by cardiovascular risk factors or aging hinder tissues, regenerative capacity as well (Powers et al. 2009). The harmful impacts of senescent cells are particularly triggered by the acquisition of the SASP, as this leads to the release of soluble elements that harm the surrounding tissue and affect their function, when it is ongoing or stated. Conversely, localized and time-restricted SASP can heal tissue injury, enhancing the immune removal of the injured cells (Tchkonia et al. 2013). Among SASP elements, is possible to recognize indicators of inflammation and age-associated molecules, like IL-6. Rodondi and colleagues evaluated that this cytokine serves as an inflammation marker and also as a predictor (Rodondi et al., 2010) (Figure 2).

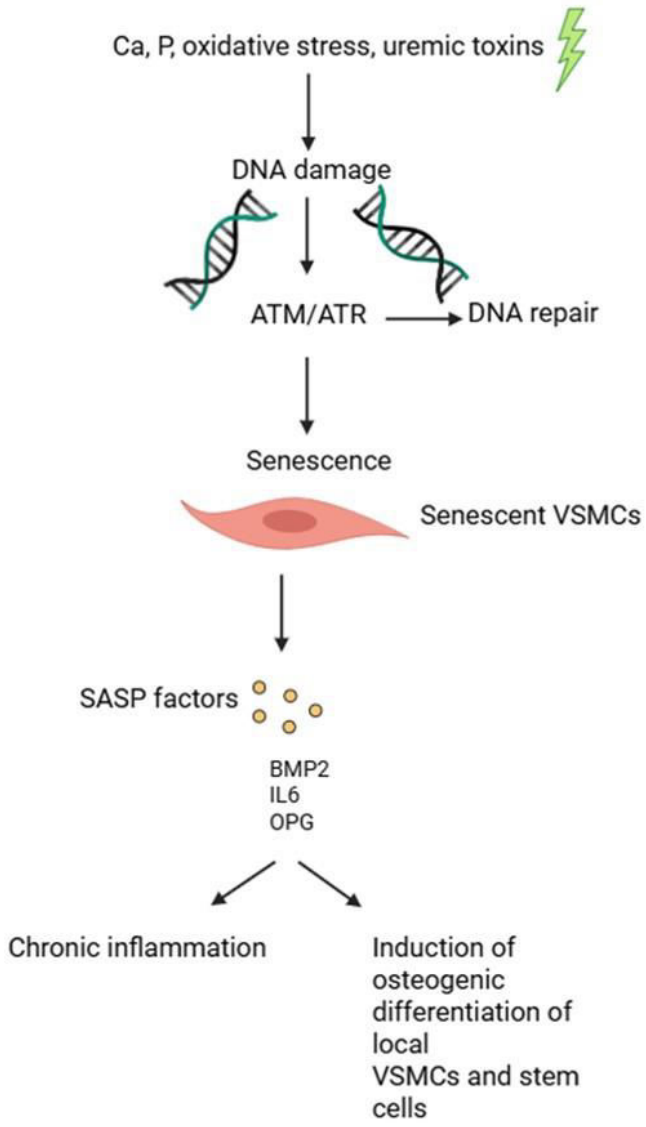

Figure 2. VSMCs senescence induce inflammation and calcification. A permanent DNA damage induces senescence in VSMCs. They release SASP factors such as BMP2, IL-6 and OPG that induce the inflammation and calcification trough the osteogenic differentiation of VSMCs. (Shanahan et al., 2013).

1.4 VSMC senescence

In VSMCs, senescence can be triggered by Angiotensin II (Ang II) and PDGF, transforming growth factor-β (TGF-β), integrin binding partners, oxidative stress, altered calcium and phosphate concentrations and uremic substances. Overproduction of ROS and the stress-related early aging of the VSMCs is a key characteristic of vascular aging (Lacolley et al., 2018). As we age, the external factors (Ang II, PDGF, TGFβ) and integrin ligands trigger a phenotypic change in VSMCs, which involves transitioning from a stable differentiated phenotype to a de-differentiated state with enhanced expansion, movement, and modified production of ECM components. In older ships, senescent VSMCs might adopt an osteo/chondrogenic phenotype and play a role in the induction of persistent inflammation due to their capability to release pro-inflammatory and pro-calcification factors (Badi et al., 2015). Also, microRNAs can influence VSMC senescence and SASP (Badi et al., 2015; Badi et al., 2018). We have reported that miR-34a is a senescence-inducer of VSMCs. miR-34a is upregulated in aged aortas and promotes VSMC senescence through the direct downregulation of the longevity-associated gene SIRT1 (sirtuin 1) and the antiapoptotic receptor tyrosine kinase Axl (AXL receptor tyrosine kinase), and the expression of a subset of SASP factors, including IL-6 (Badi et al., 2015; Badi et al., 2018).

Arterial ageing represents a progressive, multifactorial process that precedes and predisposes to overt cardiovascular disease. Wang et al. in 2010 described how structural and functional changes in the arterial wall accumulate with age, transforming healthy vessels into a pro-inflammatory, pro-fibrotic, and stiffened phenotype. At the cellular level, endothelial dysfunction, oxidative stress, and phenotypic modulation of vascular smooth muscle cells (VSMCs) drive extracellular matrix remodelling, elastin fragmentation, and collagen deposition. The authors introduce the concept of the Age-Associated Arterial Secretory Phenotype (AAASP), in which aged VSMCs lose their contractile properties and adopt a secretory behavior, releasing cytokines, matrix proteins, and calcification-promoting molecules. This active, maladaptive secretory profile contributes to chronic vascular inflammation and arterial stiffening, key features of subclinical arterial disease. Targeting molecular pathways involved in oxidative stress, inflammation, and extracellular matrix turnover may delay arterial ageing and reduce cardiovascular risk in older adults. Arterial ageing could be considered as an active biological process that establishes the substrate for later cardiovascular pathology, highlighting potential therapeutic targets to preserve vascular function with age (Wang et al., 2010).

1.5 Vascular calcification

Vascular calcification (VC) is an age-related pathological process involving the crystallization of hydroxyapatite at the extent of the ECM matrix and inside the cells of

the arterial wall (Schlieper et al. 2016). VC is a complication also associated with atherosclerosis, diabetes, and chronic kidney disease (CKD), which exhibit features of premature aging and low level of systemic chronic inflammation (Schlieper et al., 2016). Vascular wall mineralization alters vessel elasticity and hemodynamics contributing to the increased risk of cardiovascular events in these pathological conditions (Schlieper et al., 2016). Although subjects with VC are high-risk patients, effective pharmacological treatments are not available so far.

At first, VC was considered the result of a passive degenerative process. Nonetheless, recent discoveries indicate that VC is a dynamic and well-coordinated process governed by multiple signaling pathways (K. Boström et al. 1993). There are various types of VC that can be classified in different ways. From an anatomical perspective, VC can arise at the level of the intimal layer, intimal VC (VCi), or at the level of the medial layer, medial VC (VCm). Both procedures are similarly significant from a clinical perspective and occur more frequently in men than in women (Boström et al., 1993). VCi occurs in the intimal layer of blood vessels and is typically linked to atherosclerosis. Atherosclerotic plaques exhibit typical indicators of cellular aging (decreased cell multiplication, DNA damage, telomere degradation, etc.). Additionally, increasing evidence indicates that senescence can enhance it (Alique et al. 2017). Multiple risk factors are recognized to be involved in VCi, including hyperlipidaemia that occurs as a persistent inflammatory condition triggered by lipid build up in the artery wall (Alique et al., 2017). Subsequently, primarily in middle-aged and older individuals, calcification of the atherosclerotic plaque occurs, resulting in clinical symptoms such as angina (if the plaque forms in the coronary arteries) and heart attack, stroke, and ischemia assault (if the carotid is involved), along with claudication and severe limb ischemia (if the plaque interests the outer artery) (Virmani et al. 2000).

VCm is responsible for the degradation of the internal elastic lamina and vessel stiffness, and is associated with diastolic dysfunction and heart failure (Lanzer et al., 2014). It involves a variety of distinct pathological states with several causes such as aging, hyperglycaemia, a condition typical of diabetic patients, and hyperphosphatemia (high levels of inorganic phosphate (Pi) in the blood) and hypercalcemia (high levels of Ca^{2+}) observed in CKD patients (St Hilaire et al. 2011; Boström et al., 2011) (Lanzer et al., 2014).

The onset of VC has been linked to various mechanisms but is primarily a vascular smooth muscle cells (VSMCs) pathology. In response to calcification stimuli, VSMCs endorse a cellular reprogramming by differentiating in osteoblast-like cells characterized by loss of contractile protein expression and upregulation of the specific osteogenic factors, including Runt-related transcription factor 2 (RUNX2), which, in turn, modulate genes involved in bone metabolism and development like alkaline phosphatase (ALP), osteocalcin, and bone morphogenic proteins (BMPs) (Van Varik et al., 2012) (Figure 3).

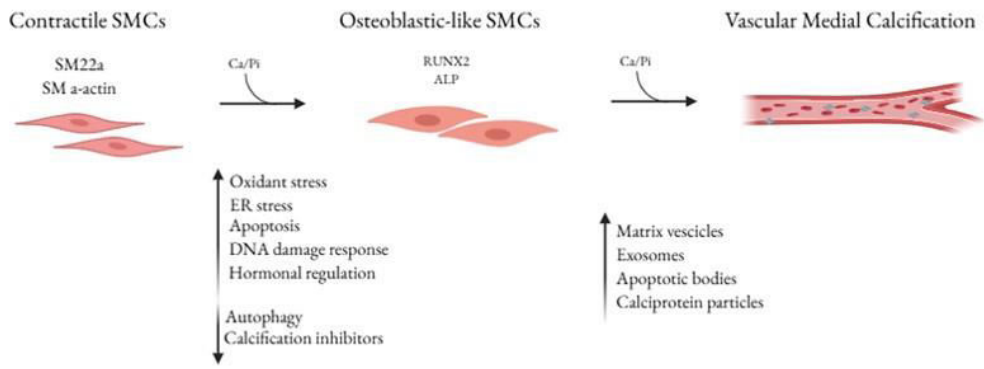

Figure 3. Mechanisms of vascular medial calcification. Contractile VSMCs undergo differentiation to osteoblast-like cells when exposed to high levels of phosphate and other cellular and/or systemic processes that facilitate vascular calcification. These osteoblast-like cells participate in medial vascular calcification. (Leopold et al., 2015).

At first, VC appeared to resemble osteogenesis because of the finding of osteoblast-like BMP-2 expression in calcified human atherosclerotic plaques (Boström et al., 1993). By the time, several evidences highlighted that VC is caused by an increase in the release of specific MMPs and extracellular vesicles (for example, exosomes, microparticles, apoptotic bodies, and matrix vesicles) (Proudfoot et al., 2000) and an unbalance among endogenous inhibitors and inducers of the mineralization process such as matrix-Gla protein (MGP), the extracellular inorganic pyrophosphate (PPi), fetuin A, osteoprotegerin (OPG), and osteopontin (OPN) (Luo et al. 1997; Schafer et al. 2003; Bucay et al. 1998). MGP, originally isolated from bones, reduces VCm through the binding to calcium ions and the inhibition of BMP-2 action in promoting VSMCs osteoblastic differentiation (Luo et al., 1997). Fetuin A, a circulating inhibitor of VCm, is a Ca^{2+}-binding protein produced by the liver and it is found in serum whereas MGP and OPG are local factors implicated in VCm at the site of calcification. VSMCs uptake serum fetuin A and store it in ECM vesicles that are used as pool for mineral nucleation. When they are released from VSMCs, fetuin A binds to calcium and prevents its accumulation (Reynolds et al., 2005). OPN is an acidic phosphoprotein expressed in mineralized tissues able to block hydroxyapatite formation and activates osteoclast function (Bennett et al., 2006). Normally OPN is not present in vessels but it is largely expressed in calcified arteries, suggesting its regulatory function in VCm. OPG is a soluble cytokine that is part of the tumour necrosis factor (TNF) receptor superfamily. It serves as an essential regulator of bone density and acts as a blocker of VCm via its function as a decoy receptor for the Receptor Activator of Nuclear Factor kappa-B ligand (RANKL) (Lacey et al., 1998). Mice lacking OPG experience significant VCm indicating its function as a calcification inhibitor *in*

vivo as well (Bennett et al. 2006). Furthermore, the expression of OPG in osteoblasts is closely controlled by estrogens like estradiol. Specifically, estradiol enhances OPG mRNA transcription, resulting in an increased frequency, more common in men than in women (Jia et al., 2017). PPi originates from the hydrolysis of nucleotide triphosphates, which is catalyzed by nucleotide pyrophosphatase phosphodiesterase family (NPP) which acts as the primary VCm inhibitor because it reduces the development of hydroxyapatite crystals (Harmey et al. 2004). Tissue-nonspecific alkaline phosphatase (TNAP, ALP) plays a crucial role in regulating tissue levels of PPi and calcification. This ectoenzyme breaks down PPi and its deficiency in humans raises plasma PPi levels and leads to impaired bone mineral formation (Lomashvili et al., 2008) (Figure 4). Additionally, PPi can also stabilize the phenotype of VSMCs by inhibiting the cartilaginous metaplasia of VSMCs and their reprogramming into chondrocytes or osteoblast-like cells (Johnson et al. 2004). VSMCs from calcified blood vessels exhibit a variety of bone-associated transcription factors such as Msh homeobox 2 (MSX2) and SRY [sex-determining region Y]-box 9 (SOX9), RUNX2, and Osterix, typical of chondrocytes and osteoblast (Leopold et al., 2015). Pro-calcification stimuli can trigger MSX2 and Wnt signaling, leading to elevated expression of RUNX2 and Osterix (Boström et al., 2011). RUNX2, consequently enhances the expression of bone-associated proteins such as osteocalcin and RANKL. In contrast, Osterix, a downstream element of RUNX2, enhances various proteins associated with PPi metabolism and Ca^{2+} content comprising ALP and bone sialoprotein (Lian et al., 2006; Nakashima et al., 2002). Recently, it has emerged that molecular mechanisms that promote senescence and the acquisition of SASP facilitate the propensity of VSMCs to undergo osteogenic transition (Badi et al., 2018; Zuccolo et al., 2020). Senescent VSMCs express bone-related genes, like Runx2, ALP and osteocalcin that favor the maladaptive differentiation to the osteoblastic phenotype and VC (Badi et al., 2018; Zuccolo et al., 2020).

Our recent work shows that miR-34a is a promoter of senescence-induced VC. Its overexpression in senescent VSMCs promotes osteoblastic differentiation and mineralization. *In vivo*, miR-34a is upregulated before aortas calcification and *Mir34a* deficiency reduces the expression of the VC markers Sox9 and Runx2 and senescence proteins p16 and p21 and, consequently soft tissue and aortic VCm (Badi et al., 2018). Furtheremore, miR-34a is also able to enhance the transcriptional expression of a subset of SASP molecules that promote VSMC mineralization (Badi et al., 2018; Zuccolo et al., 2020).

The mechanism by which VSMCs reprogram their genetic code to switch into osteoblast-like cells remains still poorly understood.

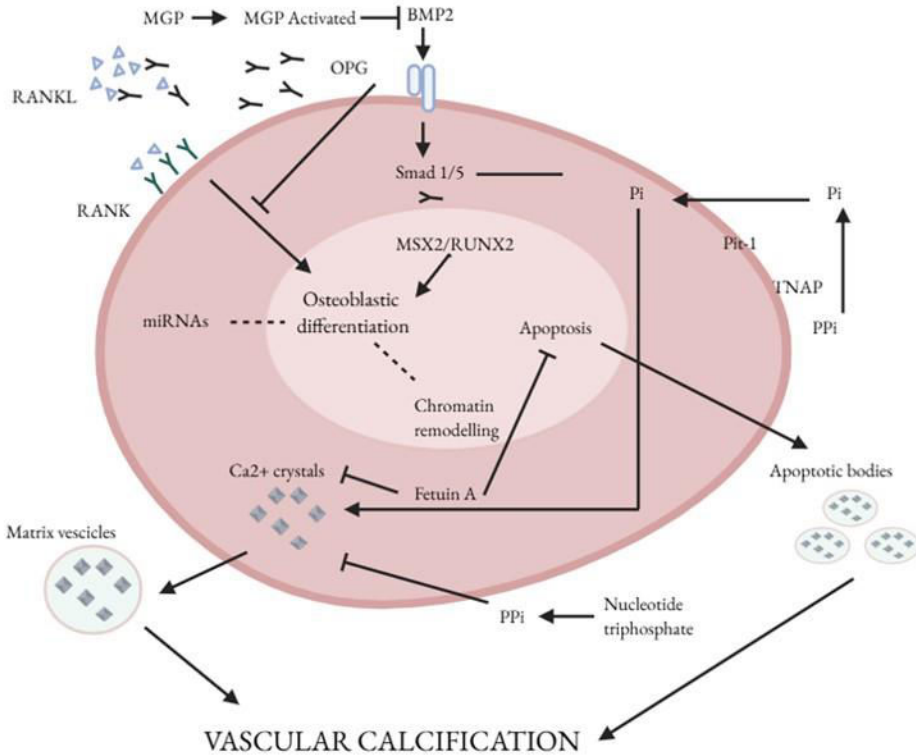

Figure 4. Mechanisms of medial vascular calcification (VC) in vascular smooth muscle cells (VSMCs). Numerous overlapping mechanisms are involved in VC. The main event is the osteoblastic differentiation of VSMCs which can be supported by the MSX2/RUNX-2 axis through the activation of BMP2. Moreover, the unbalance between calcification inhibitors (MGP, OPG, Fetuin-A and extracellular PPi) and promoters (Pi) can encourage VC development.

1.6 Role of inflammation in VC

The causal link between inflammation and VC has been explored but not fully resolved. While atherosclerotic plaque calcification has a strong inflammatory component with infiltration of inflammatory cells, VCm is characterized by the absence of immune cells in the medial layer (Alexander et al., 2021). Significantly, anti-inflammatory treatments can lower cardiovascular (CV) events but do not affect VCi (Alfaddagh et al., 2020). Indeed, statins with anti-inflammatory properties beyond cholesterol reduction, decrease CV risk and accelarate the advancement of coronary artery calcification, which subsequently influences plaque stability (Lee et al., 2019; Puri et al., 2015). Multiple studies indicate that the activation of VSMCs with certain inflammatory substances initiate calcification. For example, IL-8 increases the uraemic toxins-triggered HASMC calcification by inhibiting the production of OPN (Bouabdallah et al., 2019) and IL-29 enhances calcification in rat VSMCs induced by elevated Pi levels (Hao et al., 2023). Conversely, our group and others have demonstrated that IL-6 alone is inadequate to affect HASMC calcification in hyperphosphatemia conditions (Zuccolo et al., 2020; Kurozumi et al., 2019).

We recently demonstrated that HASMC calcification, induced by elevated concentrations of Pi, is associated with the onset of an inflammatory secretory phenotype consisting of the release of IL-6, IL-8, MCP-1, and the calcification inhibitor OPG under the control of the JAK-STAT pathway. A JAK inhibitor reduced HASMC proliferation and enhanced VSMC calcification *in vitro* and in murine aortic rings along with higher RUNX2 expression and lower OPG levels (Macrì et al., 2023). Thereby, it is likely that the JAK-STAT pathway establishes a protective inflammatory condition which diminishes VSMC pathogenic differentiation emphasizing a different connection between inflammation and VCm.

Further investigation are necessary to highlight the relationship between inflammation and VC.

2. HIGH MOBILITY GROUP BOX 1

High Mobility Group Box 1 (HMGB1) is a non-histone chromatin binding protein and it belongs to the HMGB family, which also comprises HMGB2 and HMGB3. Together, they belong to the HMG (high mobility group) family and contain an 80 amino acids region that enables binding to the minor groove of DNA with minimal or no sequence specificity (Bustin et al., 2001; Bianchi et al., 2005). HMGB1 has a molecular mass of roughly 25 KDa and comprises 215 amino acids arranged into a negatively charged residue (30 aspartate and glutamate residues) at the C-terminus along with two DNA-binding domains that carry a positive charge, referred to as box A and box B at the N-terminus (Štros et al., 2010; Bianchi et al., 1992). It also includes two nuclear localization signals (NLS1 e NLS2) and two nuclear export signals (NESs) (Bonaldi et al., 2003). These two signals, along with post-translational modification,

facilitate localization both intracellularly (nucleus and cytoplasm) and extracellularly; however, HMGB1 is primarily situated within the nucleus. The movement from the nucleus to the cytoplasm is facilitated through the acetylation of NLS lysines (Bonaldi et al., 2003). HMGB1 is expressed throughout the body. Additionally, HMGB1 is preserved in eukaryotic cells (Klune et al., 2008) and exists in non-mammalian organisms, including yeasts and Drosophila Melanogaster (Bianchi et al., 2005). These characteristics indicate that HMGB1 is essential for living beings and survival after birth. Calogero et al. have demonstrated that the removal of HMGB1 causes mortality in mice 24 hours post-birth (Calogero et al., 1999).

HMGB1 is a component of the damage-associated molecular pattern (DAMP) molecules, additionally referred to as “alarmins”, extracellular proteins that are recognized for triggering a swift inflammatory reaction. HMGB1 is actively secreted by macrophages in response to infectious or sterile triggers after activation of inflammasomes, and passively from necrotic cells. Consequently, HMGB1 may be regarded as an initial indicator of localized or systemic inflammation in various inflammatory conditions. Upon being released in the extracellular environment, it promotes tissue repair or inflammation through binding to receptor for advanced glycation end-products (RAGE), Toll-like receptor (TLR) 2 and 4 (Bertheloot et al., 2017; Harris et al., 2006; Colavita et al., 2020). Consequently, HMGB1 performs various functions based on its cellular localization: at nuclear level, it preserves the configuration of the nucleosome and it controls DNA replication, transcription, recombination, and repair (Bianchi et al., 2005); at cytoplasmic level, it controls autophagy, apoptosis, inflammation and it induces a pro-calcification effect (Müller et al., 2004; Chen et al., 2017); at extracellular level, it plays a role in tissue inflammation, regeneration, and remodeling including bone remodeling and abnormal calcification (Chen et al., 2017; Raucci et al., 2019) (Figure 5).

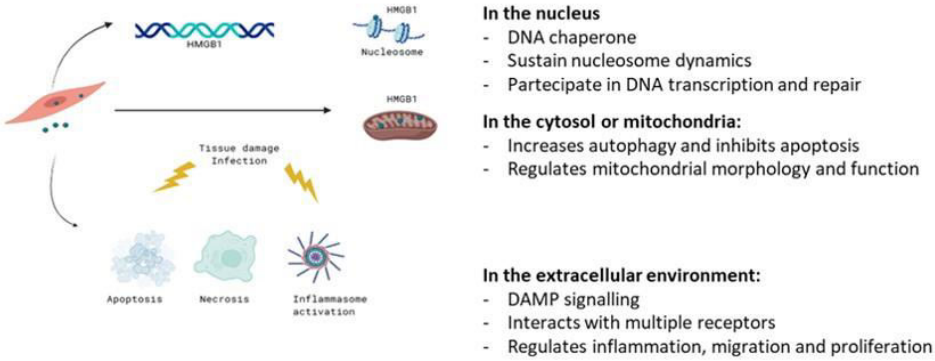

Figure 5. Functions of HMGB1. HMGB1 has many roles depending on its cellular localization. In the nucleus HMGB1 binds to the minor groove of DNA in a no – sequence specific manner, regulating chromatin structure, gene expression and gene transcription; in the cytosol HMGB1 has been showing to regulate cellular autophagy and apoptosis during inflammation and also it partecipates in mitochondrial functions. In the extracellular space HMGB1 functions as a DAMP and regulates tissue inflammation and regeneration during an injury depending on its redox state.

2.1 Nuclear roles of HMGB1

Within the nucleus, HMGB1 binds the minor groove of DNA in a non specific manner, controlling chromatin architecture, gene transcription, and gene expression (Agresti et al., 2003). Evidence showed that HMGB1 additionally associates with higher affinity to twisted and relaxed non-B-type DNA formations (Iacomino et al., 2016). Interestingly, HMGB1 can engage with fresh nucleosomes each second while scanning the DNA searching for the appropriate binding site (Iacomino et al., 2016). Other interactors could influence HMGB1- DNA correlation. For example, nuclear aggregates of polyamines (NAPs) create complexes using DNA to facilitate the conformational alterations of the double helix and to safeguard DNA integrity and regulate DNA-protein interactions; thus, they play a direct role in the dynamic simulation of chromatin (Iacomino et al., 2016). It has been suggested that NAPs play a crucial role in the packaging of DNA into chromatin (Iacomino et al. 2016).p
HMGB1 functions as a chaperone facilitating the assembly of nucleosomes (Celona et al., 2011). Thus, mammalian cells that do not have HMGB1 exhibit a reduced quantity of nucleosomes because of a reduced count of histones. Hmgb1 knockout ($Hmgb1^{-/-}$) mouse embryonic fibroblasts contain approximately 20% fewer total histones (Celona et al., 2011). Alterations in nucleosomes number and depletion of histones can lead to increased genomic instability and sensitivity to DNA-damaging substances due to the heightened exposure of DNA to harmful agents, such as hydroxyl free radicals (Hu et al., 2014). Consequently, the absence of HMGB1 is linked to age-related nuclear defects. Additionally, the reduction of nucleosomes does not

affect their spacing or positioning, but decreases occupancy that indicates an increase in transcript levels, implying that transcription relies on the accessibility of DNA regulated by nucleosomes (Celona et al., 2011). The release of HMGB1 in response to inflammatory stimuli decreases the histone levels in macrophages (De Toma et al., 2014). In activated macrophages, HMGB1 is released from the nuclear pool (Bonaldi et al., 2003) and the loss of HMGB1 hinders macrophages' response to inflammation (De Toma et al., 2014). Collectively, this shows that the secretion of HMGB1 by activated macrophages results in chromatin alterations resulting from the loss of nucleosomes and histones, which subsequently influences and controls the inflammatory reaction (De Toma et al., 2014).
As a nuclear factor, HMGB1 has several additional functions. It assists the enhanceosome assembly, stabilizes nucleoprotein complexes and is involved in chromatin renovation and gene transcription through the modulation of various DNA-binding factor activities (Lotze et al. 2005). For example, HMGB1 plays a crucial role in the V(D)J recombinase assembly (Little et al., 2013). Additionally, HMGB1 is capable of attaching to various members of the tumor suppressor gene p53 family to boost their binding to Bax and Mdm2 promoters (Stros et al., 2002). Other functions of HMGB1 are associated with histone H1 which contend identical DNA binding configurations (curved DNA, supercoiled DNA) (Thomas et al., 2012). The displacement of histone H1 by HMGB1 may lead to chromatin destabilization and the attraction of additional factors and transcriptional stimulation (Polanská et al., 2014).

2.2 Extracellular roles of HMGB1

The initial proof of an extracellular role for HMGB1 originates from Wang et al. who first described HMGB1 released by murine macrophage-like RAW 264.7 cells following stimulation with lipopolisaccaride (LPS), acting as a late mediator of endotoxemia (Wang et al., 1999). Importantly, the neutralization of HMGB1 using an anti-HMGB1 antibody enhanced survival rate of LPS-treated mice (Wang et al., 1999). As previously stated, upon stress or danger stimuli, HMGB1 is released into the extracellular environment where it functions as a DAMP (Harris et al., 2006). Thus, it has the ability to stimulate both innate and acquired immunological defense, enhance tissue healing, activate monocytes/macrophages and dendritic cells, and induce fibroblast, EC and VSMCs migration (Treutiger et al., 2003). The suppression of extracellular HMGB1 reduces inflammation and provides defense in various animal models of trial diseases including ischemia/reperfusion injury of the heart and liver, diabetes, autoimmune disorders and epilepsy (Andrassy et al., 2008; Wang et al., 2014; Ulloa et al., 2003; Maroso et al., 2010)
This pleiotropic effect relies on HMGB1's sensitivity to the surroundings oxidizing environments that trigger redox post-translational modifications. Depending on the redox state of 3 cysteine residues, several redox forms of HMGB1 may exist. The

first one is the completely reduced HMGB1 (fr-HMGB1) where all cysteines are in a reduced state; the second one is the disulfide HMGB1 (ds-HMGB1) where C23 and C45 are partially oxidized to create a disulphide bond, whereas the unpaired C106 is reduced. The third variant is the sulfonyl HMGB1 (ox-HMGB1) where all cysteines have undergone oxidation (Venereau et al., 2012). Fr-HMGB1 has chemotactic effects and encourages polarization of macrophages into a regenerative phenotype (Venereau et al., 2012). Ds-HMGB1 promotes the generation of proinflammatory cytokines and chemokines within immune cells and the development of new blood vessels in endothelial cells (Venereau et al., 2012). Ox-HMGB1 could influence the activation of neutrophils (Maugeri et al., 2014).
Moreover, the diverse functions of HMGB1 depend on the ability of redox variants to bind to different receptors, individually or in heterocomplex with additional ligands (Tsung et al., 2014). The receptors that have been studied the most extensively are RAGE, TLR2-4 and CXCR4 (Tsung et al., 2014). RAGE is a membrane-spanning receptor for advanced glycation end-products (AGEs). The RAGE-HMGB1 pathway is implicated in various diseases, including cancer and inflammation (Tirone et al., 2018). Every redox state of HMGB1 engages with RAGE, ds-HMGB1 interacts with greater affinity (Tirone et al., 2018). TLRs are a group of transmembrane proteins that play a role in the defense of the host and possess comparable structure yet vary in their subcellular positioning and ligands (Leifer et al., 2016). TLR2 and TLR4 engage with HMGB1, resulting in nuclear translocation of NF-κB and the production of pro-inflammatory cytokines in macrophages and neutrophils (Park et al., 2004). The TLR2/HMGB1 pathway is recognized for enhancing natural killer (NK) and activation of cancer stem cells (Conti et al., 2013). CXCR4 serves as a receptor for SDF-1/CXCL12, a significant chemotactic trigger for leukocytes. (Hummel et al., 2014). Fr-HMGB1 creates a heterocomplex with CXCL12 which safeguards CXCL12 from being broken down and enhances migration mediated by CXCR4 in mouse embryonic fibroblasts (MEFs), human cardiac fibroblasts (hcFbs), macrophages, dendritic cells, and my-oblasts (Venereau et al., 2012). Hence, extracellular HMGB1 experiences gradual redox alterations necessary to start, control, and settle the inflammatory reaction. These changes are also essential for coordinating tissue repair and regeneration via the identification of various receptors and interactors.

2.3 HMGB1 and senescence

Cellular senescence results from the shortening of telomeres and the induction of DNA damages (Calcinotto et al., 2019). Considering that HMGB1 is involved in DNA repair, it is evident that it can also contribute to senescence and organismal aging. Enokido and colleagues studied the function of HMGB1 in the aging of the brain. They discovered that HMGB1 levels diminish with advancing age in the nuclei of neurons and in astrocytes, resulting in a rise of DNA double-strand breaks and cellular harm (Enokido et al., 2008). Lately, it has been suggested that nuclear HMGB1

levels associates with changes in cell proliferation potency (Yasom et al., 2022). Notably, HMGB1 is depleted from the nuclei of some primary cells approaching senescence and it is re-localized to the extracellular environment to trigger proinflammatory gene activation and the acquisition of a SASP (Sofiadis et al., 2021, Davalos et al., 2013). Moreover, nuclear HMGB1 engages with a specific subset of topologically associating domains (TADs) and active chromatin loci relevant for the induction of the senescence gene expression program and its loss is causal for cell cycle arrest and senescence entry (Sofiadis et al., 2021). Davalos et al. showed that both reduction and overexpression of HMGB1 promotes senescence in MEFs and Human Mammary Epithelial Cells (HMECs), due to the activation of p53 (Davalos et al., 2013). HMGB1 released by senescent cells and after binding to RAGE and TLRs receptors, triggers the expression of cytokines that promote inflammation, like IL-6 (Davalos et al., 2013). Furthermore, extracellular HMGB1 activates the immune response and triggers SASP-driven paracrine senescence (Di Micco et al., 2021). It has been suggested that since senescent cells secrete HMGB1, loss of intracellular HMGB1 may be considered an additional marker of senescence (Davalos et al., 2013; Stojanovic et al., 2020; Sofiadis et al., 2021). Thereby, HMGB1 could invoke various roles during senescence. It has been demonstrated that HMGB1 expression decreases in human coronary smooth muscle cells undergoing senescence (Sofiadis et al., 2021), however, the consequences of nuclear reduction of HMGB1 in VSMC senescence and calcification as well as medial VC has never been investigated.

2.3 HMGB1 and calcification

HMGB1 is essential in both pathological and nonpathological calcification processes. Specifically, HMGB1 is found in the nucleus of human dental pulp cells (hDPCs) and throughout odontoblastic differentiation it moves into the cytoplasm. Extracellular HMGB1 stimulates the development of mineral nodules (Qi et al., 2013). It has been shown that HMGB1 is engaged in the onset of calcification in several disorders, including diabetes, calcific aortic valve disease (CAVD), and CKD. In CAVD, extracellular HMGB1 promotes the osteoblastic differentiation of aortic valve interstitial cells (AVICs) through interaction with TLR4, resulting in expression of genes associated with bone formation (Shen et al., 2017). Jin et al. showed that in CKD patients, cytosolic HMGB1 levels are elevated due to the higher phosphate levels that causes HMGB1 movement from the nucleus into the cytosol of aortic cells in CDK models. They showed that the silencing of HMGB1 improved kidney and vascular function, also improving some aspects of renal function. HMGB1 promotes the calcification of the aorta in CKD via the stimulation of β-catenin (Jin et al., 2018). Wang et al. revealed that elevated glucose concentration leads to HMGB1 relocation from the nucleus to the cytosol, triggers the expression of TLR2, TLR4, and RAGE and stimulates NFkB. They have additionally shown that *in vitro*, in conditions of high glucose

and HMGB1 silencing there is an absence of intracellular calcium accumulation (Wang et al., 2013). Additionally, extracellular HMGB1 enhances the expression of RUNX2, OPN and BMP-2 and controls chondrocyte activity and maturation, osteoblast differentiation and promotes migration of macrophages into calcified nodules (Chen et al., 2017). HMGB1 also promotes the secretion of matrix vesicles from macrophages, *in vivo* and *in vitro* via RAGE/p38/nSMase2 signaling (Chen et al. 2016). Some evidences show that degradation of HMGB1 inhibits pathological calcification. Zhang et al. identified the protein Lethal Giant Larve (LGL1), the lack of which encourages aggravation of high phosphate-triggered calcification in VSMCs through enhancing the breakdown of HMGB1 through the lysosomal route (Zhang et al., 2020). HMGB1 is involved in inflammation associated to calcification acting as an inflammatory cytokine. During inflammation, levels of expression HMGB1 increase, promoting vascular calcification. Moreover, oxidative stress and generation of ROS can trigger VC *via* HMGB1. Elevated ROS levels, found near calcified foci, facilitate osteochondrogenic processes and differentiation of different cell types, including VSMCs and pericytes, by prompting the expression of osteogenic genes via TNF-α release, which subsequently modulates HMGB1 release (Chen et al., 2017; Al-Aly et al., 2011).

In contrast to published evidences on the involvement of extracellular HMGB1 in VC, the specific role of nuclear HMGB1 functions to VS and VC remains unexplored.

3. PRELIMINARY RESULTS

Our preliminary results show that HMGB1 levels decrease during vascular aging and in senescent VSMCs. In particular, we found that aortas isolated from 21-month-old (Old) C57BL6 male mice displayed a significant reduction of HMGB1 protein levels compared with aortas of 2.5-month-old (Young) animals (Figure 6A). Accordingly, senescent human aortic smooth muscle cells (HASMCs) isolated from donors of different age (22, 30, 43 years) displayed a reduction in both mRNA and protein HMGB1 expression compared to replicative cells while no translocation to the cytosol was observed (Figure 6B-D). We also found that lower HMGB1 levels promote senescence-like alterations in HASMCs. We silenced HMGB1 in HASMCs generating shB1/HASMCs and control shCTR/HASMCs and cultured both clones to obtain proliferative (P8) and senescent (P15) cells. HMGB1 was reduced during replicative senescence and after silencing in both P8 and P15 shB1/HASMCs compared to corresponding shCTR/HASMCs (Figure 7A). Similar expression was observed for extracellular HMGB1 (Figure 7B). Interestingly, HASMCs silenced for HMGB1 (shB1/HASMCs) exhibited bigger nuclear size (nucleomegaly) (Figure 7C-D) and lower proliferation in comparison with matched control cells (shCTR/HASMCs) (Figure 7F-G). Notably, we also observed an inverse correlation between HMGB1 nuclear content and the nuclei area (Figure 7E). Overall, P8 shB1/HASMCs shows similar features of P15 shCTR/HASMCs.

Altogether, these data indicate that reduced nuclear HMGB1 content promotes VSMC senescence and may play a role in senescence-induced VSMC mineralization and VC.

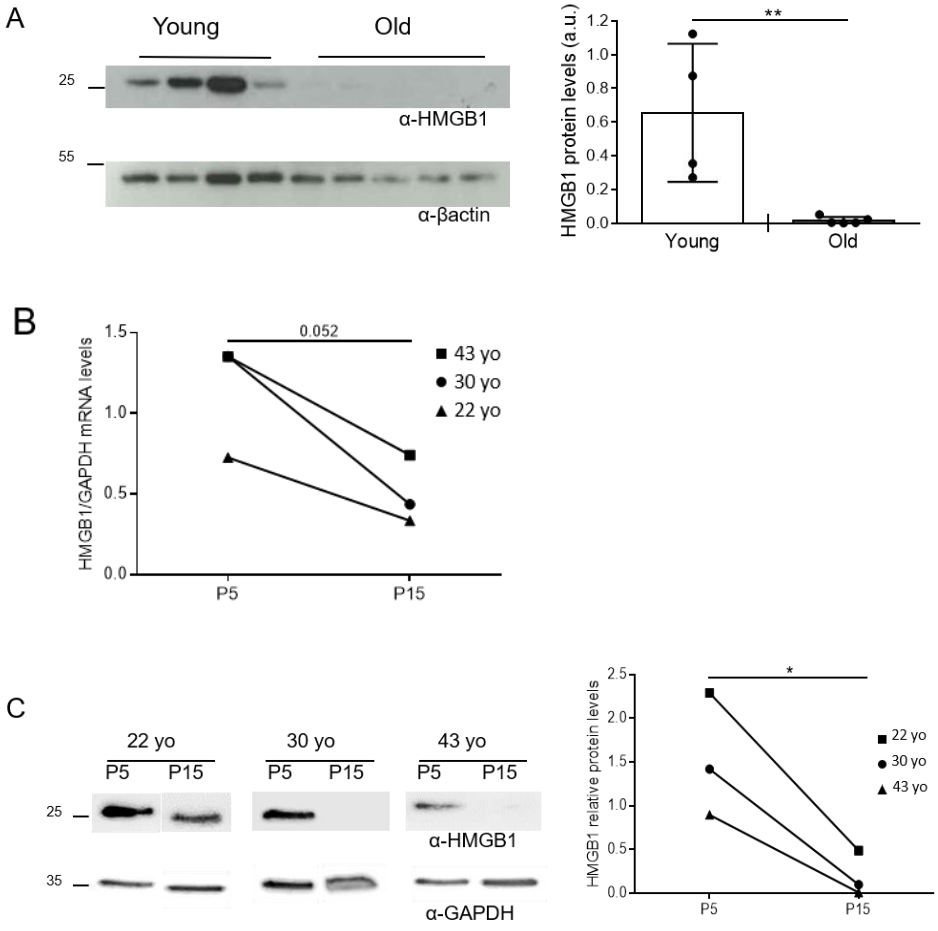

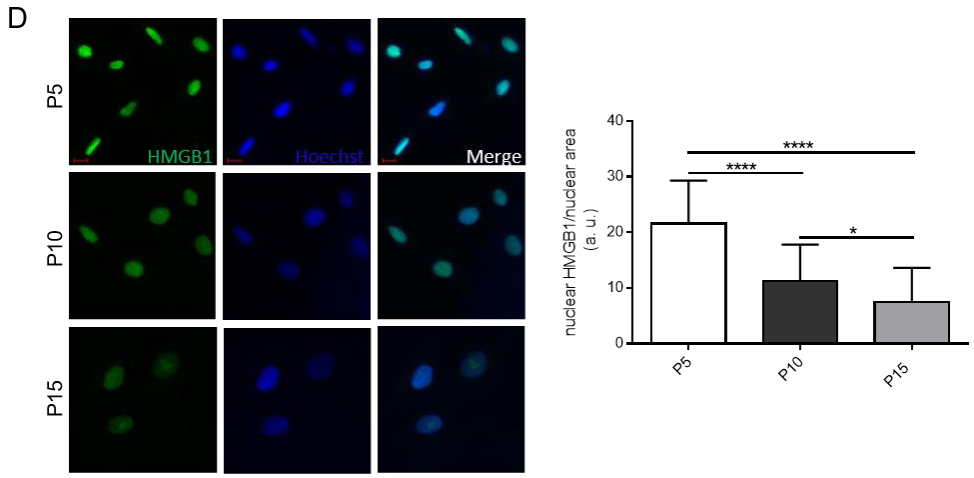

Figure 6. HMGB1 decreases during vascular aging and in senescent VSMCs. (A) (Left panel) Western blot images showing HMGB1 protein levels in the aortas of Young (2.5 months-old) and Old (21 months-old) male mice; β-actin was used as loading control. (Right panel) Quantification of HMGB1 expression. Student's t-test; *p < 0.05; P5 n = 3, P15 n = 3. **(B)** HMGB1 mRNA expression normalized on GAPDH levels in proliferative Young (P5) and senescent Old (P15) human aortic smooth muscle cells (HASMCs) isolated from donors of different ages (22-30-43 years old (yo)). Student's t-test; P5 n=3, P15 n=3. **(C) (**Left panel) Western blot showing HMGB1 protein levels in P5 and P15 HASMCs isolated from donors at different ages (22-30-43 years old (yo); GAPDH was used as loading control. (Right panel). Quantification of HMGB1 expression. Student's t-test; *p<0.05; P5 n=3, P15 n=3. **(D)** (Left panel) Representative immunofluorescence images showing HMGB1 protein levels (green) in HASMCs isolated from a 43 years-old donor at the indicated passages (P). Nuclei were stained with Hoechst (blue); scale bar: 10µm. (Right panels) Quantification of nuclear HMGB1 signal/nuclear area. Bars show

values mean ± SD; 1-way ANOVA plus Bonferroni post-hoc test; *p < 0.05, ****p < 0.0001; number of cells n=41-46.

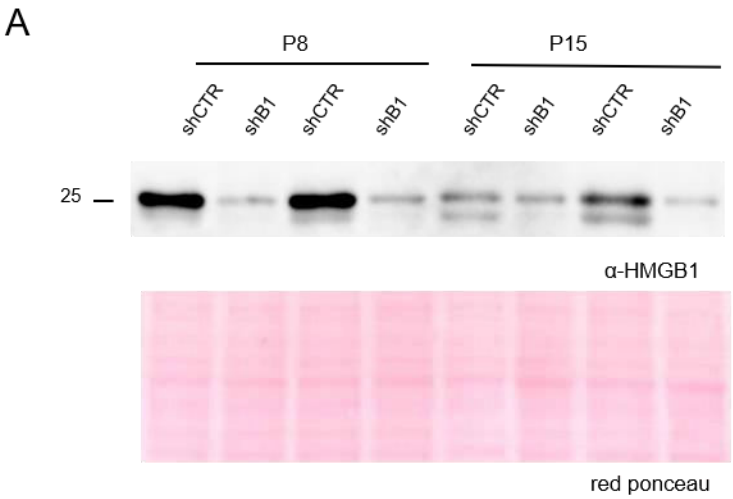

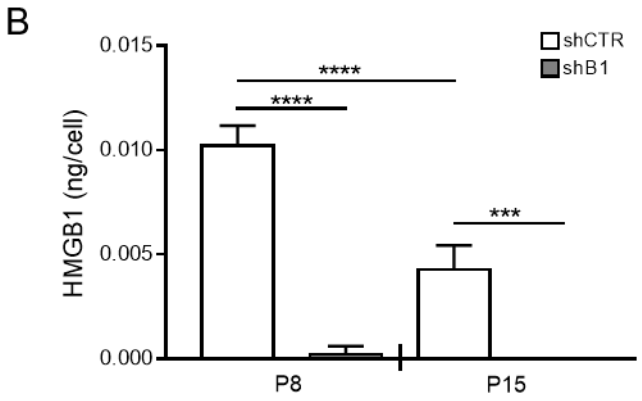

C

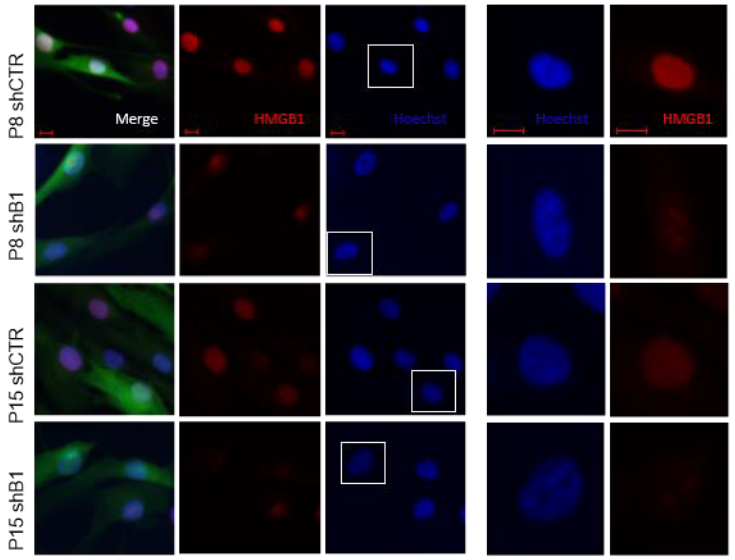
P8 shCTR
P8 shB1
P15 shCTR
P15 shB1
Merge
HMGB1
Hoechst
Hoechst
HMGB1

D

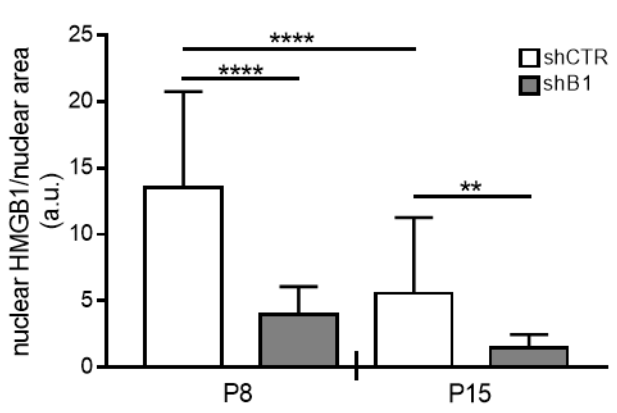
nuclear HMGB1/nuclear area (a.u.)
25
20
15
10
5
0
****
****
**
shCTR
shB1
P8
P15

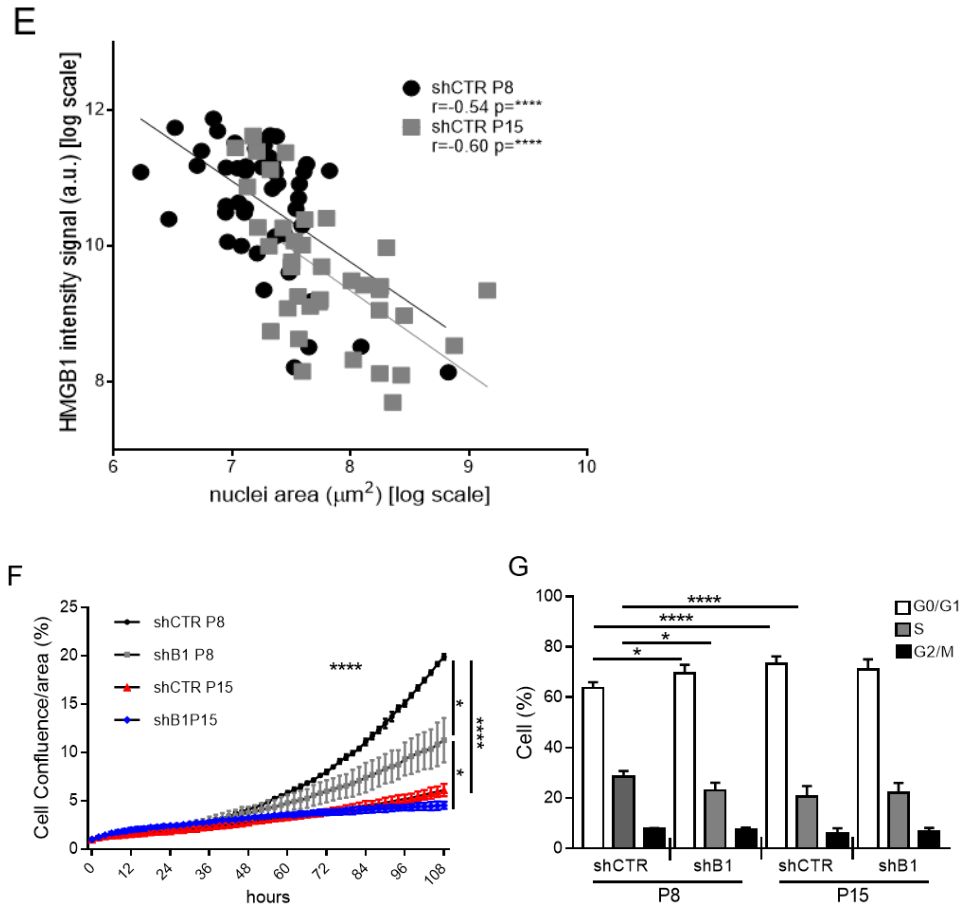

Figure 7. Generation and characterization of HASMCs silenced for HMGB1. (A) Western blot for HMGB1 on P8 and P15 shB1/HASMCs and shCTR/HASMCs. Red ponceau staining was used as loading control. **(B)** Extracellular HMGB1 secreted by P8 and P15 shCTR/HASMCs a and shB1/HASMCs after 48 hours of culturing and determined by ELISA. Bars show values as mean ± SD; 1-way ANOVA plus Bonferroni post-hoc test; **p < 0.01, ****p < 0.0001; n=3. **(C)** Representative immunofluorescence images of P8 and P15 shCTR/HASMCs and shB1/HASMCs expressing GFP (Merge) and labeled for HMGB1 (red). Nuclei were stained with Hoechst (blue); scale bars: 10μm. **(D)** Quantification of nuclear HMGB1 relative to panel C. Bars show values as mean ± SD; 1-way ANOVA plus Bonferroni post-hoc test; **p < 0.01, ****p < 0.0001; number of cells = 27-37. **(E)** Correlation analysis between HMGB1 content and nuclear size of P8 (n = 48 cells, black circle) and P15 (n = 37 cells, gray square) shCTR/HASMCs showed in panel C (log scale). Pearson test. **(F)** Proliferation analysis of indicated HASMCs clones. Graph represents the percentage of cell confluence per area during time. Indicated significance among different clones refers at 96 hours; 1-way ANOVA plus Bonferroni post-hoc test; *p < 0.05, ****p < 0.0001; n=3. **(G)** Cell cycle analysis by FACS of P8 and P15 shCTR/HASMCs and shB1/HASMCs after 48 hours of culture. Bars show values as mean ± SD; 1-way ANOVA plus Bonferroni post-hoc test; *p < 0.05, ****p < 0.0001; P8 n = 6, P15 n = 10.

4. AIMS

Based on our preliminary data, we hypothesized that vascular HMGB1 decline induced by aging affects VC by promoting senescence and the acquisition of SASP in VSMCs that, in turn, facilitate the trans-differentiation to an osteogenic phenotype in pro-calcification conditions.

In order to achieve our goal, we took advantage of *in vitro* and *in vivo* approaches with the following aims:

Aim 1: Investigation of HMGB1 role in VSMCs senescence and osteoblastic trans-differentiation *in vitro*.

Aim 2: Assessment of HMGB1-dependent transcriptional changes during VSMCs mineralization.

Aim 3: Assessment of HMGB1 role in VS and VC in preclinical animal model and in human specimens.

5. MATHERIALS AND METHODS

5.1 Human aortic smooth muscle cells culture

Human aortic smooth muscle cells (HASMCs) were purchased from Lonza (Basel, Switzerland) and cultured in SmGM-2 Basal Medium (#CC-3182, Lonza). The donors were Caucasian males of 22, 30 and 43 years. Replicative senescence was induced by keeping cells in culture and splitting them repeatedly after reaching 90% confluence until they stop proliferating. Low-passage cells (P5-P9) with normal growth rate were defined as "Young", while low-proliferative/senescent cells (P12-15) as "Old".

5.2 Generation of HASMCs silenced for HMGB1

HASMCs isolated from the 22-year-old donor were used for silencing experiments. Human embryonic kidney HEK293T cells, cultured in DMEM (#LOBE12604, Lonza) supplemented with 10% fetal bovine serum (#10270106, Thermo Fisher Scientific, Waltham, Massachussets, US), 100U/mL penicillin, 100U/mL streptomycin (Penicillin-Streptomycin (5,000 U/mL; #1507006, Thermo Fisher Scientific) L-Glutamine (#LOBE17605E, Lonza) were used for virus production. Two hours before transfection, the medium was changed with IMDM (#21980032, Thermo Fisher Scientific) supplemented with 10% FBS, penicillin 100U/mL, streptomycin 100U/mL, and L-glutamine. HEK293T cells ($9x10^6$) were transfected with the packaging plasmids and the lentivirus vectors carrying short hairpin for human HMGB1(shHMGB1 Dharmacon™ GIPZ™ Lentiviral shRNA, #RHS4531, GE Healthcare, Chicago, Illinois, US) or short hairpin control (shCNTRL Dharmacon™ GIPZ™ Lentiviral shRNA, # FE6RHS4351, GE Healthcare) along with Green Fluorescence Protein (GFP) using calcium/phosphate method.
Twenty-two years-old donor P3-P4 HASMCs were seeded in a 6-well plate ($2.1x10^4$ cells/cm^2) and transduced in SmGM-2 Basal Medium with lentivirus carrying pGIPZ-shHMGB1 (shB1/HASMCs) or pGIPZ-shCNTRL (shCTR/HASMCs) using a multiplicity of infection (MOI) = 20. After 24 hours, the medium was replaced with a complete SmGM-2 Basal Medium containing puromycin (1μg/mL) for at least 4 days to select infected cells. All experiments involving "Young" shB1/HASMCs and shCTR/HASMCs were conducted at P8. To generate "Old" shB1/HASMCs and shCTR/HASMCs, P8 shB1/HASMCs and shCTR/HASMCs were cultured until reaching passage P15.

5.3 Western Blot

HASMCs ($1x10^5$) were lysed in RIPA buffer (10 mM Tris pH 7.4, 100 mM NaCl, 1 mM EDTA, 1 mM EGTA, 1% Triton X-100, 10% glycerol, 0.1% SDS, 0.5% deoxycholate) in presence of phoshatase inhibitors (PhosSTOP™; #04906837001; Sigma-Aldrich) and protease inhibitor cocktail (#P8849; Sigma-Aldrich). Nitrocellulose membranes were stained with red ponceau (#P7170, Sigma-Aldrich) e and then incubated with different antibodies. Proteins were visualized by ECL Western Blotting Detection Reagents ClarityTM or Clarity MaxTM Western ECL substrate (#170-5060, 170-5062, Biorad, Hercules, CA, US). Images were acquired with ChemiDoc™ MP Imaging System (Bio-Rad) and densitometric analysis was performed using ImageJ. Red ponceau is used like equal loading to normalize protein expression density because we found that housekeeping protein like GAPDH and a-actin are modulated in shHMGB1 cells.

5.4 Quantitative RT-PCR (q-RT-PCR)

For HASMCs, the total RNA was extracted using Illustra RNAspin Mini RNA Isolation Kit reagent (#25 0500-72, GE Healthcare) following the manufacturer's protocol. cDNA was synthesized with iScript™ Reverse Transcription Supermix for RT-qPCR (#1708841BUN, Bio-Rad). qRT-PCR was performed on a Bio-Rad C1000 Touch™ Thermal Cycler with CFX 96™ Real-Time PCR Detection System using the iTaq Universal SYBR® Green Supermix (#1725124, Bio-Rad). Relative gene expression levels were determined using the 2 method and *GAPDH* or *UBC* and *ZNF* levels as reference genes.

5.5 Senescence-associated β-galactosidase (SA-β-gal) staining

Senescence was assessed with the SA-β-gal staining kit (Cell Signaling Technology, Danvers, MA, US) following the manufacturer's protocol. Briefly, $5x10^3$ cells were seeded in a 24 well plate and cultured for 72 hours. After washing in PBS, cells were fixed for 10 minutes at room temperature and then treated with a staining solution containing the substrate X-gal was added and incubated overnight at 37°C in a dry incubator. Images of ten random fields were acquired using a Zeiss Axiovert 200M microscope equipped with a HITACHI HV-D30 Compact 3-CCD Camera (Zeiss). Percentage of SA-β-gal-positive cells was calculated as the fraction of SA-β-gal-positive staining to the total number of cells multiply by one hundred.

5.6 Cell proliferation assay

HASMCs were seeded in a 96-well plate ($7x10^3$ cells/cm^2) and cultured in SmGM-2 Basal Medium with the addition of the IncuCyte® NucLight Rapid Red Reagent for Cell Labeling (#4717, Essen BioScience, Ann Arbor, Michigan, US). The growth was evaluated for 108 hours and the images were acquired every 2 hours with IncuCyte®S3 System (Essen Instruments, Ann Arbor, MI, US). Growth curves were extrapolated automatically from data points acquired during round-the-clock kinetic imaging considering cell confluence obtained by red nuclei object count/image normalized to h "0".

5.7 ELISA assay

Supernatant from $1x10^5$ HASMCs was collected. ELISA kits specific for different cytokines were used to test the extracellular levels of these proteins following manufacturer's instruction. The absorbance at 450nm was read by using a spectrophotometer (Infinite® M200 PRO- TECAN). Finally, cytokines concentration was normalized to the number of cells (pg/mL/number of cells).

5.8 Calcification assay for cells

5.8.1 Colorimetric Assay

HASMCs ($5x10^4$) were seeded in a 24 well-plate and after 6-8 hours growth medium was replaced with calcification medium (DMEM supplemented with 15% FBS, 5 mM phosphate, 10 mM sodium pyruvate and 50ug/mL ascorbic acid) and further cultured for 3, 7 and 11 days. The calcification medium was replaced every 2 days. Calcium was quantified by colorimetric analysis with the QuantiChrom™ Calcium Assay Kit Kit (#DICA-500, Gentaur, Kampenhout, Belgium) following manufacturer's instructions. In order to extract protein for normalization, cells were washed with PBS and incubated overnight at 4°C with 250µL of 0.1% SDS-0.1 N NaOH lysis buffer. Protein concentration was determined with the Bio-Rad protein assay (Bio-Rad Laboratories, Hercules, CA, US). Calcium content was expressed as µg of calcium/µg of protein.

5.8.2 Alizarin red staining

The staining was performed with Alizarin Red S Staining Quantification Assay (#8678, ScienCell, San Diego, California, US) according to the manufacturer's protocol. Briefly, HASMCs cultured in osteogenic media were washed with PBS and fixed with 4% PFA. Alizarin red S (40mM) was added and incubated for 30 minutes at room temperature with gentle shaking. Then, cells were washed with H_2O and images were acquired with a Zeiss Axiovert 200M microscope equipped with a HITACHI HV-D30 Compact 3-CCD Camera (Zeiss).

5.9 Label-free quantitative mass spectrometry (LC-MSE) analysis

For secretome analysis of the supernatant of HASMCs/shHMGB1 or HASMCs/shCTRL, $1x10^5$ cells were seeded into 100 mm plate and let them grown for 72 hours. Briefly, the cell culture medium from each condition was collected and centrifuged for 5 minutes at 1000 x g at 4°C before dialysis with 3500 molecular weight cut-off dialysis tubes (Spectrum Laboratories, Rancho Dominguez, CA, US) against 5 mmol/L NH_4HCO_3, and a last step against distilled water for 4 hours. The samples were then concentrated by means of lyophilisation and stored at -80°C. After lyophilisation, the secreted protein pellets were dissolved in 25 mmol/L NH_4HCO_3 containing 0.1% RapiGest (Waters Corporation, Milfors, MA, US), sonicated and centrifuged at 13,000 g for 10 min. The supernatants were collected and the protein concentration was determined by Bradford's method. The samples were then reduced with 5 mmol/L DTT, carbamidomethylated with 10 mmol/L iodacetamide, and digested by adding 1µg of sequencing-grade trypsin (Promega, Milan, Italy). Tryptic peptides were used for label-free mass spectrometry analysis, LC-MSE, performed on a hybrid quadrupole-time of flight mass spectrometer coupled with nanoUPLC system and equipped with a Trizaic source (Waters Corporation). Statistical analysis was performed by means of Progenesis QIP v 4.1 (Nonlinear Dynamics).

5.10 RNA-sequencing

Total RNA was isolated from shB1/HASMCs and shCTR/HASMCs), using miRNeasy® mini kit (Qiagen, Hilden, Germany) following manufacturing instruction, including DNAse treatment for genomic removal. Total RNA concentration was assessed by NanoDrop One Microvolume Spectrophotometer (Thermo Fisher Scientific) while quality was evaluated by microfluidics electrophoresis using the RNA 6000 Nano Assay Kit on a 2100 Bioanalyzer system (Agilent Technologies, Santa Clara, CA, USA), respectively. Poly(A)+RNA enrichment was performed using the Dynabeads mRNA

Direct Micro Kit (Thermo Fisher Scientific) starting from 500 ng of total RNA. Barcoded libraries were prepared using the Total RNA-Seq Kit *v2.0* and Ion Xpress™ Barcode Adapters 1-16 Kit (Thermo Fisher Scientific) following manufacturer's instruction. Briefly, after poly(A)+ RNA fragmentation with RNAse III, hybridization and ligation of barcoded adapters for stranded RNA sequencing were performed, followed by reverse transcription. Lastly, cDNA fragments of 200 bp were amplified by 16 cycles of PCR, using the specific Ion Xpress™ Barcode for library demultiplexing. Prepared sequencing libraries were then quantified using both Qubit™ dsDNA Quantification Assay Kit on Qubit 3.0 Fluorometer and Agilent High Sensitivity DNA kit (Agilent Technologies) on 2100 Bioanalyzer system. One hundred pM diluted libraries were randomly pooled (four samples/pool) and loaded on 550 chips to be sequenced. Sequencing was performed using Ion Gene Studio S5 Prime System (Thermo Fisher Scientific).

5.11 Bioinformatic analysis

Raw reads were mapped against the GRCh38 Human Genome reference (release 99) with the Spliced Transcripts Alignment to a Reference (STAR) v2.7.5c software (Dobin et al., 2013) and with Bowtie2 v2.4.1 (Langmead et al., 2012), whereas gene expression quantification was computed by featureCounts v2.0.1 (Liao et al., 2014). Raw counts were then used for data exploration by using the EDASeq and DaMiRseq R/Bioconductor packages (Risso et al., 2011; Risso et al., 2014).

Differential Gene Expression Analysis. The raw count data were first filtered to retain genes with 10 counts in at least 20% of the samples. The RUVr method of the RUVSeq R/Bioconductor package (Zhou et al., 2019) was implemented to estimate the 'unwanted variation' (W) factors by considering the residuals of a first-pass GLM regression of the counts on the covariate of interest, i.e. the aggregate variable time (Day 3, 7 and 11) plus treatment (shB1/HASMCs and shCTR/HASMCs). The number of W factors was chosen by comparing the unadjusted expression data with those adjusted by a different number of Ws, based on the use of diagnostic graphs such as the relative logical expression (RLE) plot, the scatter plot of the first two principal components (PCs) derived from the principal component analysis (PCA) performed on the total data, the correlation graph between the estimated latent variables and the known clinical/technical variables, and the histogram of the distribution of P values to test the differential expression between sh and control samples at each time point. In our setting, an unwanted variation factor of W=4 was chosen as it provided the best trade-off between data adjustment and the risk of data overcorrection. Contrasts were set to compare the gene expression differences between sh and control samples for each time point. Gene expression was considered significantly different between sh and controls at a false discovery rate-adjusted $p < 0.05$ and $|\log2\text{-fold (FC) changes}| > 0.58$. The Benjamini-Hochberg

method was used to control for false discovery rate. The scatter plots of FC differences versus significance (volcano plots) were used to graphically summarize the DEA results (EnhancedVolcano R/Bioconductor package).

Functional Enrichment Analysis. To associate specific biological functions with sh and control phenotypes, we benefited from prior biological knowledge on genes grouped by gene ontology (GO) biological processes (BP) to perform gene set enrichment analysis by the Metascape software (Zhou et al., 2019). Enrichment analysis was performed based on the over- and under-expressed genes as found by the comparison of shB1/HASMCs *vs* shCTR/HASMCs at Day 3, 7, and 11. The genes expressed in the present RNA-seq dataset was used as the background. Parameters for analysis were set with Min Overlap = 3, P-Value Cutoff = 0.05 and Min Enrichment = 1.5. Significant terms were hierarchically clustered in a tree based on Kappa-statistical similarities (threshold = 0.3) among gene memberships. The most statistically significant term within a cluster was used as the overview term to represent the cluster and then visualized as heatmaps.

5.12 Animal experiments

For the aging experiments, aortas were isolated from male C57BL/6J (Charles River Laboratories International, Inc. Wilmington, MA, US) young (2.5 months-old) and old (21 months-old) mice, immediately frozen for protein extraction or fixed in 10% formalin for immunohistochemistry analysis. For calcification experiments, sixteen-week-old male *Hmgb1*$^{+/+}$ and *Hmgb1*$^{+/-}$ mice were treated with either 500000 IU/kg/day Vitamin D (Cholecalciferol, #C1357, Sigma-Aldrich, St. Louis, MO, US) or a mock solution (1% (v/v) Ethanol, 7% (v/v) Kolliphor® EL, 3.75% (w/v) Dextrose (all from Sigma-Aldrich) administrated subcutaneously for three consecutive days, and sacrificed seven days after the first injection. Animals were weighed before the treatment and before euthanasia with an intraperitoneal injection of ketamine (100mg/Kg) and perfused with PBS. Organs were dissected out and processed.

5.13 Immunohistochemistry (IHC)

Mouse distal thoracic aortas were fixed in 10% formalin and paraffin-embedded. Seven µm sections were de-paraffinized, re-hydrated and boiled for 20 minutes in Dako Target Retrieval Solution Citrate pH 6 or pH9 (Agilent Technologies, Santa Clara, CA, US). After washing in PBS-0.1% Triton X-100 (PBS-T) slides were incubated in 3% H2O2 (Sigma-Aldrich) and then blocked in PBS-T-5% Bovine Serum Albumin (BSA; #A3294, Sigma-Aldrich) or PBS-T-5% Goat Serum (GS; #G9023, Sigma- Aldrich) in for 1 hour at room temperature. Primary antibodies were dissolved in PBS-T-1%

BSA or PBS-T-1% GS and incubated overnight at 4°C. Sections were incubated with biotin-conjugated goat anti-rabbit antibody (7.5 µg/mL, #BA-1000, Vector Laboratories, Burlingame, CA, US) or rabbit anti-goat antibody (7.5 µg/mL, #BA-5000, Vector Laboratories) and, then with VECTASTAIN Elite ABC Kit, Peroxidase (Standard) (ABC kit; #PK-6100, Vector Laboratories) for 30 min at room temperature. Immunoreactions were revealed using 3.3'-Diaminobenzidine (ImmPACT DAB substrate, #SK-4105, Vector Laboratories) as chromogen and slides were counterstained with haematoxylin. The quantification of the signal was carried out after acquiring the images with an Axioskop II microscope (Zeiss) using a digital camera (AxioCam Color, Zeiss) on the entire aorta cross section with the Axiovision Software Rel 4.7 (Zeiss). The percentage of the positive area was defined as the ratio between the signal positive area to the total aortic area. Aorta thickness was measured after Hematoxylin and Eosin (H&E) staining.

5.14 Aortic Rings

The thoracic aortas of 12 weeks old male *Hmgb1*$^{+/+}$ and *Hmgb1*$^{+/-}$ BALB/c mice were harvested from the descending part of the aortic cross to the diaphragm. The adjacent connective tissue was gently removed in a physiological solution and Penicillin–Streptomycin (5000 U/mL; Gibco™, ThermoFisher Scientific, Waltham, MA, USA). Aortas were cut in rings of about 3 mm thickness and cultured in 24-well plates in SmGM-2 medium (Basal Medium; Lonza) or in calcification medium (DMEM supplemented with 15% FBS, 5 mM of phosphate, 10 mM of sodium pyruvate, 50 µg/mL of ascorbic acid, and 1% pen/strep) for 8 days. The medium was changed every two days.

5.15 Calcification assay for murine tissues

5.15.1 Von Kossa staining on aortic sections

Mice distal thoracic aortas or aortic rings were fixed in 10% formalin and paraffin-embedded. Six µm sections were de-paraffinized and incubated with 1% silver nitrate solution under ultraviolet light for 20 minutes. After rinsing the specimens with several changes of distilled H_2O, the unreacted silver was removed with 5% sodium thiosulfate for 5 minutes at room temperature. Then, the sections were rinsed in distilled H_2O and counterstained with H&E. The quantification of Von Kossa positive area was made by taking images with an Axioskop II microscope (Zeiss) using a digital camera (AxioCam Color, Zeiss). The entire aorta cross section was analyzed with Axiovision Software Rel 4.7 (Zeiss) and calcium content was defined as Von Kossa staining positive area divided by the total area (μm^2) multiplied by one hundred.

5.16 Human samples

Human aortic tissue from young and middle-age (MA)-old control (n=3) subjects and CKD patients (n=4) were collected after signing the consent form (Table 3). Sample were fixed in 10% formalin and paraffin embedded. Sections were boiled in sodium citrate buffer and endogenous peroxidase activity was quenched by 3% hydrogen peroxide in methanol. Non-specific binding was blocked with 10% goat serum before incubation with the primary antibody rabbit anti-HMGB1 (1µg/mL, ab18256, Abcam, Cambridge, United Kingdom). Biotinylated horse anti-mouse secondary antibody was added, followed by amplification using avidin-biotin complex (#PK-6101, Vector Laboratories). Staining was developed with DAB peroxidase substrate and these sections were counterstained with haematoxylin. The slides were mounted with DPX followed by dehydration. Images were acquired with an Axioskop II microscope (Zeiss) using a digital camera (AxioCam Color, Zeiss). The quantification of the HMGB1 signal was carried out on the entire aorta cross-section with the Axiovision Software Rel 4.7 (Zeiss). The percentage of positive area was defined as the ratio of the HMGB1 positive area to the total area of the aortas.

Thirty-five samples of abdominal aortic aneurysms (AAA) from male patients with an average age of 71±8 years subjected to surgery were collected at Centro Cardiologico Monzino after signing the consent form approved by the Ethical Committee of Centro Cardiologico Monzino (Milano, Italy) on 4th November 2013 (Table 4).

5.17 Statistical analysis

Data were analyzed with GraphPad Prism software version 7 (GraphPad Software, Inc, La Jolla, CA, US). D'Agostino or Shapiro-Wilk test was used to assess the normality of distribution of investigated parameters. Student's t-test was used for comparison between two groups as indicated in the legends. Statistical analysis between more than two groups was conducted by 1-way or 2-way ANOVA with Bonferroni post-hoc test, as reported in the figure legends. Values are presented as mean ± SD. To assess the relationship between variables, Pearson's correlation was calculated between the expression values of HMGB1, IL-6 and Ca^{2+}. Moreover, linear regression analysis was performed to evaluate the relationships between clinical covariates and HMGB1, IL-6 and Ca^{2+}. A p-value < 0.05 was considered statistically significant.

6. RESULTS

6.1 HMGB1 controls senescence and SASP acquisition in VSMCs

Since P8 shB1/HASMCs show similar senescent features of P15 shCTR/HASMCs, we characterized further the HMGB1 role on the senescent phenotype of P8 HASMCs by testing other known markers of senescence. An augmentation of CDK inhibitor p21 protein levels (Figure 8A) and a higher percentage of cells positive for senescence-associated β-galactosidase (SA-β-gal) activity in shB1/HASMCs compared to shCTR/HASMCs were observed (Figure 8B). The production and release of SASP inflammatory factors is typical of senescent cells and is recognized as a mechanism influenced by HMGB1 (Sofiadis et al., 2021) thereby we investigated whether HMGB1 could influence the SASP acquisition in HASMCs. We examined whether HMGB1 could affect the acquisition of the SASP in HASMCs. To do this, we analyzed the mRNA expression of various SASP factors in HASMCs/shHMGB1 and HASMCs/shCNTRL cells at passage 8 (P8), cultured for 24, 48, and 72 hours, using RT-PCR (Figure 8C). Surprisingly, HASMCs/shHMGB1 cells showed a significant reduction in the mRNA levels of inflammatory genes (IL-6, IL-1β, IL-8, and IL-10) and migratory factors (MCP-1), while no alteration of the anti-inflammatory cytokine IL-10 with respect to control cells. We confirmed these data by assessing secretion of IL-6 and IL-8 (Figure 8D). We measured their extracellular release using ELISA after 72 hours of culture. We observed that, overall, HASMCs/shHMGB1 cells secreted less IL-6 than HASMCs/shCNTRL cells and as expected, the extracellular levels of IL-6 were higher at P15 compared to P8. The secretion of other pro-inflammatory cytokines like IL-1β was barely detectable in HASMCs/shCNTRL cells at P8. Overall, these findings suggest that HMGB1 can influence the acquisition of the SASP and, consequently, the spread of senescence in HASMCs.

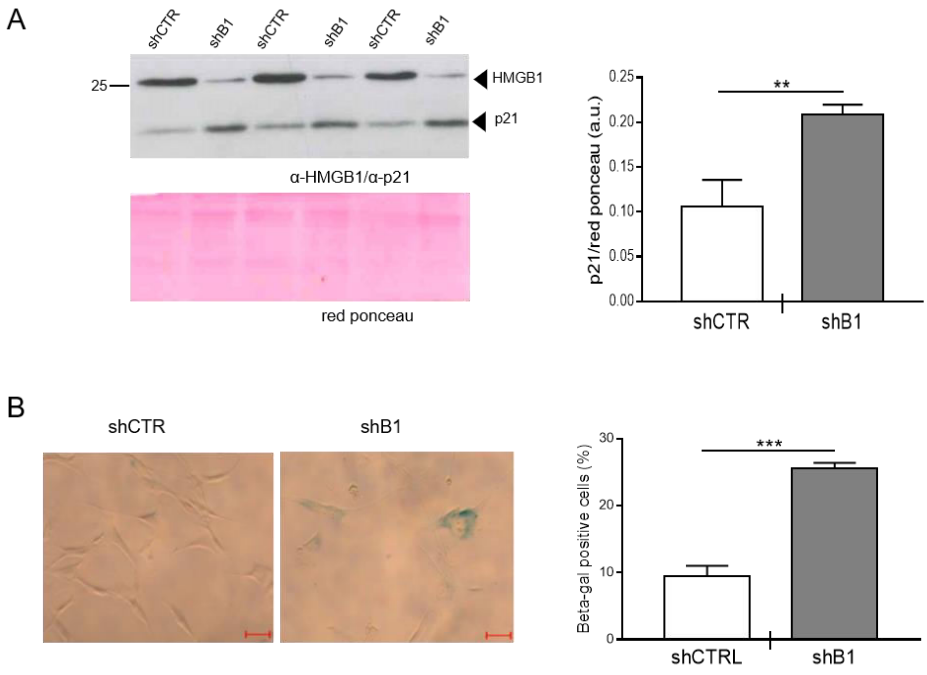
A
shCTR
shB1
shCTR
shB1
shCTR
shB1
25
HMGB1
p21
α-HMGB1/α-p21
red ponceau
p21/red ponceau (a.u.)
0.25
0.20
0.15
0.10
0.05
0.00
**
shCTR
shB1
B
shCTR
shB1
Beta-gal positive cells (%)
30
20
10
0
***
shCTRL
shB1
C
shCTR
shB1
mRNA relative expression
12
10
8
6
4
2
2.0
1.5
1.0
0.5
0.0
***
***
**
***
***
***
**
IL-6
IL-8
IL-1β
MCP-1
IL-10
24h
48h
72h

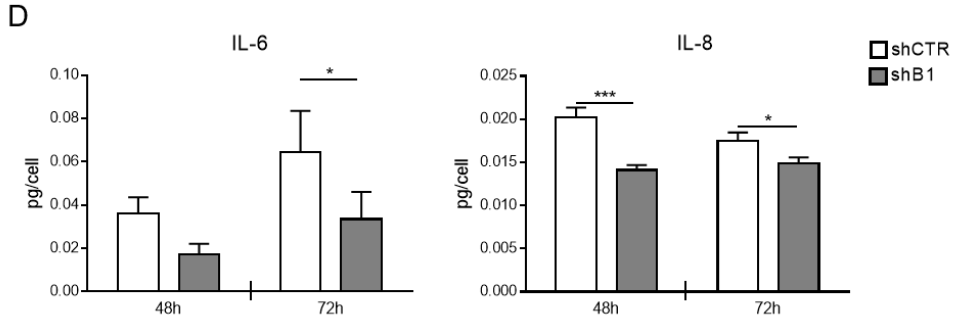

Figure 8. HMGB1 controls senescence and the SASP acquisition in VSMCs. (A) (Right panel) Western blot for p21 in P8 shCTR/HASMCs and shB1/HASMCs after 24 hours (h) of culture; red ponceau staining was used as loading control. **(B)** (Right panel) Representative images of SA-β-gal staining in P8 shCTR/HASMCs and shB1/HASMCs after 72 hours of culture (Left panel) Quantification of SA-β-gal staining. Bars show values as mean ± SD; Student's t-test; ***p < 0.001; n = 3. **(C)** SASP factors mRNA expression in P8 shCTR/HASMCs and shB1/HASMCs after 24, 48 and 72 h of growth analyzed by qRT-PCR and normalized to *GAPDH* levels. Bars show values as mean ± SD; 2-way ANOVA plus Bonferroni post-hoc test; *p < 0.05, **p < 0.01, ***p < 0.001; n = 3. **(D)** Extracellular protein levels of indicated SASP factors secreted by P8 shCTR/HASMCs and shB1/HASMCs after 48 and 72 h of growth monitored by ELISA. Bars show values as mean ± SD; 1-way ANOVA plus Bonferroni post-hoc test; *p < 0.05, **p < 0.01, ***p < 0.001; n = 3.

To better characterize the secretory phenotype of P8 shCTR/HASMCs and shB1/HASMCs, we performed a proteomic analysis of their secretome by label-free mass spectrometry (LC-MSE). We found that shB1/HASMCs released higher amount of matrix metalloproteinase-2 (MMP-2), plasminogen activator inhibitor 1 (PAI1), biglycan (BGN), gelsolin (GSN), lamin subunit α-4 (LAMA4), pigment epithelium-derived factor (PEDF) and profilin-1 (PFN1), and lower levels of decorin (DCN), insulin-like growth factor-binding protein 7 (IGFBP7), lumican (LUM), tenascin-X (TNX), collagen alpha-1(III) (COL3A1), complement C1s subcomponents, glia-derived nexin (GDN), pentraxin-related protein (PTX3), trombospondin-1 (THBS1) and tissue-type plasminogen activator (PLAT), compared to shCTR/HASMCs (Table 1). A Gene Ontology (GO) was performed on the set of proteins that exhibited significant altered levels in the secretome of shB1/HASMCs cells. The analysis of the more abundant proteins indicated a significant enrichment in the cellular compartment related to collagen-containing extracellular matrix (p = 0.00016) and extracellular space (p = 0.0017), (Figure 9). Proteins involved in the biological processes related to negative

regulation of plasminogen activation (p = 0.00024) and extracellular organization (p = 0.0123) were less abundant in the shB1/HASMCs secretome (Figure 9).
We confirmed that HMGB1 content influences the expression of some of these factors both at mRNA (Figure 10A) and protein levels (Figure 10B).
Altogether, these data indicate that the reduction of HMGB1 levels induces senescence, alters ECM proteins balance and unexpectedly mitigates the expression of inflammatory SASP factors in VSMCs.

Table 1. Secretome analysis of shCTR/HASMCs and shB1/HASMCs by la-bel-free mass spectrometry (LC-MSE). shCTR = shCTR/HASMCs, shB = shB1/HASMCs.

Description	Highest mean condition	Replicate 1	Replicate 2	Replicate 3	mean
72 kDa type IV collagenase GN=MMP2	shB1	1.214	1.475	1.517	1.40
Plasminogen activator inhibitor 1 GN=SERPINE1	shB1	2.075	2.820	1.365	2.09
Biglycan GN=BGN	shB1	1.207	1.661	-	1.43
Gelsolin GN=GSN	shB1	1.245	1.496	-	1.37
Laminin subunit alpha-4 GN=LAMA4	shB1	1.203	1.346	-	1.27
Pigment epithelium-derived factor GN=SERPINF1	shB1	1.209	1.786	-	1.50
Profilin-1 GN=PFN1	shB1	-	1.304	1.355	1.33
Decorin GN=DCN	shCTR	1.245	1.437	1.947	1.54
Insulin-like growth factor-binding protein 7 GN=IGFBP7	shCTR	1.406	1.283	1.260	1.32
Lumican GN=LUM	shCTR	1.396	1.906	4.355	2.55
Tenascin-X GN=TNXB	shCTR	1.324	2.191	1.250	1.59
Collagen alpha-1(III) GN=COL3A1	shCTR	1.229	1.953	-	1.59
Complement C1s subcomponent GN=C1S	shCTR	-	1.465	2.136	1.80
Glia-derived nexin GN=SERPINE2	shCTR	-	1.291	1.230	1.26
Pentraxin-related protein PTX3 GN=PTX3	shCTR	-	1.997	1.592	1.79
Thrombospondin-1 GN=THBS1	shCTR	2.022	-	1.987	2.00
Tissue-type plasminogen activator GN=PLAT	shCTR	1.490	-	1.955	1.72

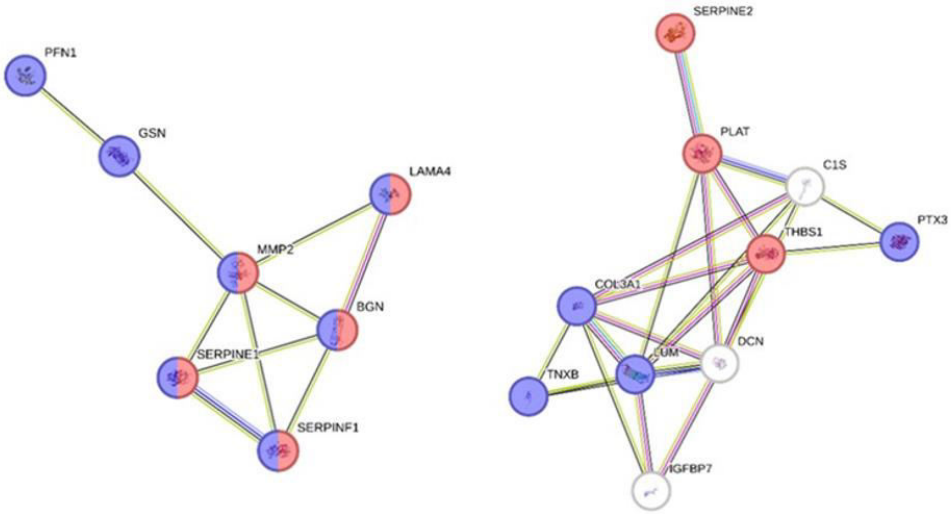

Figure 9. Secretome analysis. (Left panel) Gene Ontology analysis of proteins more abundant in the secretome of shB1/HASMCs cells. In red, proteins related to the collagen-containing extracellular matrix; in blu, proteins related to the extracellular space. (Right panel) Gene Ontology analysis of proteins less abundant in the secretome of shB1/HASMCs cells. In red, proteins related to the negative regulation of plasminogen activation biological process; in blue, proteins related to the extracellular matrix organization process.

A

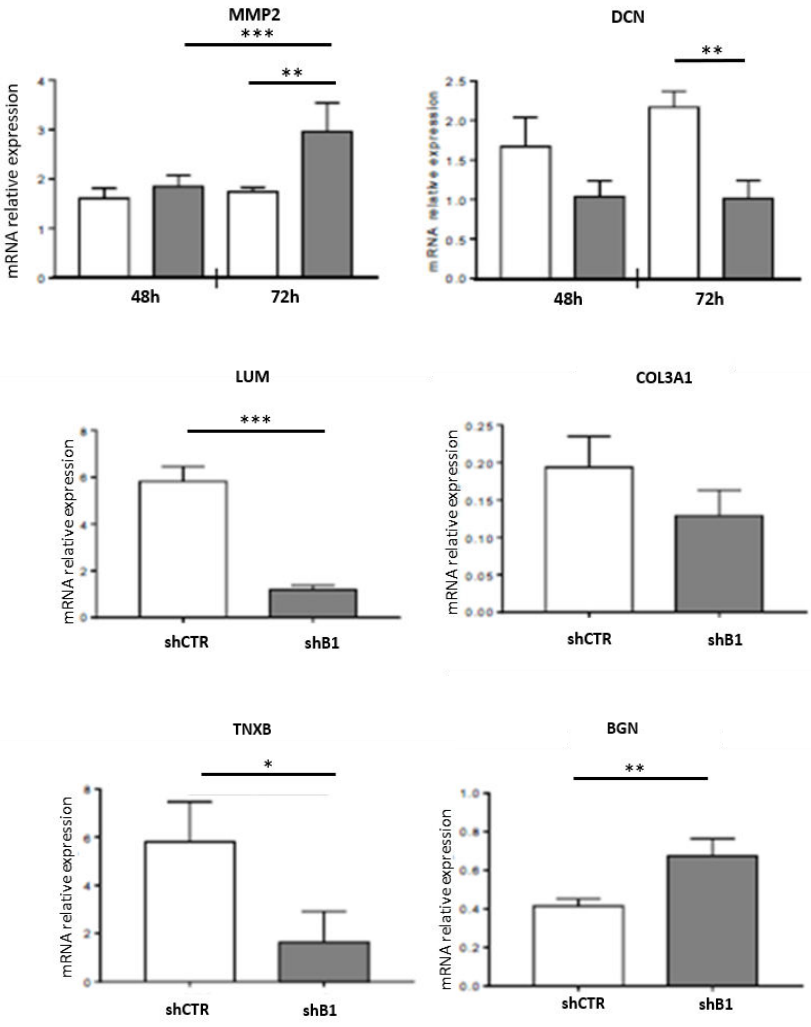
MMP2
***
**
mRNA relative expression
48h
72h
DCN
**
mRNA relative expression
48h
72h
LUM
***
mRNA relative expression
shCTR
shB1
COL3A1
mRNA relative expression
shCTR
shB1
TNXB
*
mRNA relative expression
shCTR
shB1
BGN
**
mRNA relative expression
shCTR
shB1

B

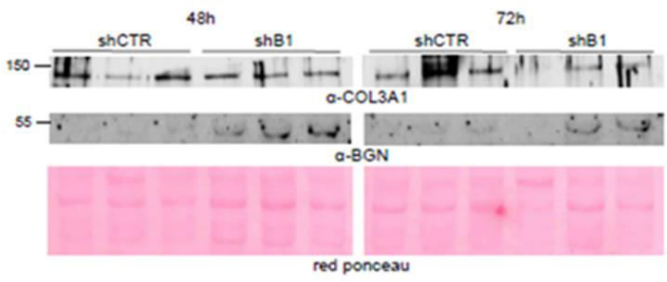
48h
72h
shCTR
shB1
shCTR
shB1
150
α-COL3A1
55
α-BGN
red ponceau

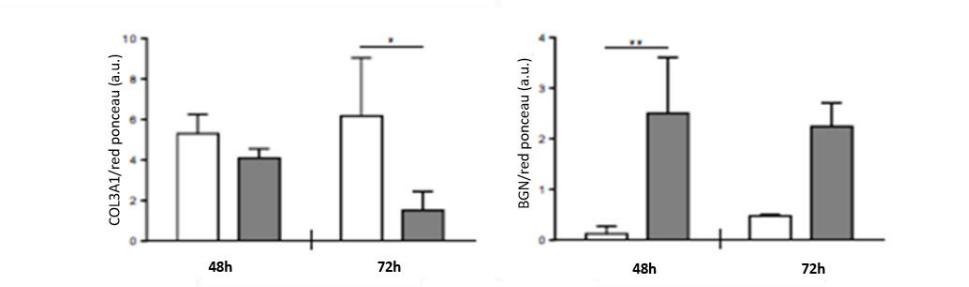

Figure 10. HMGB1 downregulation alters ECM macromolecules expression in HASMCs. (A) mRNA expression of indicated genes in P8 shCTR/HASMCs and shB1/HASMCs after 48 (LUM, COL3A1, TNXB, BGN) and 72 hours (h, DNC and MMP2) of growth analyzed by qRT-PCR and normalized to corresponding *HPRT* levels. Bars show values as mean ± SD; Student's t-test or 1-way ANOVA plus Bonferroni post-hoc test; *p < 0.05, **p < 0.01; ***p < 0.001; n = 3. **(B)** (Top panels) Western blot for COL3A1 or BGN of P8 shCTR/HASMCs and shB1/HASMCs after 48 and 72 h of culture. Red ponceau staining was used as loading control. (Lower panels) Quantification of COL3A1 or BGN expression. Bars show values as mean ± SD; 1-way ANOVA plus Bonferroni post-hoc test; *p < 0.05, **p < 0.01; n = 3.

6.2 HMGB1 downregulation promotes the expression of regulators of VSMCs osteogenic differentiation

Notably, the secretome of shB1/HASMCs resembles the proteome of calcified aortic valves and aortic valve interstitial cells (AVICs) characterized by a reduction of some ECM proteins like TNXB, DCN, LUM and an increase of BGN (De la Cuesta et al., 2013). Evidence have highlighted also a link between BGN and pro-osteogenic reprogramming in AVICs since BGN upregulates RUNX2 and ALP expression in these cells (Song et al., 2015). We have also shown that inhibition of pro-inflammatory SASP factors accelerates HASMC calcification (Macrì et al., 2023). Hence, we decided to check whether nuclear HMGB1 influences the expression of pro-calcification markers in HASMCs. We measured the expression of the transcription factor RUNX2 and the enzyme ALP, known regulators of VSMCs osteoblastic trans-differentiation and the SASP factors OPG, a well-known calcification inhibitor (Macrì et al., 2023). As shown in Figure 11A, ALP expression was significantly higher and RUNX2 showed a tendency to increase in shB1/HASMCs with respect to control cells. HMGB1 silencing significantly inhibited OPG mRNA expression and protein release (Figure 11B-C).

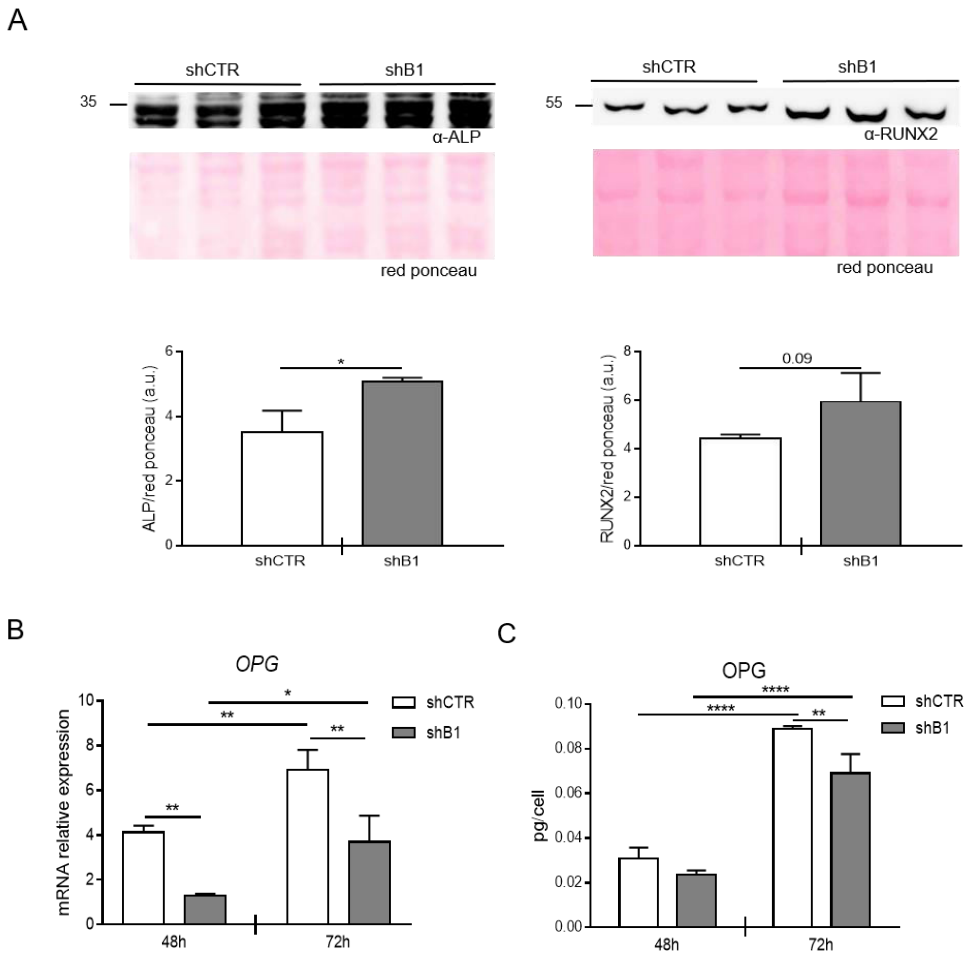

Figure 11. HMGB1 downregulation alters calcification markers expression in HASMCs. (A) (Higher panels) Western blot for Alkaline Phosphatase (ALP) and RUNX2 of P8 shCTR/HASMCs and shB1/HASMCs after 48 (h) of culture. Red ponceau staining was used as loading control. (Lower panels) Quantification of ALP and RUNX2 expression. Bars show values as mean ± SD; Student's t-test; *p < 0.05; n = 3. **(B)** OPG mRNA expression in P8 shCTR/HASMCs and shB1/HASMCs after 48 and 72 hours of growth analyzed by qRT-PCR and normalized to corresponding GAPDH levels. 1-way ANOVA plus Bonferroni post-hoc test; *p < 0.5, **p < 0.01; n = 3. **(C)** Extracellular protein levels of OPG secreted by P8 shCTR/HASMCs and shB1/HASMCs after 48-72 hours (h) of growth monitored by ELISA. Bars show values as mean ± SD; 1-way ANOVA plus Bonferroni post-hoc test; **p < 0.01, ****p < 0.0001; n = 3.

We decided to confirm the *in vitro* data on aortas isolated from Young and Old *Hmgb1*$^{+/+}$ and *Hmgb1*$^{+/-}$ mice. While Young *Hmgb1*$^{+/+}$ and *Hmgb1*$^{+/-}$ mice have a similar protein expression of ALP and RUNX2, *Hmgb1*$^{-/+}$ old mice show higher protein levels of both proteins compared to corresponding *Hmgb1*$^{+/+}$ (Figure 12A). IL-6 expression increased with age in *Hmgb1*$^{+/+}$but not in Hmgb1$^{+/-}$ mice (Figure 12A). LUM and TNXB protein expression tends to decrease while BGN increases in Old Hmgb1$^{+/-}$ mice compared to age-matched control animals (Figure 12B).
Overall, these data support the *in vitro* results, showing that HMGB1 downregulation in VSMCs affects the expression of pro-osteogenic factors, ECM proteins associated to cell calcification and inflammatory molecules in aged mice.
These findings demonstrate that HMGB1 decline promotes the expression of modulators of VSMC osteogenic trans-differentiation.

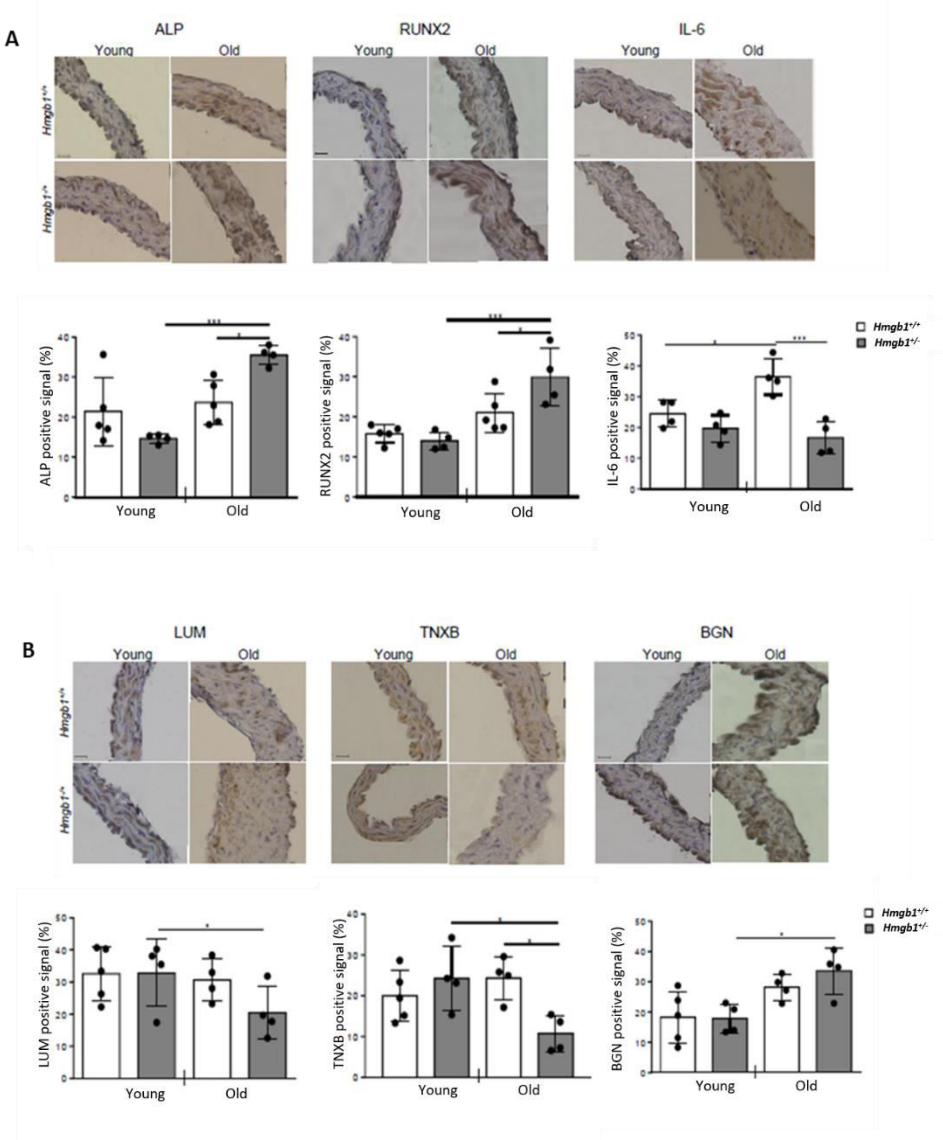

Figure 12.Expression of calcification and pro-inflammatory markers, and ECM proteoglycans in aortas isolated from Young and Old *Hmgb1*$^{+/+}$ and *Hmgb1*$^{+/-}$ *mice*. (A) Aortas were isolated from Young (4 months-old) and Old (18 months-old) Hmgb1$^{+/+}$ and Hmgb1$^{+/-}$ male mice. Calcification and pro-inflammatory markers. (Upper panels) Representative images of ALP, RUNX2, and IL-6 staining. Scale bar: 20 µm. (Lower panels) Quantification of ALP, RUNX2, and IL-6 signal. **(B)** ECM proteoglycans. (Upper panels) Representative images TNXB, LUM and BGN staining. Scale bar: 20 µm. (Lower panels) Quantification of TNXB, LUM and BGN signal. Bars show values as mean ± SD; 1-way ANOVA plus Bonferroni post-hoc test; *p < 0.05, ***p < 0.001; n = 4-5.

6.3 HMGB1 reduction accelerates Pi-induced VSMC osteogenic transition and calcification

To investigate whether HMGB1 decline play a direct role in VSMC osteogenic transdifferentiation, we cultured P8 shCTR/HASMCs and shB1/HASMCs in calcification medium containing high concentration of Pi (hyperphosphatemia) (Cozzolino et al., 2019) for 3, 7 and 11 consecutive days (Day). Qualitative alizarin red staining and quantitative calcium colorimetric assay show that calcification increased overtime in both clones, nevertheless, shB1/HASMCs accumulated higher amount of calcium at Day 7 and Day 11 in respect to shCTR/HASMCs (Figure 13A-B). We observed a downregulation of HMGB1 expression, which almost disappeared after 11 days of calcification in both shCTR/HASMCs and shB1/HASMCs, however, silenced cells displayed a more drastic and earlier downregulation (Figure 13C).

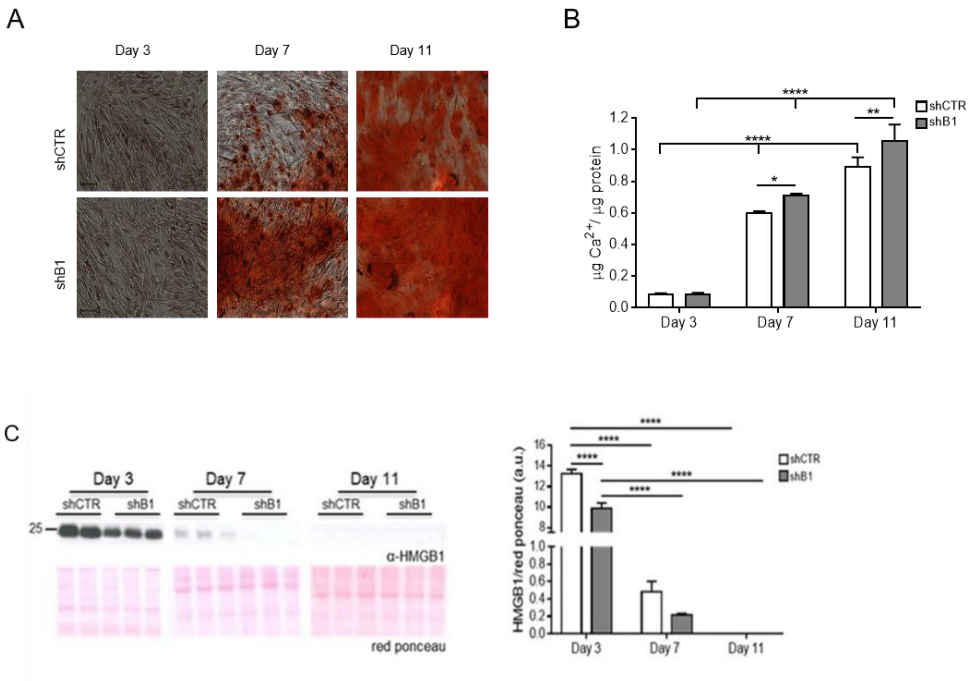

Figure 13. HMGB1 reduction in HASMCs modulates calcification process. (A) HMGB1 downregulation enhances HASMCs calcification. P8 shCTR/HASMCs and shB1/HASMCs were cultured in calcification medium for 3, 7 and 11 days (Day) (A) Representative images of P8 shCTR/HASMCs and shB1/HASMCs after alizarin red staining to re reveal calcium deposits (red). **(B)** Calcium content of P8 shCTR/HASMCs and shB1/HASMCs quantified by colorimetric analysis. Bars show values as mean ± SD; 2-way ANOVA

plus Bonferroni post-hoc test; *p < 0.05, **p < 0.01, ****p < 0.0001; n = 3. **(C)** (Left panels) Cell extracts of HASMC clones were processed for WB analysis with a α-HMGB1 antibody. Red ponceau was used as loading control. (Right panel) Quantification of HMGB1 protein expression. Bars show values as mean ± SD; 2-way ANOVA plus Bonferroni post-hoc test; ****p < 0.0001; n = 2-3.

To gain more insight into the molecular mechanisms by which HMGB1 may repress VSMC osteogenic transition, we performed transcriptomic analyses on shCTR/HASMCs and shB1/HASMCs, both grown in osteogenic medium for 3, 7 and 11 days. Differential expression analysis (DEA), adjusted for the effects of confounders (i.e. latent variables), showed specific mean changes in HASMC gene expression between shB1/HASMCs and control samples for each time point. We summarise the main findings in Table 2. The large number of differentially expressed genes, which include both protein coding and long non-coding genes, suggests a profound effect of HMGB1 silencing on the overall transcriptome of HASMCs, with a more pronounced number of total DE genes (DEG) at Day 11 compared to Days 3 and 7 (Table 2, Figure 14A, Volcano plot). To better infer the biological functions underlying the phenotype of HASMCs silenced for HMGB1, we performed a gene set enrichment analysis on the DEA result obtained from the comparisons at each time point. Among the most significantly altered RNAs in HMGB1-silenced cells, both the lncRNA H19 and the SOST gene were consistently upregulated at all time points examined. This lncRNA acts as a sponge for several microRNAs, facilitating vascular calcification. (Xhiong-Zi et al., 2023, Qiang et al., 2022, Feng et al., 2022, Wei et al., 2022).

We found a considerable number of significant Gene Ontology Biological Processes (GO-BP) that were over- or under-represented in the shB1/HASMCs vs shCTR/HASMCs. The most representative GO-BP that were positively associated with the HMGB1 silenced phenotype were suggestive of “biomineral tissue development” and “cell fate commitment” at any stage of osteogenic transdifferentiation (Figure 14B right panel). These GO-BP terms contain genes such as NOTCH3 and ALPL, respectively that are upregulated during VSMC osteogenic transition (Liu et al., 2011). The downregulated DEG were enriched for GO-BP terms related to the regulation of cell cycle process and nuclear division, innate immune response, including the defence response to virus and to bacterium, the response to type I interferon and tissue migration (Figure 14B left panel).

We confirmed by RT-PCR that during HASMC calcification the mRNA level of pro-inflammatory SASP IL-6 and IL-8 and the inhibitor of calcification OPG (TNFRSF11B) were lower while ALP (ALPL) was higher in shB1/HASMCs (Figure 14C). Accordingly, shB1/HASMCs released lower amount of the OPG protein as well (Figure 14D). Although RUNX2 mRNA levels did not vary during calcification, the protein was significantly more expressed in shB1/HASMCs compared to control cells (Figure 14E).

Overall, this data show that HMGB1 decreases during HASMC calcification and its loss influences VSMC fate commitment.

Table 2. Differentially expressed genes in shCTR/HASMCs vs shB1/HASMCs after challenge with osteogenic differentiation medium. Genes were considered as differentially expressed if adj. $p < 0.05$ and $|\log2 \text{ fold change}| > 0.58$. DE = Differentially expressed.

shB1/HASMCs *vs* shCTR/HASMCs	Day 3	Day 7	Day 11
Total DE genes	1707	1236	2982
Over-expressed genes	392	318	2131
Under-expressed genes	1315	918	851

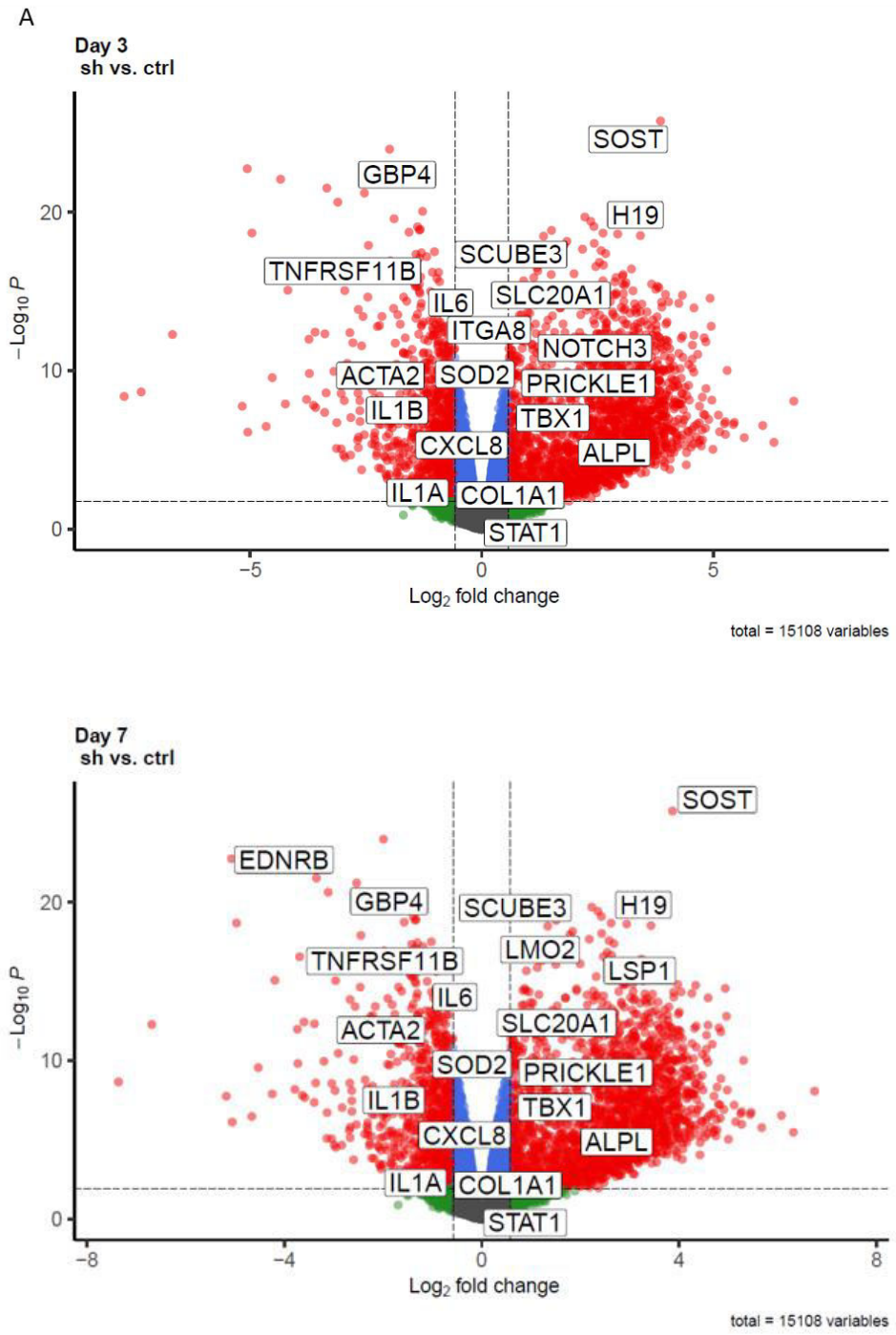
A
Day 3
sh vs. ctrl
SOST
GBP4
H19
SCUBE3
TNFRSF11B
SLC20A1
IL6
ITGA8
NOTCH3
ACTA2
SOD2
PRICKLE1
IL1B
TBX1
CXCL8
ALPL
IL1A
COL1A1
STAT1
20
10
0
−5
0
5
−Log10 P
Log2 fold change
total = 15108 variables
Day 7
sh vs. ctrl
SOST
EDNRB
GBP4
SCUBE3
H19
LMO2
TNFRSF11B
LSP1
IL6
ACTA2
SLC20A1
SOD2
PRICKLE1
IL1B
TBX1
CXCL8
ALPL
IL1A
COL1A1
STAT1
20
10
0
−8
−4
0
4
8
−Log10 P
Log2 fold change
total = 15108 variables

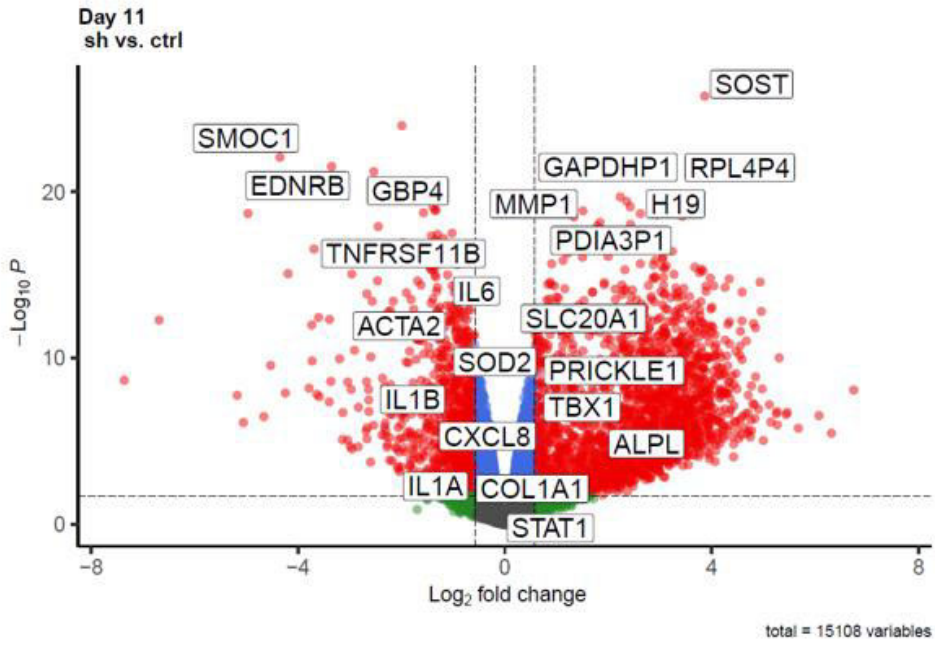
Day 11
sh vs. ctrl
SOST
SMOC1
EDNRB
GBP4
GAPDHP1
RPL4P4
MMP1
H19
PDIA3P1
TNFRSF11B
IL6
ACTA2
SLC20A1
SOD2
PRICKLE1
IL1B
TBX1
CXCL8
ALPL
IL1A
COL1A1
STAT1
20
10
0
−8
−4
0
4
8
−Log10 P
Log2 fold change
total = 15108 variables

B

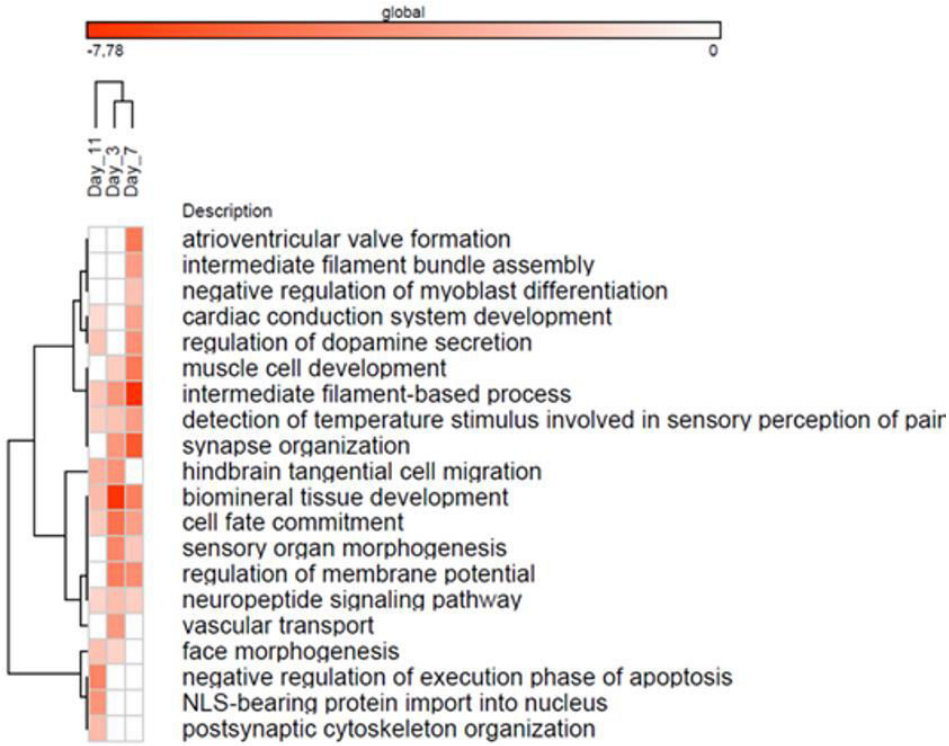
global
-7,78
0
Day_11
Day_3
Day_7
Description
atrioventricular valve formation
intermediate filament bundle assembly
negative regulation of myoblast differentiation
cardiac conduction system development
regulation of dopamine secretion
muscle cell development
intermediate filament-based process
detection of temperature stimulus involved in sensory perception of pair
synapse organization
hindbrain tangential cell migration
biomineral tissue development
cell fate commitment
sensory organ morphogenesis
regulation of membrane potential
neuropeptide signaling pathway
vascular transport
face morphogenesis
negative regulation of execution phase of apoptosis
NLS-bearing protein import into nucleus
postsynaptic cytoskeleton organization

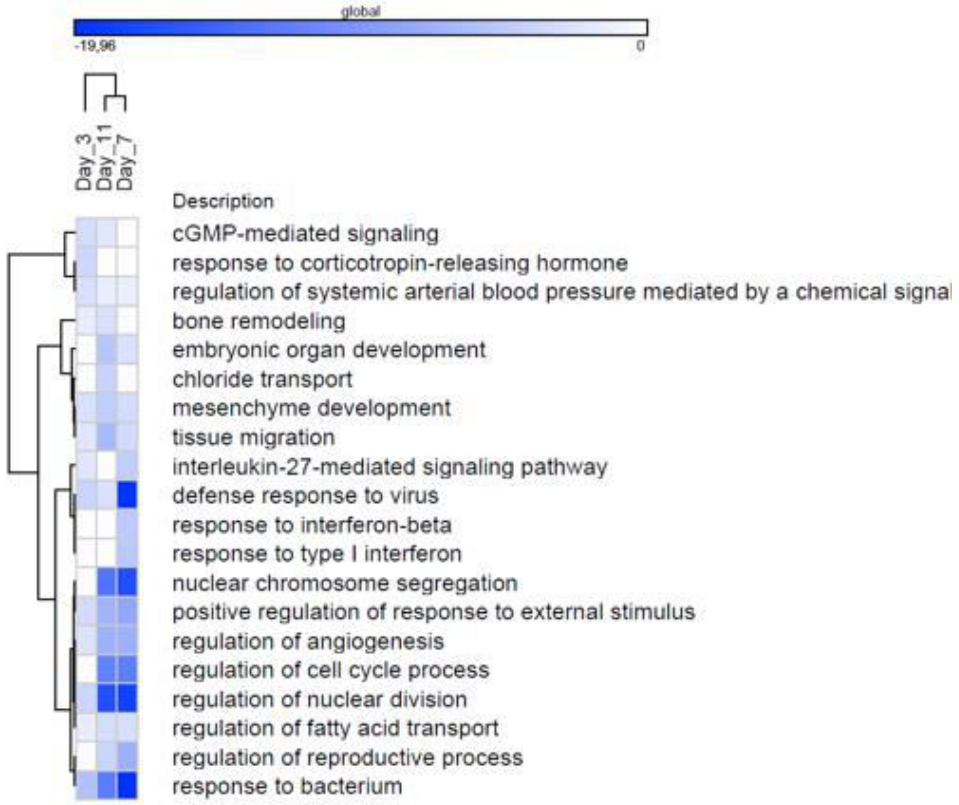
global
-19,96
0
Day_3
Day_11
Day_7
Description
cGMP-mediated signaling
response to corticotropin-releasing hormone
regulation of systemic arterial blood pressure mediated by a chemical signal
bone remodeling
embryonic organ development
chloride transport
mesenchyme development
tissue migration
interleukin-27-mediated signaling pathway
defense response to virus
response to interferon-beta
response to type I interferon
nuclear chromosome segregation
positive regulation of response to external stimulus
regulation of angiogenesis
regulation of cell cycle process
regulation of nuclear division
regulation of fatty acid transport
regulation of reproductive process
response to bacterium

C

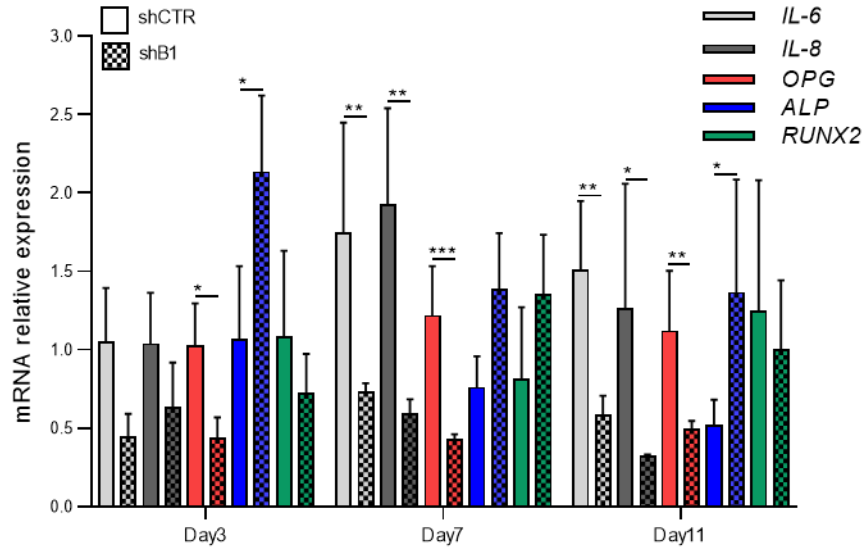
shCTR
shB1
IL-6
IL-8
OPG
ALP
RUNX2
mRNA relative expression
3.0
2.5
2.0
1.5
1.0
0.5
0.0
Day3
Day7
Day11

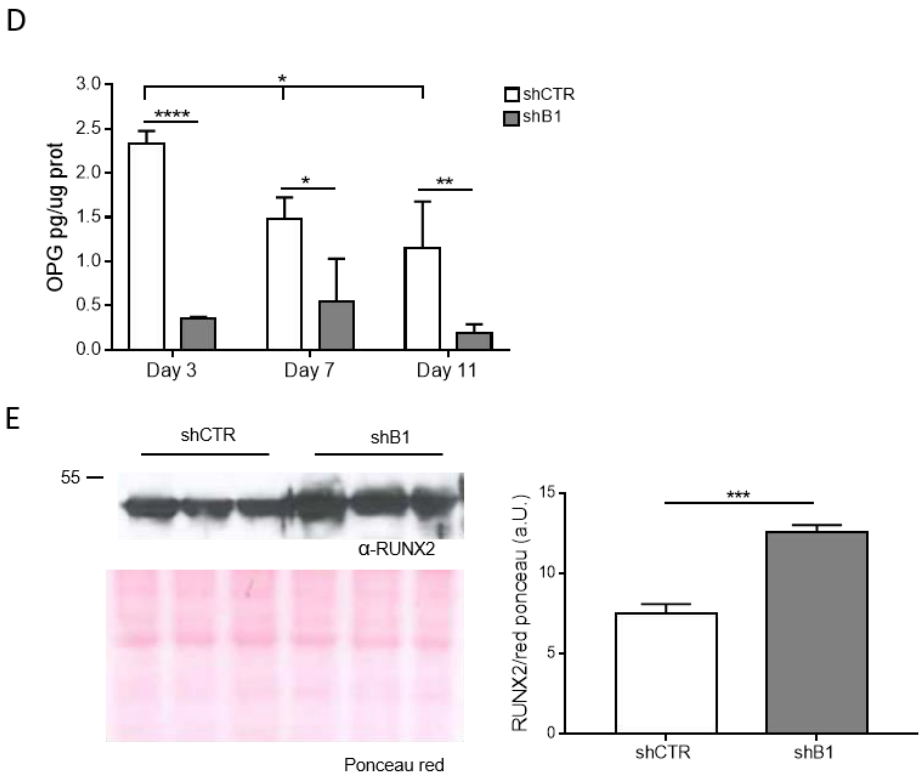

Figure 14. HMGB1 loss during HASMC calcification influences VSMC fate commitment. (A) Volcano plots. (B) Gene set enrichment analysis. (C) Indicated genes were analyzed by qRT-PCR and normalized to UBC and ZNF levels. Bars show values as mean ± SD; 2-way ANOVA plus Bonferroni post-hoc test; ns= not significant; *p < 0.05, **p < 0.01, ***p < 0.001; n = 3-4. (D) Supernatants of cells were subjected to ELISA assay for OPG detection. Bars show values as mean ± SD; 2-way ANOVA plus Bonferroni post-hoc test; *p < 0.05, **p < 0.01, ****p < 0.0001; n = 3. (E) (Left panel) P8 shCTR/HASMCs and shB1/HASMCs cultured for 11 days in calcification medium and cell extracts were processed for WB analysis with a α-RUNX2 antibody. Ponceau red was used as loading control. (Right panel) Quantification of RUNX2 protein expression. Bars show values as mean ± SD; Student's t-test; ***p < 0.001; n = 3.

6.4 HMGB1 reduction enhances tissue VC

In order to verify if HMGB1 could alter also VC *in vivo*, we took advantage of a well-established mouse model of soft tissue calcification induced by a high dose of vitamin D (Vit D). We have already demonstrated that Vit D treatment induces VSMC senescence along with calcification (Badi et al., 2018). $Hmgb1^{+/+}$ and $Hmgb1^{+/-}$ mice were treated with Vit D or a mock solution as control (Ctrl) and calcium deposits, determined by Von Kossa staining, were detected in aortas of mice receiving Vit D (Figure 15A). Notably, aortas of Vit D-injected $Hmgb1^{+/-}$mice showed higher calcification than $Hmgb1^{+/+}$(Figure 15A).
Accordingly, $Hmgb1^{+/-}$mice displayed higher aortic ALP expression but lower aortic inflammation, as indicated by IL-6 signal, in respect to $Hmgb1^{+/+}$following Vit D treatment (Figure 15 B-C). In order to check whether HMGB1 influences directly VC onset despite the systemic inflammation or organ dysfunction that may be induced by Vit D, we isolated and cultured aortic rings in calcification medium (Macrì et al., 2023). Aortic rings of $Hmgb1^{+/-}$mice accumulate more calcium compared to $Hmgb1^{+/+}$ mice (Figure 15D). Kidneys and heart of Vit D-injected $Hmgb1^{+/-}$also accumulate more calcium than $Hmgb1^{+/+}$animals (Figure 15E-F).
Altogether, these data indicate that HMGB1 loss promotes medial VC and, in particular, enhances vessels and soft tissues mineralization while reduces local vascular inflammation in response to a calcification stimulus.

A

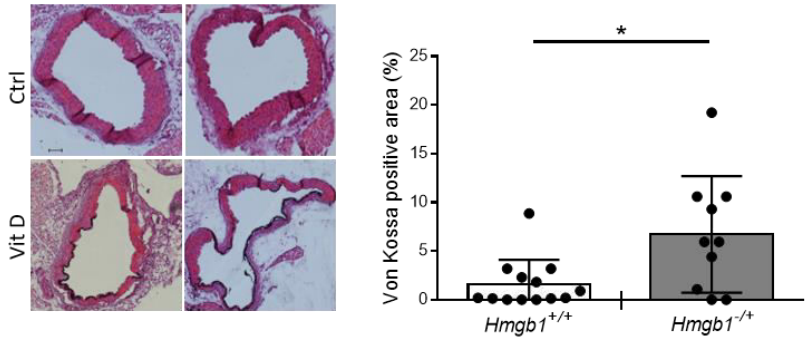
Ctrl
Vit D
Von Kossa positive area (%)
25
20
15
10
5
0
*
Hmgb1+/+
Hmgb1-/+

B

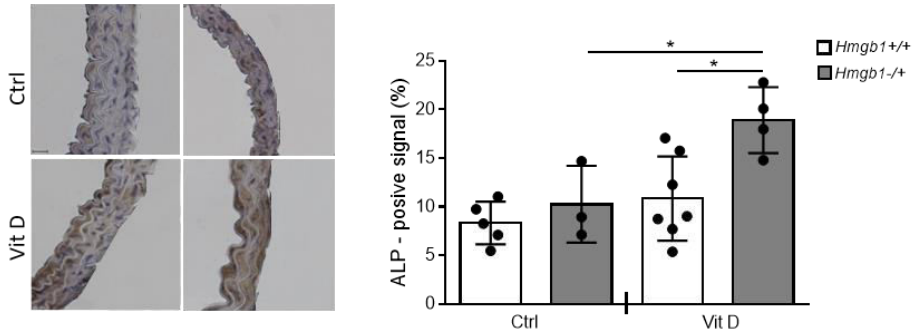
Ctrl
Vit D
ALP - posive signal (%)
25
20
15
10
5
0
*
*
Hmgb1+/+
Hmgb1-/+
Ctrl
Vit D

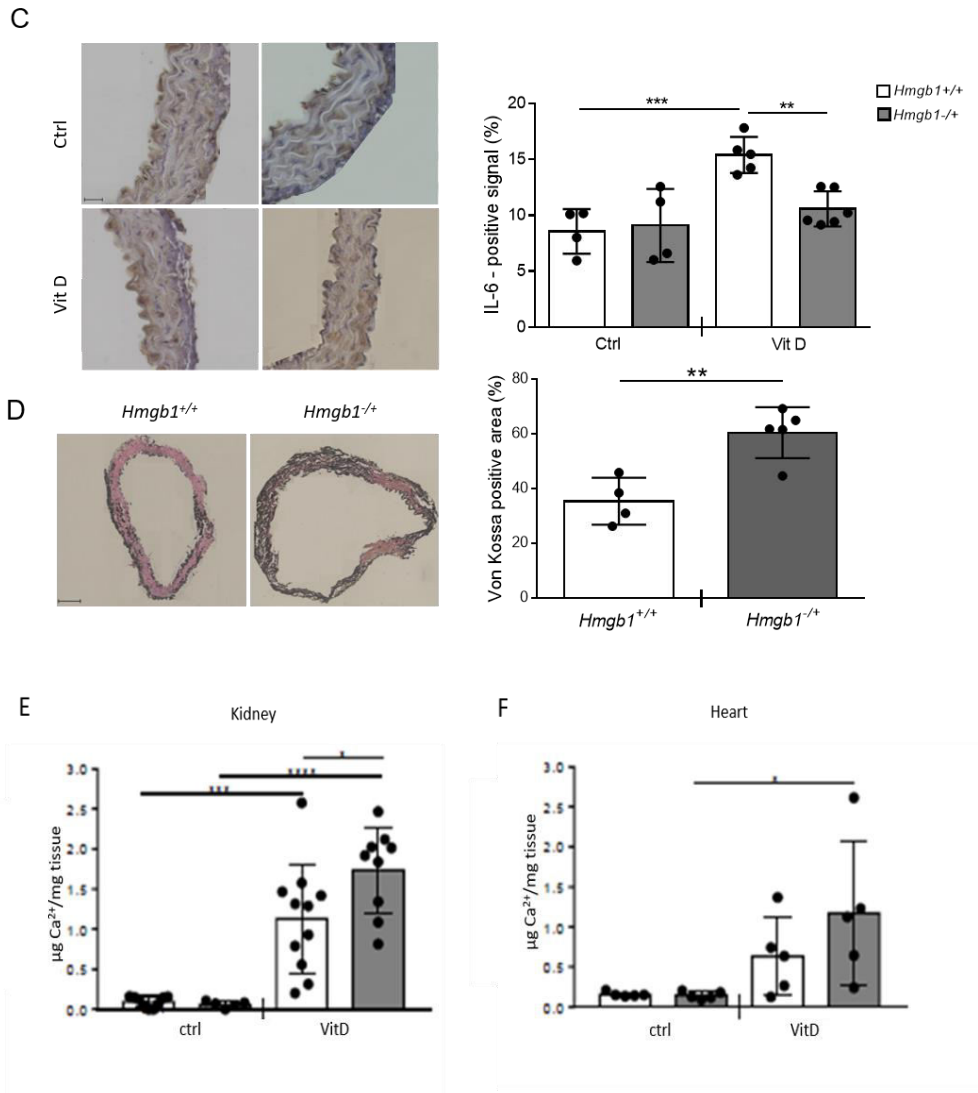

Figure 15. Hmgb1+/- mice show enhanced VC. (A-C) Sixteen week-old Hmgb1$^{+/+}$ and Hmgb1$^{+/-}$ male mice were treated subcutaneously with either vitamin D (Vit D) or a mock solution (Ctrl) for three consecutive days and sacrificed 7 days after the first injection. (A) (Left panel) Representative images of Von Kossa staining to reveal calcium deposits (black) on section from distal thoracic aortas. Scale bar: 50 µm. (Right panel) Quantification of calcium deposits shown as percentage of Von Kossa positive area to the total aortic area. Bars show values as mean ± SD; Student's t-test; * $p < 0.5$; n = 10-13. (B-C) (Left panels) Representative images of ALP (B) and IL-6 (C) staining in aortas of indicated groups of mice. Scale bar: 20 µm. (Right panels) Quantification of ALP (B) and IL-6 (C) signal. Bars show values as mean ± SD; 1-way ANOVA plus Bonferroni post-hoc test; *$p < 0.05$, **$p < 0.01$, ***$p < 0.001$; n = 3-7. (D) Aortic rings derived from Hmgb1+/+ and Hmgb1-/+ male mice. Aortic rings were exposed to calcification medium for 8 days. (Left) representative images of sections from aortic rings after Von Kossa staining (black); scale bars: 100 µm. (Right) quantification of calcium signal (t-test; **, $p < 0.01$; n = 4-5). HMGB1 alters soft tissue calcification in vivo. (E-F) Sixteen week-old Hmgb1+/+ and Hmgb1-

/+ male mice were treated subcutaneously with either vitamin D (Vit D) or a mock solution (Ctrl) for three consecutive days and sacrificed 7 days after the first injection. Calcium content in kidney and heart of mice was quantified by colorimetric analysis and normalized to mg of tissue. Bars show values as mean ± SD; 2-way ANOVA plus Bonferroni post-hoc test; *p < 0.05, ***p < 0.001, ****p < 0.0001; n = 5-11.

6.5 HMGB1 reduction is a marker of VSMC senescence and calcification in humans

Reduction of nuclear HMGB1 expression has been proposed has a marker of senescence in some primary cells including human coronary smooth muscle cells (Stojanovic et al., 2020). Our results suggest that HMGB1 loss may be a marker of HASMC calcification as well.

Thus, we investigated HMGB1 protein levels along with calcium content in aortas isolated from young and middle-age (MA)/old healthy subjects (Controls) (n=3) and CKD patients (n=4). Calcium deposits were undetectable in the vessels isolated from young and MA/old Controls while vessels of MA/old CKD patient have a tendency to show more calcification than young CKD patients (Figure 16A).

Immunohistochemistry revealed that HMGB1 is mainly present in the nucleus and in a less extent in the cytosol of VSMCs of young Controls and decreases significantly in young CKD patients and more drastically in MA/old healthy individuals (Figure 16B). MA/old CKD subjects show similar levels of HMGB1 compared to MA/old healthy subjects (Figure 16B), however the age average of MA/old controls is higher than MA/old CKD patients (Table3).

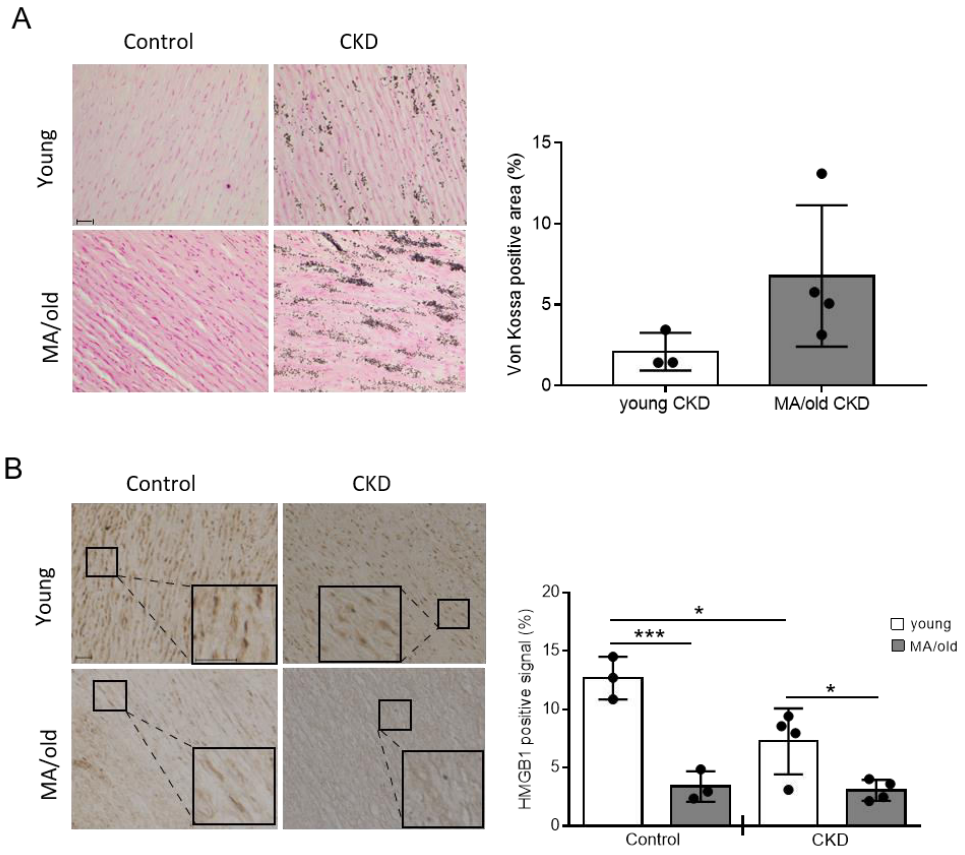

Figure 16. HMGB1 loss is a marker of vascular aging and VC associated with chronic kidney disease (CKD) in humans. (A-B) Vessels from young and old control subjects and CKD patients show decreased levels of HMGB1. **(A)** (Left panel) Representative images of Von Kossa staining to reveal calcium deposits (black) on aortic sections; scale bar: 50 µm. (Right panel) Quantification of calcium deposits shown as percentage of Von Kossa positive area to the total aortic area. **(B)** (Left panel) Immunohistochemistry for HMGB1; scale bars: 50 µm (large panel), 100 µm (small panel). (Right panel) Quantification of HMGB1 expression. Bars show values as mean ± SD; 1-way ANOVA plus Bonferroni post-hoc test; *$p < 0.05$, ***$p < 0.001$; n = 3-4.

Table 3. General information in Control subjects and CKD patients. Data are represented as mean ± SD. 1-way ANOVA plus Bonferroni post-hoc test for multiple comparisons between MA/old CKD vs MA/old Control ‖, $p < 0.05$; young CKD vs young Control *, $p < 0.05$; MA/old Control vs young Control ###, $p < 0.001$; MA/old CKD vs young CKD, §, $p < 0.05$, §§§, $p < 0.001$. MA = middle-age, CKD = chronic kidney disease, HMGB1 = High Mobility Group Box 1. (n=3 control; n=4 CKD).

Variable	young		MA-old	
	Control	CKD	Control	CKD
n	3	4	3	4
Sex (n/% male)	3/100%	1/25%	1/33.3%	0/0%
Age (years)	20.00±2.65	23.00±2.94	76.33±9.02###	63.00±6.06‖,§§§
Von Kossa signal (%)	0	2.11±1.16	0	6.78±4.36
HMGB1 signal (%)	12.68±1.82	7.25±2.83*	3.38±1.31###	3.06±0.90§

Then, we assessed the relationship between HMGB1 protein levels, IL-6 transcript and calcium content in a cohort of male patients undergone surgery for AAA, which is a vascular pathology characterized by massive calcification (Table4) (Shi et al., 2025). A significant negative and positive correlation was found, comparing calcium (Ca^{2+}) with HMGB1 ($R = -0.37$, $p = 0.03$; p) and IL-6 ($R = 0.43$, $p = 0.02$), respectively; however, there was no significant correlation between HMGB1 and IL-6 levels ($R = -0.03$, $p = 0.88$; (Figure 17).

Therefore, these results confirm that HMGB1 is down-regulated in human aortic tissues during both aging and VC associated with various diseases.

Table 4. Biochemical, metabolic, and anthropometric variables of patients undergoing open AAA repair. Variables are expressed as mean ± SD. LDL = Low Density Lipoprotein, HDL = High Density, BMI = body mass index, HMGB1 = High Mobility Group Box 1, Ca^{2+} = Calcium, IL-6 = Interleukin 6.

Variable	Cohort
	n=35
Age (years)	70.9 ± 7.78
Sex (n/% male)	35/100%
Dilated cardiomyopathy	1 (2.9%)
Valve Intervention	0 (0%)
congenital atrial fibrillation	0 (0%)
Stroke	1 (2.9%)
Cancer	4 (11.4%)
Other risk factors	3 (8.6%)
Hypertension	28 (80.0%)
Dyslipidemia	30 (85.7%)
Diabetes Mellitus	8 (22.9%)
Smoke	8 (22.9%)
Total Cholesterol	169 ± 34.4
LDL Cholesterol	100 ± 29.7
HDL Cholesterol	47.3 ± 10.3
Triglycerides	117 ± 55.7
Glycemia	114 ± 21.7
Creatinine	1.05 ± 0.258
BMI	26.8 ± 3.20
Height	1.72 ± 0.0485
Weight	78.9 ± 10.4
Clopidogrel	1 (2.9%)
Ticlopidine	0 (0%)
Ca^{2+} Antagonists	17 (48.6%)
Beta Blockers	19 (54.3%)
Statins	23 (65.7%)
Proton pump inhibitors	15 (42.9%)
Oral diabetes medications	5 (14.3%)
Insulin	2 (5.7%)
HMGB1	179 ± 261
Ca^{2+}	17.4 ± 35.2
IL-6	0.467 ± 0.524

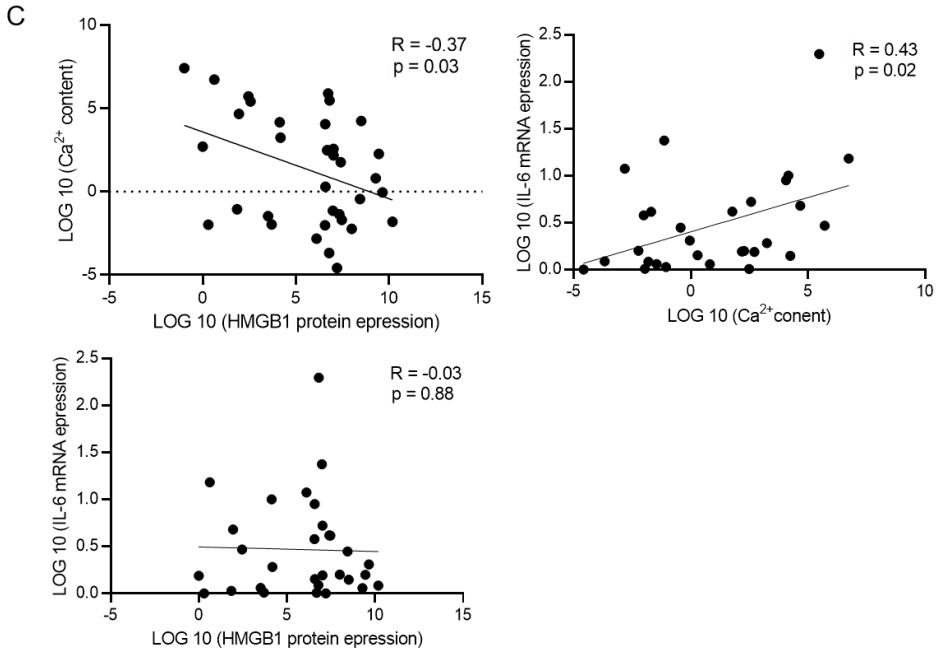

Figure 17. Scatter plots showing correlation between HMGB1, Ca2+ and IL-6 in human AAA specimens. Variables were log-transformed. R = Pearson's coefficient; $p < 0.05$ was considered statistically significant; n=35.

7. DISCUSSION

Vascular aging is the principal risk factor for CVD and VCm is a prominent age-associated complication. VCm is also typical of CKD patients that exhibit accelerated vascular aging driven in part by VSMC senescence and activation of pro-inflammatory SASP (Sanchis et al., 2019). High Mobility Group Box 1 (HMGB1) is an abundant ubiquitous non-histone chromatin binding protein (Bustin et al., 2001; Bianchi et al., 2005; Muller et al., 2001). Upon stress, HMGB1 is released in the extracellular milieu where acts as an "alarmin" and a DAMP (Harris et al., 2006), activating innate and acquired immunity, and promoting tissue repair and regeneration (Bianchi et al., 2007; Tsung et al., 2014). Nuclear HMGB1 is fundamental for chromatin topology and homeostasis (Celona et al., 2011) and it regulates DNA recombination, damage response and repair as well as gene transcription (Bianchi et al., 2005). Lately, it has been suggested that nuclear HMGB1 levels associates with changes in cell proliferation potency and thus, may be involved in organismal aging (Bou, S.M. et al., 2020). Notably, HMGB1 is depleted from the nuclei of primary cells approaching senescence and it is re-localized to the extracellular environment to trigger proinflammatory gene activation and the acquisition of a SASP (Papantonis et al., 2021). Moreover, nuclear HMGB1 binds active chromatin loci relevant for the induction of the senescence gene expression program (Sofiadis et al., 2021). HMGB1 expression decreases in human coronary smooth muscle cells undergoing senescence (Stojanovic et al., 2020), however, the consequences of nuclear reduction of HMGB1 in VSMC senescence and calcification as well as medial VC has never been investigated.

Initial findings from our lab along with the data we obtained herein, demonstrated for the first time that vascular aging is characterized by loss of nuclear HMGB1 expression in mice and humans and that HMGB1 reduction drives VSMC senescence and accelerates VSMC osteogenic differentiation and medial VC induced by altered mineral metabolism. Noteworthy, HMGB1 downregulation in VSMCs *in vitro* and in aortas *in vivo* reduces levels of pro-inflammatory SASP molecules and phenotypic commitment. Finally, HMGB1 progressive decline is a feature of aortas of old healthy subjects and calcified aortas of CKD patients, and the level of the protein inversely correlates with calcium content in human AAA specimens.

Moreover, our results suggest that the loss of HMGB1 may also serve as a marker for VSMC calcification in chronic kidney disease (CKD) patients.

Thus, we investigated HMGB1 protein levels along with calcium content in aortas isolated from young, MA and elderly healthy subjects (n=3), as well as from CKD patients (n=4). Calcium deposits were undetectable in vessels isolated from young and MA/elderly Controls, while vessels from MA/elderly CKD patients showed a tendency for more calcification compared to young CKD patients (Figure 16A). HMGB1 levels decrease significantly in young CKD patients and drop even more drastically in MA/elderly healthy individuals (Figure 16B). MA/elderly CKD patients exhibit similar levels of HMGB1 compared to MA/elderly healthy subjects (Figure 16B), although the average age of the MA/elderly Controls is higher than that of MA/elderly

CKD patients (Table 3).This data seems to be coherent even if the limited sample size could result in an interpretative constraint.
We then examined the relationship between HMGB1 protein levels, IL-6 transcript levels, and calcium content in a cohort of male patients who underwent surgery for abdominal aortic aneurysm (AAA) (Table 4) (Shi et al., 2025). A significant negative correlation was found between calcium and HMGB1, while a significant positive correlation was observed between calcium and IL-6. However, no significant correlation was detected between HMGB1 and IL-6 levels (Figure 17).
Even if this analysis shows very low correlation values (R), making these data exploratory and preliminary, these findings further support the notion that HMGB1 expression is down-regulated in human aortic tissues during both aging and vascular calcification (VC) associated with various diseases, independent of IL-6 levels.
Overall, our data suggest that proper levels of nuclear HMGB1 are protective against vascular senescence and calcification. Furthermore, loss of HMGB1 expression could be considered a marker of VC associated to different pathologies.
Cellular senescence is characterized by permanent growth arrest and a proinflammatory SASP responsible for organismal aging (Di Micco et al., 2021). However, identification of senescent cells, especially in tissues, is limited because of their heterogeneity and lack of specific markers common to all cell types (Di Micco et al., 2021). With the attempt to profile a phenotypical and molecular signature of senescent VSMCs, Stojanovic et al reported that loss of HMGB1 expression may be considered a marker of senescence in human coronary smooth muscle cells (Stojanovic et al., 2020). We extended these findings to HASMCs *in vitro*, and in mouse and human aortas (Figures 6A-C and 15B). We further demonstrated that decline of nuclear HMGB1 levels causes senescence-related changes in VSMCs. Indeed, HASMCs silenced for HMGB1 possess larger nuclei, reduced proliferation because of G0/G1 blocking, and exhibit increased levels of senescent markers such as p21 and SA-β-gal activity (Figure 7 and 8A-B).
Interestingly, HMGB1 decline causes a decrease in pro-inflammatory SASP factor release such as IL-6, IL-8, IL-1β, and MCP1 (Figure 8C-D). Significantly, aortas of *Hmgb1*$^{+/-}$ old mice also show a reduction in IL-6 expression (Figure 12A) suggesting that age-dependent HMGB1 downregulation may hinder inflammation spreading in vessels. Indeed, in contrast with published evidences reporting that some senescent cells (i. e. human fibroblast) relocate HMGB1 into the extracellular environment to activate inflammation and SASP on surrounding cells (Davalos et al., 2013; Papantonis et al., 2021; Bou, S.M. et al., 2020), our findings demonstrate that nuclear HMGB1 decline in senescent VSMCs is not due to its secretion extracellularly but rather to decreased mRNA transcription (Figures 6B-C and 7B). Therefore, the absence of extracellular HMGB1 blunts the acquisition of an inflammatory phenotype in senescent VSMC. Moreover, loss of nuclear HMGB1 can results in chromatin alterations which control transcription of inflammatory genes (Sofiadis et al., 2021).

Hence, as already observed in other cells (De Toma et al., 2014), the anti-inflammatory phenotype of VSMCs may be due to the combination of nuclear and extracellular HMGB1 loss.
We have published that senescent VSMCs have more propensity toward a shift to an osteogenic phenotype and enhances VC onset (Badi et al., 2018; Zuccolo et al., 2020). Accordingly, shB1/HASMCs exhibited higher expression of pro-calcification factors such as RUNX2 and ALP, and decreased levels of the calcification inhibitor OPG (Figure 11). As we recently published, low levels of proinflammatory factors can also enhance VSMC mineralization (Macrì et al., 2023). Furthermore, we found that silencing of HMGB1 in HASMCs results in a shift in ECM components abundance (Table 1); specifically, it influences the expression of TNXB, LUM, COLL-III, BGN, DCN and MMP2 (Figure 10), proteins previously linked to tissue calcification (Matsumoto et al. 2012; Lim et al. 2020). The proteomic profile of calcific aortic valve (CAV) shows a decrease in TNXB and DCN, along with an increase of BGN (Matsumoto et al. 2012; Lim et al. 2020). Certain proteoglycans play a role in the ECM organization that supports the correct function of vessels, others are engaged in calcification of tissue. Specifically: the TNX family participates in the production or application of collagen; DCN stabilizes the ECM; LUM is crucial for ECM integrity and COLL-III supports the vessel elasticity (Imanaka-Yoshida et al., 2018; Neill et al., 2012; Nannan et al., 2020; Osidak et al. 2015). Conversely, both BGN and MMP2 are directly engaged in the osteogenic mechanism crucial for bone development and VC (Polonskaya et al. 2021). Additionally, BGN through drives the pro-osteogenic reprogramming of AVICs (Song et al. 2015). In this study, we discovered that, following the silencing of HMGB1, TNXB, LUM, COLL-III, and DCN expression diminished while levels of BGN and MMP2 increase (Figure 10) probably resulting in an adverse modification of ECM that favors calcification. Significantly, our *in vivo* aging model corroborates the *in vitro* findings. Old *Hmgb1*$^{+/-}$ mice show a reduction in TNXB levels along with an increase in BGN, ALP and RUNX2 (Figure 12). Taken together, these findings demonstrate that the age-dependent decline in HMGB1 in the vasculature plays a causal role in VSMC senescence, predisposing cells to an osteogenic switch.
When cultured in high concentration of Pi, HASMCs silenced for HMGB1 calcify more than control cells (Figure 13A-B); likewise, *Hmgb1*$^{+/-}$ mice treated with an overdose of Vit D, that causes VCm (Badi et al 2015), accumulates more calcium deposits than control mice (Figure 15A). The transcriptomic analyses on shCTR/HASMCs and shB1/HASMCs, both grown in osteogenic medium for 3, 7 and 11 days supported the role of HMGB1 in preventing VSMC osteogenic trans-differentiation. HMGB1 silencing affects profoundly the overall transcriptome of HASMCs considering the large number of differentially expressed genes (Table2). Among the top dysregulated RNAs in HMGB1-silenced cells, the lncRNA H19 and *SOST* gene were found upregulated at all the investigated time points. This lncRNA sponges a number of microRNAs to promote vascular calcification (Xhiong-Zi et al., 2023, Qiang et al., 2022, Feng et al., 2022, Wei et al., 2022). *SOST* gene encodes sclerostin that is a glycoprotein mainly secreted by osteocytes to increase bone resorption and whose

role in vascular calcification is still debated (De Maré et al., 2020); however, its expression levels are increased in calcified arteries (Bisson et al., 2019). Among the top 20 GO terms for the upregulated genes nearly half were related to development/morphogenesis or differentiation/cell commitment. At every assessed stage of osteogenic trans-differentiation upregulated RNAs were significantly enriched in the term "biomineral tissue development" that encompasses genes such as *ALPL*, *COL1A1*, *SLC20A1* (also known as PIT-1), and *PHOSPO1* that are vascular calcification promoters (Bobryshev et al., 2014, Iqbal et al., 2023; Li et al., 2007). Another top GO term was "face morphogenesis" that encompasses genes involved in craniofacial bone development, such as *TBX*1 and *PRICKLE1* (Funato et al., 2022, Wan et al., 2018), and also described to have a role in VC, namely *COL1A1* and *MSX1* (Iqbal et al., 2023; Hayashi et al., 2006). Genes present in other three GO terms linked to development ("atrioventricular valve formation", "cardiac conduction system development", and "sensory organ morphogenesis") are linked to Notch and Wnt signalling pathways that are known to promote VC (Liu et al., 2011; Cai et al., 2016; Lai et al., 2012). "Cell fate commitment" GO term encompasses genes such as *NOTCH3* and *TBX1*, that promote respectively VC and Runx2 expression (Liu et al., 2011; 25209980). The top 20 GO terms for the downregulated genes were linked not only to development, but also to cell cycle progression and inflammation. *ACTA2,* that is a vascular smooth muscle cell contractile marker whose expression is lost in osteogenic-like VSMC was present in both "mesenchyme development" and "tissue migration" GO terms (Funato et al., 2015). Also, *SOD2*, that is believed to have a protective effect against VC, is found in the latter GO term (Tsai et al., 2021). The common genes in GO terms linked to cell cycle progression and inflammation are interleukins, such as *IL1B*, *IL1A*, and *IL6*. Of note, also *STAT1* was found in a number of GO terms enriched for downregulated genes. We have previously shown that despite sustaining inflammation in high phosphate-treated VSMC, JAK-STAT signalling limits the calcification of these cells (Macrì et al., 2023).

In conclusion, our study shows that HMGB1 acts as a crucial player in vascular aging and VCm onset. Its downregulation enhances VSMCs senescence, establishes an anti-inflammatory SASP phenotype, affects ECM organization and the expression of modulators of osteoblast trans-differentiation that ultimately leads to VCm. HMGB1 loss can be also considered a marker of VSMC senescence and calcification. Hence, HMGB1 is a regulator of VSMCs plasticity and contributes to physiological function of vessel but also to age-dependent vascular disease onset.

8. REFERENCES

- Lacolley P, Regnault V, Avolio AP. Smooth muscle cell and arterial aging: basic and clinical aspects. Cardiovasc Res. 2018 Mar 15;114(4):513-528. doi: 10.1093/cvr/cvy009. PMID: 29514201.

- Chamley-Campbell J, Campbell GR, Ross R. The smooth muscle cell in culture. Physiol Rev. 1979 Jan;59(1):1-61. doi: 10.1152/physrev.1979.59.1.1. PMID: 108688.

- Majesky MW. Developmental basis of vascular smooth muscle diversity. Arterioscler Thromb Vasc Biol. 2007 Jun;27(6):1248-58. doi: 10.1161/ATVBAHA.107.141069. Epub 2007 Mar 22. PMID: 17379839.

- Di Micco R, Krizhanovsky V, Baker D, d'Adda di Fagagna F. Cellular senescence in ageing: from mechanisms to therapeutic opportunities. Nat Rev Mol Cell Biol. 2021 Feb;22(2):75-95. doi: 10.1038/s41580-020-00314-w. Epub 2020 Dec 16. PMID: 33328614; PMCID: PMC8344376.

- López-Otín C, Blasco MA, Partridge L, Serrano M, Kroemer G. Hallmarks of aging: An expanding universe. Cell. 2023 Jan 19;186(2):243-278. doi: 10.1016/j.cell.2022.11.001. Epub 2023 Jan 3. PMID: 36599349.

- Costantino S, Paneni F, Cosentino F. Ageing, metabolism and cardiovascular disease. J Physiol. 2016 Apr 15;594(8):2061-73. doi: 10.1113/JP270538. Epub 2015 Oct 22. PMID: 26391109; PMCID: PMC4933114.

- Ohyama Y, Redheuil A, Kachenoura N, Ambale Venkatesh B, Lima JAC. Imaging Insights on the Aorta in Aging. Circ Cardiovasc Imaging. 2018 Apr;11(4):e005617. doi: 10.1161/CIRCIMAGING.117.005617. PMID: 29653929; PMCID: PMC6029255.

- Frismantiene A, Philippova M, Erne P, Resink TJ. Smooth muscle cell-driven vascular diseases and molecular mechanisms of VSMC plasticity. Cell Signal. 2018 Dec;52:48-64. doi: 10.1016/j.cellsig.2018.08.019. Epub 2018 Aug 30. PMID: 30172025.

- Wang M, Monticone RE, McGraw KR. Proinflammatory Arterial Stiffness Syndrome: A Signature of Large Arterial Aging. J Vasc Res. 2018;55(4):210-223. doi: 10.1159/000490244. Epub 2018 Aug 2. PMID: 30071538; PMCID: PMC6174095.

- Hayflick L, Moorhead PS. The serial cultivation of human diploid cell strains. Exp Cell Res. 1961 Dec;25:585-621. doi: 10.1016/0014-4827(61)90192-6. PMID: 13905658.

- Bodnar AG, Ouellette M, Frolkis M, Holt SE, Chiu CP, Morin GB, Harley CB, Shay JW, Lichtsteiner S, Wright WE. Extension of life-span by introduction of telomerase into

normal human cells. Science. 1998 Jan 16;279(5349):349-52. doi: 10.1126/science.279.5349.349. PMID: 9454332.

- d'Adda di Fagagna F, Reaper PM, Clay-Farrace L, Fiegler H, Carr P, Von Zglinicki T, Saretzki G, Carter NP, Jackson SP. A DNA damage checkpoint response in telomere-initiated senescence. Nature. 2003 Nov 13;426(6963):194-8. doi: 10.1038/nature02118. Epub 2003 Nov 5. PMID: 14608368.

- Morgan RG, Donato AJ, Walker AE. Telomere uncapping and vascular aging. Am J Physiol Heart Circ Physiol. 2018 Jul 1;315(1):H1-H5. doi: 10.1152/ajpheart.00008.2018. Epub 2018 Mar 16. PMID: 29547021; PMCID: PMC6087771.

- Campisi J. Cellular senescence: putting the paradoxes in perspective. Curr Opin Genet Dev. 2011 Feb;21(1):107-12. doi: 10.1016/j.gde.2010.10.005. Epub 2010 Nov 17. PMID: 21093253; PMCID: PMC3073609.

- Burton DG, Krizhanovsky V. Physiological and pathological consequences of cellular senescence. Cell Mol Life Sci. 2014 Nov;71(22):4373-86. doi: 10.1007/s00018-014-1691-3. Epub 2014 Jul 31. PMID: 25080110; PMCID: PMC4207941.

- Powers ET, Morimoto RI, Dillin A, Kelly JW, Balch WE. Biological and chemical approaches to diseases of proteostasis deficiency. Annu Rev Biochem. 2009;78:959-91. doi: 10.1146/annurev.biochem.052308.114844. PMID: 19298183.

- Koga H, Kaushik S, Cuervo AM. Protein homeostasis and aging: The importance of exquisite quality control. Ageing Res Rev. 2011 Apr;10(2):205-15. doi: 10.1016/j.arr.2010.02.001. Epub 2010 Feb 10. PMID: 20152936; PMCID: PMC2888802.

- Tchkonia T, Zhu Y, van Deursen J, Campisi J, Kirkland JL. Cellular senescence and the senescent secretory phenotype: therapeutic opportunities. J Clin Invest. 2013 Mar;123(3):966-72. doi: 10.1172/JCI64098. Epub 2013 Mar 1. PMID: 23454759; PMCID: PMC3582125.

- Rodondi N, Marques-Vidal P, Butler J, Sutton-Tyrrell K, Cornuz J, Satterfield S, Harris T, Bauer DC, Ferrucci L, Vittinghoff E, Newman AB; Health, Aging, and Body Composition Study. Markers of atherosclerosis and inflammation for prediction of coronary heart disease in older adults. Am J Epidemiol. 2010 Mar 1;171(5):540-9. doi: 10.1093/aje/kwp428. Epub 2010 Jan 28. PMID: 20110287; PMCID: PMC2842214.

- Badi I, Burba I, Ruggeri C, Zeni F, Bertolotti M, Scopece A, Pompilio G, Raucci A. MicroRNA-34a Induces Vascular Smooth Muscle Cells Senescence by SIRT1 Down-

regulation and Promotes the Expression of Age-Associated Pro-inflammatory Secretory Factors. J Gerontol A Biol Sci Med Sci. 2015 Nov;70(11):1304-11. doi: 10.1093/gerona/glu180. Epub 2014 Oct 28. PMID: 25352462.

- Shanahan CM. Mechanisms of vascular calcification in CKD-evidence for premature ageing? Nat Rev Nephrol. 2013 Nov;9(11):661-70. doi: 10.1038/nrneph.2013.176. Epub 2013 Sep 10. PMID: 24018414.

- Badi I, Mancinelli L, Polizzotto A, Ferri D, Zeni F, Burba I, Milano G, Brambilla F, Saccu C, Bianchi ME, Pompilio G, Capogrossi MC, Raucci A. miR-34a Promotes Vascular Smooth Muscle Cell Calcification by Downregulating SIRT1 (Sirtuin 1) and Axl (AXL Receptor Tyrosine Kinase). Arterioscler Thromb Vasc Biol. 2018 Sep;38(9):2079-2090. doi: 10.1161/ATVBAHA.118.311298. PMID: 30026277.

- Wang M, Monticone RE, Lakatta EG. Arterial aging: a journey into subclinical arterial disease. Curr Opin Nephrol Hypertens. 2010 Mar;19(2):201-7. doi: 10.1097/MNH.0b013e3283361c0b. PMID: 20040868; PMCID: PMC2943205.

- Schlieper G, Schurgers L, Brandenburg V, Reutelingsperger C, Floege J. Vascular calcification in chronic kidney disease: an update. Nephrol Dial Transplant. 2016 Jan;31(1):31-9. doi: 10.1093/ndt/gfv111. Epub 2015 Apr 26. PMID: 25916871.

- Boström K, Watson KE, Horn S, Wortham C, Herman IM, Demer LL. Bone morphogenetic protein expression in human atherosclerotic lesions. J Clin Invest. 1993 Apr;91(4):1800-9. doi: 10.1172/JCI116391. PMID: 8473518; PMCID: PMC288161.

- Alique M, Ruíz-Torres MP, Bodega G, Noci MV, Troyano N, Bohórquez L, Luna C, Luque R, Carmona A, Carracedo J, Ramírez R. Microvesicles from the plasma of elderly subjects and from senescent endothelial cells promote vascular calcification. Aging (Albany NY). 2017 Mar 8;9(3):778-789. doi: 10.18632/aging.101191. PMID: 28278131; PMCID: PMC5391231.

- Virmani R, Kolodgie FD, Burke AP, Farb A, Schwartz SM. Lessons from sudden coronary death: a comprehensive morphological classification scheme for atherosclerotic lesions. Arterioscler Thromb Vasc Biol. 2000 May;20(5):1262-75. doi: 10.1161/01.atv.20.5.1262. PMID: 10807742.

- Lanzer P, Boehm M, Sorribas V, Thiriet M, Janzen J, Zeller T, St Hilaire C, Shanahan C. Medial vascular calcification revisited: review and perspectives. Eur Heart J. 2014 Jun 14;35(23):1515-25. doi: 10.1093/eurheartj/ehu163. Epub 2014 Apr 16. PMID: 24740885; PMCID: PMC4072893.

- St Hilaire C, Ziegler SG, Markello TC, Brusco A, Groden C, Gill F, Carlson-Donohoe H, Lederman RJ, Chen MY, Yang D, Siegenthaler MP, Arduino C, Mancini C, Freudenthal B, Stanescu HC, Zdebik AA, Chaganti RK, Nussbaum RL, Kleta R, Gahl WA, Boehm M. NT5E mutations and arterial calcifications. N Engl J Med. 2011 Feb 3;364(5):432-42. doi: 10.1056/NEJMoa0912923. PMID: 21288095; PMCID: PMC3049958.

- Boström KI, Rajamannan NM, Towler DA. The regulation of valvular and vascular sclerosis by osteogenic morphogens. Circ Res. 2011 Aug 19;109(5):564-77. doi: 10.1161/CIRCRESAHA.110.234278. PMID: 21852555; PMCID: PMC3167074.

- van Varik BJ, Rennenberg RJ, Reutelingsperger CP, Kroon AA, de Leeuw PW, Schurgers LJ. Mechanisms of arterial remodeling: lessons from genetic diseases. Front Genet. 2012 Dec 13;3:290. doi: 10.3389/fgene.2012.00290. PMID: 23248645; PMCID: PMC3521155.

- Leopold JA. Vascular calcification: Mechanisms of vascular smooth muscle cell calcification. Trends Cardiovasc Med. 2015 May;25(4):267-74. doi: 10.1016/j.tcm.2014.10.021. Epub 2014 Oct 30. PMID: 25435520; PMCID: PMC4414672.

- Proudfoot D, Skepper JN, Hegyi L, Bennett MR, Shanahan CM, Weissberg PL. Apoptosis regulates human vascular calcification in vitro: evidence for initiation of vascular calcification by apoptotic bodies. Circ Res. 2000 Nov 24;87(11):1055-62. doi: 10.1161/01.res.87.11.1055. PMID: 11090552.

- Luo G, Ducy P, McKee MD, Pinero GJ, Loyer E, Behringer RR, Karsenty G. Spontaneous calcification of arteries and cartilage in mice lacking matrix GLA protein. Nature. 1997 Mar 6;386(6620):78-81. doi: 10.1038/386078a0. PMID: 9052783.

- Schafer C, Heiss A, Schwarz A, Westenfeld R, Ketteler M, Floege J, Muller-Esterl W, Schinke T, Jahnen-Dechent W. The serum protein alpha 2-Heremans-Schmid glycoprotein/fetuin-A is a systemically acting inhibitor of ectopic calcification. J Clin Invest. 2003 Aug;112(3):357-66. doi: 10.1172/JCI17202. PMID: 12897203; PMCID: PMC166290.

- Bucay N, Sarosi I, Dunstan CR, Morony S, Tarpley J, Capparelli C, Scully S, Tan HL, Xu W, Lacey DL, Boyle WJ, Simonet WS. osteoprotegerin-deficient mice develop early onset osteoporosis and arterial calcification. Genes Dev. 1998 May 1;12(9):1260-8. doi: 10.1101/gad.12.9.1260. PMID: 9573043; PMCID: PMC316769.

- Reynolds JL, Skepper JN, McNair R, Kasama T, Gupta K, Weissberg PL, Jahnen-Dechent W, Shanahan CM. Multifunctional roles for serum protein fetuin-a in inhibition of human vascular smooth muscle cell calcification. J Am Soc Nephrol. 2005

Oct;16(10):2920-30. doi: 10.1681/ASN.2004100895. Epub 2005 Aug 10. PMID: 16093453.

- Bennett BJ, Scatena M, Kirk EA, Rattazzi M, Varon RM, Averill M, Schwartz SM, Giachelli CM, Rosenfeld ME. Osteoprotegerin inactivation accelerates advanced atherosclerotic lesion progression and calcification in older ApoE-/- mice. Arterioscler Thromb Vasc Biol. 2006 Sep;26(9):2117-24. doi: 10.1161/01.ATV.0000236428.91125.e6. Epub 2006 Jul 13. PMID: 16840715.

- Lacey DL, Timms E, Tan HL, Kelley MJ, Dunstan CR, Burgess T, Elliott R, Colombero A, Elliott G, Scully S, Hsu H, Sullivan J, Hawkins N, Davy E, Capparelli C, Eli A, Qian YX, Kaufman S, Sarosi I, Shalhoub V, Senaldi G, Guo J, Delaney J, Boyle WJ. Osteoprotegerin ligand is a cytokine that regulates osteoclast differentiation and activation. Cell. 1998 Apr 17;93(2):165-76. doi: 10.1016/s0092-8674(00)81569-x. PMID: 9568710.

- Jia J, Zhou H, Zeng X, Feng S. Estrogen stimulates osteoprotegerin expression via the suppression of miR-145 expression in MG-63 cells. Mol Med Rep. 2017 Apr;15(4):1539-1546. doi: 10.3892/mmr.2017.6168. Epub 2017 Feb 6. PMID: 28260003; PMCID: PMC5364970.

- Harmey D, Hessle L, Narisawa S, Johnson KA, Terkeltaub R, Millán JL. Concerted regulation of inorganic pyrophosphate and osteopontin by akp2, enpp1, and ank: an integrated model of the pathogenesis of mineralization disorders. Am J Pathol. 2004 Apr;164(4):1199-209. doi: 10.1016/S0002-9440(10)63208-7. PMID: 15039209; PMCID: PMC1615351.

- Lomashvili KA, Garg P, Narisawa S, Millan JL, O'Neill WC. Upregulation of alkaline phosphatase and pyrophosphate hydrolysis: potential mechanism for uremic vascular calcification. Kidney Int. 2008 May;73(9):1024-30. doi: 10.1038/ki.2008.26. Epub 2008 Feb 20. PMID: 18288101; PMCID: PMC3010853.

- Johnson K, Polewski M, van Etten D, Terkeltaub R. Chondrogenesis mediated by PPi depletion promotes spontaneous aortic calcification in NPP1-/- mice. Arterioscler Thromb Vasc Biol. 2005 Apr;25(4):686-91. doi: 10.1161/01.ATV.0000154774.71187.f0. Epub 2004 Dec 29. PMID: 15625282.

- Lian JB, Stein GS, Javed A, van Wijnen AJ, Stein JL, Montecino M, Hassan MQ, Gaur T, Lengner CJ, Young DW. Networks and hubs for the transcriptional control of osteoblastogenesis. Rev Endocr Metab Disord. 2006 Jun;7(1-2):1-16. doi: 10.1007/s11154-006-9001-5. PMID: 17051438.

- Nakashima K, Zhou X, Kunkel G, Zhang Z, Deng JM, Behringer RR, de Crombrugghe B. The novel zinc finger-containing transcription factor osterix is required for osteoblast differentiation and bone formation. Cell. 2002 Jan 11;108(1):17-29. doi: 10.1016/s0092-8674(01)00622-5. PMID: 11792318.

- Zuccolo E, Badi I, Scavello F, Gambuzza I, Mancinelli L, Macrì F, Tedesco CC, Veglia F, Bonfigli AR, Olivieri F, Raucci A. The microRNA-34a-Induced Senescence-Associated Secretory Phenotype (SASP) Favors Vascular Smooth Muscle Cells Calcification. Int J Mol Sci. 2020 Jun 23;21(12):4454. doi: 10.3390/ijms21124454. PMID: 32585876; PMCID: PMC7352675.

- Alexander Y, Osto E, Schmidt-Trucksäss A, Shechter M, Trifunovic D, Duncker DJ, Aboyans V, Bäck M, Badimon L, Cosentino F, De Carlo M, Dorobantu M, Harrison DG, Guzik TJ, Hoefer I, Morris PD, Norata GD, Suades R, Taddei S, Vilahur G, Waltenberger J, Weber C, Wilkinson F, Bochaton-Piallat ML, Evans PC. Endothelial function in cardiovascular medicine: a consensus paper of the European Society of Cardiology Working Groups on Atherosclerosis and Vascular Biology, Aorta and Peripheral Vascular Diseases, Coronary Pathophysiology and Microcirculation, and Thrombosis. Cardiovasc Res. 2021 Jan 1;117(1):29-42. doi: 10.1093/cvr/cvaa085. PMID: 32282914; PMCID: PMC7797212.

- Bouabdallah J, Zibara K, Issa H, Lenglet G, Kchour G, Caus T, Six I, Choukroun G, Kamel S, Bennis Y. Endothelial cells exposed to phosphate and indoxyl sulphate promote vascular calcification through interleukin-8 secretion. Nephrol Dial Transplant. 2019 Jul 1;34(7):1125-1134. doi: 10.1093/ndt/gfy325. PMID: 30481303.

- Hao N, Zhou Z, Zhang F, Li Y, Hu R, Zou J, Zheng R, Wang L, Xu L, Tan W, Li C, Wang F. Interleukin-29 Accelerates Vascular Calcification via JAK2/STAT3/BMP2 Signaling. J Am Heart Assoc. 2023 Jan 3;12(1):e027222. doi: 10.1161/JAHA.122.027222. Epub 2022 Dec 20. PMID: 36537334; PMCID: PMC9973608.

- Kurozumi A, Nakano K, Yamagata K, Okada Y, Nakayamada S, Tanaka Y. IL-6 and sIL-6R induces STAT3-dependent differentiation of human VSMCs into osteoblast-like cells through JMJD2B-mediated histone demethylation of RUNX2. Bone. 2019 Jul;124:53-61. doi: 10.1016/j.bone.2019.04.006. Epub 2019 Apr 11. PMID: 30981888.

- Alfaddagh A, Martin SS, Leucker TM, Michos ED, Blaha MJ, Lowenstein CJ, Jones SR, Toth PP. Inflammation and cardiovascular disease: From mechanisms to therapeutics. Am J Prev Cardiol. 2020 Nov 21;4:100130. doi: 10.1016/j.ajpc.2020.100130. PMID: 34327481; PMCID: PMC8315628.

- Lee SE, Sung JM, Andreini D, Budoff MJ, Cademartiri F, Chinnaiyan K, Choi JH, Chun EJ, Conte E, Gottlieb I, Hadamitzky M, Kim YJ, Kumar A, Lee BK, Leipsic JA, Maffei E,

Marques H, Pontone G, Raff G, Shin S, Stone PH, Samady H, Virmani R, Narula J, Berman DS, Shaw LJ, Bax JJ, Lin FY, Min JK, Chang HJ. Differential association between the progression of coronary artery calcium score and coronary plaque volume progression according to statins: the Progression of AtheRosclerotic PlAque DetermIned by Computed TomoGraphic Angiography Imaging (PARADIGM) study. Eur Heart J Cardiovasc Imaging. 2019 Nov 1;20(11):1307-1314. doi: 10.1093/ehjci/jez022. PMID: 30789215; PMCID: PMC6806249.

- Puri R, Nicholls SJ, Shao M, Kataoka Y, Uno K, Kapadia SR, Tuzcu EM, Nissen SE. Impact of statins on serial coronary calcification during atheroma progression and regression. J Am Coll Cardiol. 2015 Apr 7;65(13):1273-1282. doi: 10.1016/j.jacc.2015.01.036. PMID: 25835438.

- Macrì F, Vigorito I, Castiglione S, Faggiano S, Casaburo M, Fanotti N, Piacentini L, Vigetti D, Vinci MC, Raucci A. High Phosphate-Induced JAK-STAT Signalling Sustains Vascular Smooth Muscle Cell Inflammation and Limits Calcification. Biomolecules. 2023 Dec 24;14(1):29. doi: 10.3390/biom14010029. PMID: 38254629; PMCID: PMC10813375.

- Bustin M. Revised nomenclature for high mobility group (HMG) chromosomal proteins. Trends Biochem Sci. 2001 Mar;26(3):152-3. doi: 10.1016/s0968-0004(00)01777-1. PMID: 11246012.

- Bianchi ME, Agresti A. HMG proteins: dynamic players in gene regulation and differentiation. Curr Opin Genet Dev. 2005 Oct;15(5):496-506. doi: 10.1016/j.gde.2005.08.007. PMID: 16102963.

- Stros M. HMGB proteins: interactions with DNA and chromatin. Biochim Biophys Acta. 2010 Jan-Feb;1799(1-2):101-13. doi: 10.1016/j.bbagrm.2009.09.008. PMID: 20123072.

- Bianchi ME, Falciola L, Ferrari S, Lilley DM. The DNA binding site of HMG1 protein is composed of two similar segments (HMG boxes), both of which have counterparts in other eukaryotic regulatory proteins. EMBO J. 1992 Mar;11(3):1055-63. doi: 10.1002/j.1460-2075.1992.tb05144.x. PMID: 1547772; PMCID: PMC556546.

- Bonaldi T, Talamo F, Scaffidi P, Ferrera D, Porto A, Bachi A, Rubartelli A, Agresti A, Bianchi ME. Monocytic cells hyperacetylate chromatin protein HMGB1 to redirect it towards secretion. EMBO J. 2003 Oct 15;22(20):5551-60. doi: 10.1093/emboj/cdg516. PMID: 14532127; PMCID: PMC213771.

- Klune JR, Dhupar R, Cardinal J, Billiar TR, Tsung A. HMGB1: endogenous danger signaling. Mol Med. 2008 Jul-Aug;14(7-8):476-84. doi: 10.2119/2008-00034.Klune. PMID: 18431461; PMCID: PMC2323334.

- Calogero S, Grassi F, Aguzzi A, Voigtländer T, Ferrier P, Ferrari S, Bianchi ME. The lack of chromosomal protein Hmg1 does not disrupt cell growth but causes lethal hypoglycaemia in newborn mice. Nat Genet. 1999 Jul;22(3):276-80. doi: 10.1038/10338. PMID: 10391216.

- Bertheloot D, Latz E. HMGB1, IL-1α, IL-33 and S100 proteins: dual-function alarmins. Cell Mol Immunol. 2017 Jan;14(1):43-64. doi: 10.1038/cmi.2016.34. Epub 2016 Aug 29. PMID: 27569562; PMCID: PMC5214941.

- Harris HE, Raucci A. Alarmin(g) news about danger: workshop on innate danger signals and HMGB1. EMBO Rep. 2006 Aug;7(8):774-8. doi: 10.1038/sj.embor.7400759. Epub 2006 Jul 21. PMID: 16858429; PMCID: PMC1525157.

- Colavita L, Ciprandi G, Salpietro A, Cuppari C. HMGB1: A pleiotropic activity. Pediatr Allergy Immunol. 2020 Nov;31 Suppl 26(Suppl 26):63-65. doi: 10.1111/pai.13358. PMID: 33236418; PMCID: PMC7753284.

- Müller S, Ronfani L, Bianchi ME. Regulated expression and subcellular localization of HMGB1, a chromatin protein with a cytokine function. J Intern Med. 2004 Mar;255(3):332-43. doi: 10.1111/j.1365-2796.2003.01296.x. PMID: 14871457.

- Chen Q, Wang ZY, Chen LY, Hu HY. Roles of High Mobility Group Box 1 in Cardiovascular Calcification. Cell Physiol Biochem. 2017;42(2):427-440. doi: 10.1159/000477591. Epub 2017 Jun 5. PMID: 28571029.

- Raucci A, Di Maggio S, Scavello F, D'Ambrosio A, Bianchi ME, Capogrossi MC. The Janus face of HMGB1 in heart disease: a necessary update. Cell Mol Life Sci. 2019 Jan;76(2):211-229. doi: 10.1007/s00018-018-2930-9. Epub 2018 Oct 10. PMID: 30306212; PMCID: PMC6339675.

- Agresti A, Bianchi ME. HMGB proteins and gene expression. Curr Opin Genet Dev. 2003 Apr;13(2):170-8. doi: 10.1016/s0959-437x(03)00023-6. PMID: 12672494.

- Iacomino G, Picariello G, Sbrana F, Raiteri R, D'Agostino L. DNA-HMGB1 interaction: The nuclear aggregates of polyamine mediation. Biochim Biophys Acta. 2016 Oct;1864(10):1402-10. doi: 10.1016/j.bbapap.2016.07.006. Epub 2016 Jul 22. PMID: 27451951.

- Celona B, Weiner A, Di Felice F, Mancuso FM, Cesarini E, Rossi RL, Gregory L, Baban D, Rossetti G, Grianti P, Pagani M, Bonaldi T, Ragoussis J, Friedman N, Camilloni G, Bianchi ME, Agresti A. Substantial histone reduction modulates genomewide nucleosomal occupancy and global transcriptional output. PLoS Biol. 2011 Jun;9(6):e1001086. doi: 10.1371/journal.pbio.1001086. Epub 2011 Jun 28. PMID: 21738444; PMCID: PMC3125158.

- Hu Z, Chen K, Xia Z, Chavez M, Pal S, Seol JH, Chen CC, Li W, Tyler JK. Nucleosome loss leads to global transcriptional up-regulation and genomic instability during yeast aging. Genes Dev. 2014 Feb 15;28(4):396-408. doi: 10.1101/gad.233221.113. PMID: 24532716; PMCID: PMC3937517.

- De Toma I, Rossetti G, Zambrano S, Bianchi ME, Agresti A. Nucleosome loss facilitates the chemotactic response of macrophages. J Intern Med. 2014 Nov;276(5):454-69. doi: 10.1111/joim.12286. Epub 2014 Aug 5. PMID: 25069756.

- Lotze MT, Tracey KJ. High-mobility group box 1 protein (HMGB1): nuclear weapon in the immune arsenal. Nat Rev Immunol. 2005 Apr;5(4):331-42. doi: 10.1038/nri1594. PMID: 15803152.

- Little AJ, Corbett E, Ortega F, Schatz DG. Cooperative recruitment of HMGB1 during V(D)J recombination through interactions with RAG1 and DNA. Nucleic Acids Res. 2013 Mar 1;41(5):3289-301. doi: 10.1093/nar/gks1461. Epub 2013 Jan 15. PMID: 23325855; PMCID: PMC3597659.

- Stros M, Ozaki T, Bacikova A, Kageyama H, Nakagawara A. HMGB1 and HMGB2 cell-specifically down-regulate the p53- and p73-dependent sequence-specific transactivation from the human Bax gene promoter. J Biol Chem. 2002 Mar 1;277(9):7157-64. doi: 10.1074/jbc.M110233200. Epub 2001 Dec 17. PMID: 11748232.

- Thomas JO, Stott K. H1 and HMGB1: modulators of chromatin structure. Biochem Soc Trans. 2012 Apr;40(2):341-6. doi: 10.1042/BST20120014. PMID: 22435809.

- Polanská E, Pospíšilová Š, Štros M. Binding of histone H1 to DNA is differentially modulated by redox state of HMGB1. PLoS One. 2014 Feb 13;9(2):e89070. doi: 10.1371/journal.pone.0089070. PMID: 24551219; PMCID: PMC3923860.

- Wang H, Bloom O, Zhang M, Vishnubhakat JM, Ombrellino M, Che J, Frazier A, Yang H, Ivanova S, Borovikova L, Manogue KR, Faist E, Abraham E, Andersson J, Andersson U, Molina PE, Abumrad NN, Sama A, Tracey KJ. HMG-1 as a late mediator of endotoxin lethality in mice. Science. 1999 Jul 9;285(5425):248-51. doi: 10.1126/science.285.5425.248. PMID: 10398600.

- Treutiger CJ, Mullins GE, Johansson AS, Rouhiainen A, Rauvala HM, Erlandsson-Harris H, Andersson U, Yang H, Tracey KJ, Andersson J, Palmblad JE. High mobility group 1 B-box mediates activation of human endothelium. J Intern Med. 2003 Oct;254(4):375-85. doi: 10.1046/j.1365-2796.2003.01204.x. PMID: 12974876.

- Andrassy M, Volz HC, Igwe JC, Funke B, Eichberger SN, Kaya Z, Buss S, Autschbach F, Pleger ST, Lukic IK, Bea F, Hardt SE, Humpert PM, Bianchi ME, Mairbäurl H, Nawroth PP, Remppis A, Katus HA, Bierhaus A. High-mobility group box-1 in ischemia-reperfusion injury of the heart. Circulation. 2008 Jun 24;117(25):3216-26. doi: 10.1161/CIRCULATIONAHA.108.769331. PMID: 18574060.

- Wang WK, Lu QH, Zhang JN, Wang B, Liu XJ, An FS, Qin WD, Chen XY, Dong WQ, Zhang C, Zhang Y, Zhang MX. HMGB1 mediates hyperglycaemia-induced cardiomyocyte apoptosis via ERK/Ets-1 signalling pathway. J Cell Mol Med. 2014 Nov;18(11):2311-20. doi: 10.1111/jcmm.12399. Epub 2014 Sep 11. PMID: 25210949; PMCID: PMC4224563.

- Ulloa L, Batliwalla FM, Andersson U, Gregersen PK, Tracey KJ. High mobility group box chromosomal protein 1 as a nuclear protein, cytokine, and potential therapeutic target in arthritis. Arthritis Rheum. 2003 Apr;48(4):876-81. doi: 10.1002/art.10854. PMID: 12687528.

- Maroso M, Balosso S, Ravizza T, Liu J, Aronica E, Iyer AM, Rossetti C, Molteni M, Casalgrandi M, Manfredi AA, Bianchi ME, Vezzani A. Toll-like receptor 4 and high-mobility group box-1 are involved in ictogenesis and can be targeted to reduce seizures. Nat Med. 2010 Apr;16(4):413-9. doi: 10.1038/nm.2127. Epub 2010 Mar 28. PMID: 20348922.

- Venereau E, Casalgrandi M, Schiraldi M, Antoine DJ, Cattaneo A, De Marchis F, Liu J, Antonelli A, Preti A, Raeli L, Shams SS, Yang H, Varani L, Andersson U, Tracey KJ, Bachi A, Uguccioni M, Bianchi ME. Mutually exclusive redox forms of HMGB1 promote cell recruitment or proinflammatory cytokine release. J Exp Med. 2012 Aug 27;209(9):1519-28. doi: 10.1084/jem.20120189. Epub 2012 Aug 6. PMID: 22869893; PMCID: PMC3428943.

- Maugeri N, Rovere-Querini P, Baldini M, Baldissera E, Sabbadini MG, Bianchi ME, Manfredi AA. Oxidative stress elicits platelet/leukocyte inflammatory interactions via HMGB1: a candidate for microvessel injury in sytemic sclerosis. Antioxid Redox Signal. 2014 Mar 1;20(7):1060-74. doi: 10.1089/ars.2013.5298. Epub 2014 Jan 17. PMID: 24070090.

- Tsung A, Tohme S, Billiar TR. High-mobility group box-1 in sterile inflammation. J Intern Med. 2014 Nov;276(5):425-43. doi: 10.1111/joim.12276. PMID: 24935761.

- Tirone M, Tran NL, Ceriotti C, Gorzanelli A, Canepari M, Bottinelli R, Raucci A, Di Maggio S, Santiago C, Mellado M, Saclier M, François S, Careccia G, He M, De Marchis F, Conti V, Ben Larbi S, Cuvellier S, Casalgrandi M, Preti A, Chazaud B, Al-Abed Y, Messina G, Sitia G, Brunelli S, Bianchi ME, Vénéreau E. High mobility group box 1 orchestrates tissue regeneration via CXCR4. J Exp Med. 2018 Jan 2;215(1):303-318.

doi: 10.1084/jem.20160217. Epub 2017 Dec 4. PMID: 29203538; PMCID: PMC5748844.

- Leifer CA, Medvedev AE. Molecular mechanisms of regulation of Toll-like receptor signaling. J Leukoc Biol. 2016 Nov;100(5):927-941. doi: 10.1189/jlb.2MR0316-117RR. Epub 2016 Jun 24. PMID: 27343013; PMCID: PMC5069093.

- Park JS, Svetkauskaite D, He Q, Kim JY, Strassheim D, Ishizaka A, Abraham E. Involvement of toll-like receptors 2 and 4 in cellular activation by high mobility group box 1 protein. J Biol Chem. 2004 Feb 27;279(9):7370-7. doi: 10.1074/jbc.M306793200. Epub 2003 Dec 4. PMID: 14660645.

- Conti L, Lanzardo S, Arigoni M, Antonazzo R, Radaelli E, Cantarella D, Calogero RA, Cavallo F. The noninflammatory role of high mobility group box 1/Toll-like receptor 2 axis in the self-renewal of mammary cancer stem cells. FASEB J. 2013 Dec;27(12):4731-44. doi: 10.1096/fj.13-230201. Epub 2013 Aug 22. PMID: 23970797.

- Hummel S, Van Aken H, Zarbock A. Inhibitors of CXC chemokine receptor type 4: putative therapeutic approaches in inflammatory diseases. Curr Opin Hematol. 2014 Jan;21(1):29-36. doi: 10.1097/MOH.0000000000000002. PMID: 24275689.

- Calcinotto A, Kohli J, Zagato E, Pellegrini L, Demaria M, Alimonti A. Cellular Senescence: Aging, Cancer, and Injury. Physiol Rev. 2019 Apr 1;99(2):1047-1078. doi: 10.1152/physrev.00020.2018. PMID: 30648461.

- Yasom S, Watcharanurak P, Bhummaphan N, Thongsroy J, Puttipanyalears C, Settayanon S, Chalertpet K, Khumsri W, Kongkaew A, Patchsung M, Siriwattanakankul C, Pongpanich M, Pin-On P, Jindatip D, Wanotayan R, Odton M, Supasai S, Oo TT, Arunsak B, Pratchayasakul W, Chattipakorn N, Chattipakorn S, Mutirangura A. The roles of HMGB1-produced DNA gaps in DNA protection and aging biomarker reversal. FASEB Bioadv. 2022 Mar 28;4(6):408-434. doi: 10.1096/fba.2021-00131. Erratum in: FASEB Bioadv. 2023 Jan 25;5(2):85-87. doi: 10.1096/fba.1365. PMID: 35664831; PMCID: PMC9164245.

- Sofiadis K, Josipovic N, Nikolic M, Kargapolova Y, Übelmesser N, Varamogianni-Mamatsi V, Zirkel A, Papadionysiou I, Loughran G, Keane J, Michel A, Gusmao EG, Becker C, Altmüller J, Georgomanolis T, Mizi A, Papantonis A. HMGB1 coordinates SASP-related chromatin folding and RNA homeostasis on the path to senescence. Mol Syst Biol. 2021 Jun;17(6):e9760. doi: 10.15252/msb.20209760. PMID: 34166567; PMCID: PMC8224457.

- Davalos AR, Kawahara M, Malhotra GK, Schaum N, Huang J, Ved U, Beausejour CM, Coppe JP, Rodier F, Campisi J. p53-dependent release of Alarmin HMGB1 is a central

mediator of senescent phenotypes. J Cell Biol. 2013 May 13;201(4):613-29. doi: 10.1083/jcb.201206006. Epub 2013 May 6. PMID: 23649808; PMCID: PMC3653366.

- Stojanović SD, Fuchs M, Kunz M, Xiao K, Just A, Pich A, Bauersachs J, Fiedler J, Sedding D, Thum T. Inflammatory Drivers of Cardiovascular Disease: Molecular Characterization of Senescent Coronary Vascular Smooth Muscle Cells. Front Physiol. 2020 May 25;11:520. doi: 10.3389/fphys.2020.00520. PMID: 32523550; PMCID: PMC7261939.

- Lee JJ, Park IH, Rhee WJ, Kim HS, Shin JS. HMGB1 modulates the balance between senescence and apoptosis in response to genotoxic stress. FASEB J. 2019 Oct;33(10):10942-10953. doi: 10.1096/fj.201900288R. Epub 2019 Jul 5. PMID: 31284735.

- Enokido Y, Yoshitake A, Ito H, Okazawa H. Age-dependent change of HMGB1 and DNA double-strand break accumulation in mouse brain. Biochem Biophys Res Commun. 2008 Nov 7;376(1):128-33. doi: 10.1016/j.bbrc.2008.08.108. Epub 2008 Aug 30. PMID: 18762169.

- Qi SC, Cui C, Yan YH, Sun GH, Zhu SR. Effects of high-mobility group box 1 on the proliferation and odontoblastic differentiation of human dental pulp cells. Int Endod J. 2013 Dec;46(12):1153-63. doi: 10.1111/iej.12112. Epub 2013 Apr 19. PMID: 23600680.

- Shen W, Zhou J, Wang C, Xu G, Wu Y, Hu Z. High mobility group box 1 induces calcification of aortic valve interstitial cells via toll-like receptor 4. Mol Med Rep. 2017 May;15(5):2530-2536. doi: 10.3892/mmr.2017.6287. Epub 2017 Mar 3. PMID: 28260034; PMCID: PMC5428883.

- Jin X, Rong S, Yuan W, Gu L, Jia J, Wang L, Yu H, Zhuge Y. High Mobility Group Box 1 Promotes Aortic Calcification in Chronic Kidney Disease via the Wnt/β-Catenin Pathway. Front Physiol. 2018 Jun 5;9:665. doi: 10.3389/fphys.2018.00665. PMID: 29922171; PMCID: PMC5996195.

- Wang Y, Shan J, Yang W, Zheng H, Xue S. High mobility group box 1 (HMGB1) mediates high-glucose-induced calcification in vascular smooth muscle cells of saphenous veins. Inflammation. 2013 Dec;36(6):1592-604. doi: 10.1007/s10753-013-9704-1. PMID: 23928875.

- Chen Q, Bei JJ, Liu C, Feng SB, Zhao WB, Zhou Z, Yu ZP, Du XJ, Hu HY. HMGB1 Induces Secretion of Matrix Vesicles by Macrophages to Enhance Ectopic Mineralization. PLoS One. 2016 May 31;11(5):e0156686. doi: 10.1371/journal.pone.0156686. PMID: 27243975; PMCID: PMC4887028.

- Zhang T, Cao G, Meng X, Ouyang C, Gao J, Sun Y, Wu J, Min Q, Zhang C, Zhang W. Lethal giant larvae 1 inhibits smooth muscle calcification via high mobility group box 1. J Mol Cell Cardiol. 2020 May;142:39-52. doi: 10.1016/j.yjmcc.2020.03.017. Epub 2020 Apr 5. Erratum in: J Mol Cell Cardiol. 2022 Feb;163:187-189. doi: 10.1016/j.yjmcc.2021.11.012. PMID: 32268148.

- Zhang T, Li H, Ouyang C, Cao G, Gao J, Wu J, Yang J, Yu N, Min Q, Zhang C, Zhang W. Liver kinase B1 inhibits smooth muscle calcification via high mobility group box 1. Redox Biol. 2021 Jan;38:101828. doi: 10.1016/j.redox.2020.101828. Epub 2020 Dec 6. PMID: 33338919; PMCID: PMC7750422.

- Al-Aly Z. Phosphate, oxidative stress, and nuclear factor-κB activation in vascular calcification. Kidney Int. 2011 May;79(10):1044-7. doi: 10.1038/ki.2010.548. PMID: 21527943.

- Dobin A, Davis CA, Schlesinger F, Drenkow J, Zaleski C, Jha S, Batut P, Chaisson M, Gingeras TR. STAR: ultrafast universal RNA-seq aligner. Bioinformatics. 2013 Jan 1;29(1):15-21. doi: 10.1093/bioinformatics/bts635. Epub 2012 Oct 25. PMID: 23104886; PMCID: PMC3530905.

- Langmead B, Salzberg SL. Fast gapped-read alignment with Bowtie 2. Nat Methods. 2012 Mar 4;9(4):357-9. doi: 10.1038/nmeth.1923. PMID: 22388286; PMCID: PMC3322381.

- Liao Y, Smyth GK, Shi W. featureCounts: an efficient general purpose program for assigning sequence reads to genomic features. Bioinformatics. 2014 Apr 1;30(7):923-30. doi: 10.1093/bioinformatics/btt656. Epub 2013 Nov 13. PMID: 24227677.

- Risso D, Schwartz K, Sherlock G, Dudoit S. GC-content normalization for RNA-Seq data. BMC Bioinformatics. 2011 Dec 17;12:480. doi: 10.1186/1471-2105-12-480. PMID: 22177264; PMCID: PMC3315510.

- Risso D, Ngai J, Speed TP, Dudoit S. Normalization of RNA-seq data using factor analysis of control genes or samples. Nat Biotechnol. 2014 Sep;32(9):896-902. doi: 10.1038/nbt.2931. Epub 2014 Aug 24. PMID: 25150836; PMCID: PMC4404308.

- Zhou Y, Zhou B, Pache L, Chang M, Khodabakhshi AH, Tanaseichuk O, Benner C, Chanda SK. Metascape provides a biologist-oriented resource for the analysis of systems-level datasets. Nat Commun. 2019 Apr 3;10(1):1523. doi: 10.1038/s41467-019-09234-6. PMID: 30944313; PMCID: PMC6447622.

- Shi D, Zhang M, Zhang Y, Shi Y, Liu X, Wu X, Yang Z. The Pathophysiological Role of Vascular Smooth Muscle Cells in Abdominal Aortic Aneurysm. Cells. 2025 Jul

2;14(13):1009. doi: 10.3390/cells14131009. PMID: 40643529; PMCID: PMC12248496

- de la Cuesta F, Alvarez-Llamas G, Gil-Dones F, Darde VM, Calvo E, López JA, Vivanco F, Barderas MG. Secretome of human aortic valves. Methods Mol Biol. 2013;1005:237-43. doi: 10.1007/978-1-62703-386-2_19. PMID: 23606262.

- Song R, Fullerton DA, Ao L, Zheng D, Zhao KS, Meng X. BMP-2 and TGF-β1 mediate biglycan-induced pro-osteogenic reprogramming in aortic valve interstitial cells. J Mol Med (Berl). 2015 Apr;93(4):403-12. doi: 10.1007/s00109-014-1229-z. Epub 2014 Nov 22. PMID: 25412776; PMCID: PMC4369167.

- Cozzolino M, Ciceri P, Galassi A. Hyperphosphatemia: a novel risk factor for mortality in chronic kidney disease. Ann Transl Med. 2019 Feb;7(3):55. doi: 10.21037/atm.2018.06.50. PMID: 30906759; PMCID: PMC6389588.

- Liu Y, Wang T, Yan J, Jiagbogu N, Heideman DA, Canfield AE, Alexander MY. HGF/c-Met signalling promotes Notch3 activation and human vascular smooth muscle cell osteogenic differentiation in vitro. Atherosclerosis. 2011 Dec;219(2):440-7. doi: 10.1016/j.atherosclerosis.2011.08.033. Epub 2011 Aug 26. PMID: 21920521; PMCID: PMC3925803.

- Karuppagounder V, Giridharan VV, Arumugam S, Sreedhar R, Palaniyandi SS, Krishnamurthy P, Quevedo J, Watanabe K, Konishi T, Thandavarayan RA. Modulation of Macrophage Polarization and HMGB1-TLR2/TLR4 Cascade Plays a Crucial Role for Cardiac Remodeling in Senescence-Accelerated Prone Mice. PLoS One. 2016 Apr 12;11(4):e0152922. doi: 10.1371/journal.pone.0152922. PMID: 27070323; PMCID: PMC4829159.

- Fiuza C, Bustin M, Talwar S, Tropea M, Gerstenberger E, Shelhamer JH, Suffredini AF. Inflammation-promoting activity of HMGB1 on human microvascular endothelial cells. Blood. 2003 Apr 1;101(7):2652-60. doi: 10.1182/blood-2002-05-1300. Epub 2002 Nov 27. PMID: 12456506.

- Zhao HX, Huang YX, Tao JG. ST1926 Attenuates Steroid-Induced Osteoporosis in Rats by Inhibiting Inflammation Response. J Cell Biochem. 2017 Aug;118(8):2072-2086. doi: 10.1002/jcb.25812. Epub 2017 May 15. PMID: 27918081.

- Harmey D, Hessle L, Narisawa S, Johnson KA, Terkeltaub R, Millán JL. Concerted regulation of inorganic pyrophosphate and osteopontin by akp2, enpp1, and ank: an integrated model of the pathogenesis of mineralization disorders. Am J Pathol. 2004 Apr;164(4):1199-209. doi: 10.1016/S0002-9440(10)63208-7. PMID: 15039209; PMCID: PMC1615351.

- Matsumoto K, Satoh K, Maniwa T, Araki A, Maruyama R, Oda T. Noticeable decreased expression of tenascin-X in calcific aortic valves. Connect Tissue Res. 2012;53(6):460-8. doi: 10.3109/03008207.2012.702818. Epub 2012 Jul 24. PMID: 22827484.

- Lim J, Aguilan JT, Sellers RS, Nagajyothi F, Weiss LM, Angeletti RH, Bortnick AE. Lipid mass spectrometry imaging and proteomic analysis of severe aortic stenosis. J Mol Histol. 2020 Oct;51(5):559-571. doi: 10.1007/s10735-020-09905-5. Epub 2020 Aug 13. PMID: 32794037; PMCID: PMC7672660.

- Imanaka-Yoshida K, Matsumoto KI. Multiple Roles of Tenascins in Homeostasis and Pathophysiology of Aorta. Ann Vasc Dis. 2018 Jun 25;11(2):169-180. doi: 10.3400/avd.ra.17-00118. PMID: 30116408; PMCID: PMC6094038.

- Neill T, Schaefer L, Iozzo RV. Decorin: a guardian from the matrix. Am J Pathol. 2012 Aug;181(2):380-7. doi: 10.1016/j.ajpath.2012.04.029. Epub 2012 Jun 23. PMID: 22735579; PMCID: PMC3409438.

- Nannan L, Untereiner V, Proult I, Boulagnon-Rombi C, Colin-Pierre C, Sockalingum GD, Brézillon S. Label-Free Infrared Spectral Histology of Skin Tissue Part I: Impact of Lumican on Extracellular Matrix Integrity. Front Cell Dev Biol. 2020 May 12;8:320. doi: 10.3389/fcell.2020.00320. PMID: 32478070; PMCID: PMC7235349.

- Osidak MS, Osidak EO, Akhmanova MA, Domogatsky SP, Domogatskaya AS. Fibrillar, fibril-associated and basement membrane collagens of the arterial wall: architecture, elasticity and remodeling under stress. Curr Pharm Des. 2015;21(9):1124-33. doi: 10.2174/1381612820666141013122906. PMID: 25312736.

- Polonskaya YV, Kashtanova EV, Murashov IS, Striukova EV, Kurguzov AV, Stakhneva EM, Shramko VS, Maslatsov NA, Chernyavsky AM, Ragino YI. Association of Matrix Metalloproteinases with Coronary Artery Calcification in Patients with CHD. J Pers Med. 2021 Jun 3;11(6):506. doi: 10.3390/jpm11060506. PMID: 34205079; PMCID: PMC8228219.

- Song R, Fullerton DA, Ao L, Zheng D, Zhao KS, Meng X. BMP-2 and TGF-β1 mediate biglycan-induced pro-osteogenic reprogramming in aortic valve interstitial cells. J Mol Med (Berl). 2015 Apr;93(4):403-12. doi: 10.1007/s00109-014-1229-z. Epub 2014 Nov 22. PMID: 25412776; PMCID: PMC4369167.

- Bruderer M, Richards RG, Alini M, Stoddart MJ. Role and regulation of RUNX2 in osteogenesis. Eur Cell Mater. 2014 Oct 23;28:269-86. doi: 10.22203/ecm.v028a19. PMID: 25340806.

- O'Grady S, Morgan MP. Deposition of calcium in an in vitro model of human breast tumour calcification reveals functional role for ALP activity, altered expression of osteogenic genes and dysregulation of the TRPM7 ion channel. Sci Rep. 2019 Jan 24;9(1):542. doi: 10.1038/s41598-018-36496-9. PMID: 30679450; PMCID: PMC6345823.

- Sharma U, Pal D, Prasad R. Alkaline phosphatase: an overview. Indian J Clin Biochem. 2014 Jul;29(3):269-78. doi: 10.1007/s12291-013-0408-y. Epub 2013 Nov 26. PMID: 24966474; PMCID: PMC4062654.

- Lin CP, Huang PH, Lai CF, Chen JW, Lin SJ, Chen JS. Simvastatin Attenuates Oxidative Stress, NF-κB Activation, and Artery Calcification in LDLR-/- Mice Fed with High Fat Diet via Down-regulation of Tumor Necrosis Factor-α and TNF Receptor 1. PLoS One. 2015 Dec 1;10(12):e0143686. doi: 10.1371/journal.pone.0143686. Erratum in: PLoS One. 2016 Jan 29;11(1):e0148590. doi: 10.1371/journal.pone.0148590. PMID: 26625143; PMCID: PMC4666466.

- Sanchis P, Ho CY, Liu Y, Beltran LE, Ahmad S, Jacob AP, Furmanik M, Laycock J, Long DA, Shroff R, Shanahan CM. Arterial "inflammaging" drives vascular calcification in children on dialysis. Kidney Int. 2019 Apr;95(4):958-972. doi: 10.1016/j.kint.2018.12.014. Epub 2019 Mar 1. PMID: 30827513; PMCID: PMC6684370.

- Bianchi ME, Manfredi AA. High-mobility group box 1 (HMGB1) protein at the crossroads between innate and adaptive immunity. Immunol Rev. 2007 Dec;220:35-46. doi: 10.1111/j.1600-065X.2007.00574.x. PMID: 17979838.

- Li XZ, Xiong ZC, Zhang SL, Hao QY, Liu ZY, Zhang HF, Wang JF, Gao JW, Liu PM. Upregulated LncRNA H19 Sponges MiR-106a-5p and Contributes to Aldosterone-Induced Vascular Calcification via Activating the Runx2-Dependent Pathway. Arterioscler Thromb Vasc Biol. 2023 Sep;43(9):1684-1699. doi: 10.1161/ATVBAHA.123.319308. Epub 2023 Jul 6. PMID: 37409531.

- Liu Q, Qi H, Yao L. A long non-coding RNA H19/microRNA-138/TLR3 network is involved in high phosphorus-mediated vascular calcification and chronic kidney disease. Cell Cycle. 2022 Aug;21(16):1667-1683. doi: 10.1080/15384101.2022.2064957. Epub 2022 Apr 18. PMID: 35435133; PMCID: PMC9302514.

- Xu F, Zhong JY, Guo B, Lin X, Wu F, Li FX, Shan SK, Zheng MH, Wang Y, Xu QS, Lei LM, Tan CM, Liao XB, Yuan LQ. H19 Promotes Osteoblastic Transition by Acting as ceRNA of miR-140-5p in Vascular Smooth Muscle Cells. Front Cell Dev Biol. 2022 Feb 7;10:774363. doi: 10.3389/fcell.2022.774363. PMID: 35198556; PMCID: PMC8859097.

- Zhou W, Feng Q, Cheng M, Zhang D, Jin J, Zhang S, Bai Y, Xu J. LncRNA H19 sponges miR-103-3p to promote the high phosphorus-induced osteoblast phenotypic transition of vascular smooth muscle cells by upregulating Runx2. Cell Signal. 2022 Mar;91:110220. doi: 10.1016/j.cellsig.2021.110220. Epub 2021 Dec 16. PMID: 34923106.

- Maré A, D'Haese PC, Verhulst A. The Role of Sclerostin in Bone and Ectopic Calcification. Int J Mol Sci. 2020 Apr 30;21(9):3199. doi: 10.3390/ijms21093199. PMID: 32366042; PMCID: PMC7246472.

- Bisson SK, Ung RV, Picard S, Valade D, Agharazii M, Larivière R, Mac-Way F. High calcium, phosphate and calcitriol supplementation leads to an osteocyte-like phenotype in calcified vessels and bone mineralisation defect in uremic rats. J Bone Miner Metab. 2019 Mar;37(2):212-223. doi: 10.1007/s00774-018-0919-y. Epub 2018 Mar 30. PMID: 29603070.

- Bobryshev YV, Orekhov AN, Sobenin I, Chistiakov DA. Role of bone-type tissue-nonspecific alkaline phosphatase and PHOSPO1 in vascular calcification. Curr Pharm Des. 2014;20(37):5821-8. doi: 10.2174/1381612820666140212193011. PMID: 24533943.

- Iqbal F, Schlotter F, Becker-Greene D, Lupieri A, Goettsch C, Hutcheson JD, Rogers MA, Itoh S, Halu A, Lee LH, Blaser MC, Mlynarchik AK, Hagita S, Kuraoka S, Chen HY, Engert JC, Passos LSA, Jha PK, Osborn EA, Jaffer FA, Body SC, Robson SC, Thanassoulis G, Aikawa M, Singh SA, Sonawane AR, Aikawa E. Sortilin enhances fibrosis and calcification in aortic valve disease by inducing interstitial cell heterogeneity. Eur Heart J. 2023 Mar 7;44(10):885-898. doi: 10.1093/eurheartj/ehac818. PMID: 36660854; PMCID: PMC9991042.

- Li X, Giachelli CM. Sodium-dependent phosphate cotransporters and vascular calcification. Curr Opin Nephrol Hypertens. 2007 Jul;16(4):325-8. doi: 10.1097/MNH.0b013e3281c55ef1. PMID: 17565274.

- Funato N. Craniofacial Phenotypes and Genetics of DiGeorge Syndrome. J Dev Biol. 2022 May 13;10(2):18. doi: 10.3390/jdb10020018. PMID: 35645294; PMCID: PMC9149807.

- Wan Y, Lantz B, Cusack BJ, Szabo-Rogers HL. Prickle1 regulates differentiation of frontal bone osteoblasts. Sci Rep. 2018 Dec 21;8(1):18021. doi: 10.1038/s41598-018-36742-0. PMID: 30575813; PMCID: PMC6303328.

- Hayashi K, Nakamura S, Nishida W, Sobue K. Bone morphogenetic protein-induced MSX1 and MSX2 inhibit myocardin-dependent smooth muscle gene transcription.

Mol Cell Biol. 2006 Dec;26(24):9456-70. doi: 10.1128/MCB.00759-06. Epub 2006 Oct 9. PMID: 17030628; PMCID: PMC1698541.

- Cai T, Sun D, Duan Y, Wen P, Dai C, Yang J, He W. WNT/β-catenin signaling promotes VSMCs to osteogenic transdifferentiation and calcification through directly modulating Runx2 gene expression. Exp Cell Res. 2016 Jul 15;345(2):206-17. doi: 10.1016/j.yexcr.2016.06.007. Epub 2016 Jun 16. PMID: 27321958.

- Lai CF, Shao JS, Behrmann A, Krchma K, Cheng SL, Towler DA. TNFR1-activated reactive oxidative species signals up-regulate osteogenic Msx2 programs in aortic myofibroblasts. Endocrinology. 2012 Aug;153(8):3897-910. doi: 10.1210/en.2012-1216. Epub 2012 Jun 8. PMID: 22685265; PMCID: PMC3404358.

- Funato N, Nakamura M, Richardson JA, Srivastava D, Yanagisawa H. Loss of Tbx1 induces bone phenotypes similar to cleidocranial dysplasia. Hum Mol Genet. 2015 Jan 15;24(2):424-35. doi: 10.1093/hmg/ddu458. Epub 2014 Sep 10. PMID: 25209980.

- Tsai YT, Yeh HY, Chao CT, Chiang CK. Superoxide Dismutase 2 (SOD2) in Vascular Calcification: A Focus on Vascular Smooth Muscle Cells, Calcification Pathogenesis, and Therapeutic Strategies. Oxid Med Cell Longev. 2021 Feb 24;2021:6675548. doi: 10.1155/2021/6675548. PMID: 33728027; PMCID: PMC7935587.

- de Souza AW, Westra J, Limburg PC, Bijl M, Kallenberg CG. HMGB1 in vascular diseases: Its role in vascular inflammation and atherosclerosis. Autoimmun Rev. 2012 Oct;11(12):909-17. doi: 10.1016/j.autrev.2012.03.007. Epub 2012 Apr 1. PMID: 22495229.